POLITECNICO di TORINO

Corso di Laurea Magistrale in
INGEGNERIA CIVILE

Tesi di Laurea Magistrale

SEISMIC DESIGN OF HYSTERETIC DEVICES FOR RETROFITTING EXISTING RC STRUCTURES

Relatori

Prof. Paolo Castaldo
Prof. Enrico Tubaldi

Candidato

Federico Selvi

A.A 2017/2018

FIGURE INDEX

Chapter 1

1 Introduction

1.1 Aim of the thesis

Passive control systems through hysteretic devices represents one of the best technique for retrofitting, or upgrading, the numerous existing reinforced concrete framed buildings, located in Italy in areas with high seismic hazard and designed without an appropriate seismic detailing. These systems absorb the inertial actions in combination with the existing structure, increasing the stiffness of the frame and providing an additional dissipation of the energy by means of their ductility capacities to exhibit large inelastic deformations.

The thesis deals with the design of dissipative buckling restrained braces (BRBs), in order to upgrade an existing building in L'Aquila. Specifically, it is used a procedure based on the results from pushover analysis considering as design parameter the maximum inter-storey drift properly chosen in order to avoid an excessive damage of the main structure. After the design procedure, the model of the building equipped with the BRBs is tested to verify the respect of the seismic performance. The behaviour of the upgraded structure using different BRB modelling approach is studied through static nonlinear (pushover) analyses. Another important aspect that is taken into account is the influence of the infills on the design of the BRBs, comparing the response of the upgraded building with and without the presence of non-structural elements.

Chapter 2

2 Seismic performance of structural systems

2.1 Single degree of freedom system

The response of a structural system under a ground motion due to an earthquake can be represented in a simple way using a single degree of freedom (SDOF) system. This system is composed of a mass *m* concentrated on the top of the structure, a massless frame that provides an horizontal stiffness *k* and a viscous damper, with damping coefficient *c*, that simulates the energy dissipation provided by the structure. The displacement of the ground, caused by the earthquake, is u_g , the absolute displacement of the mass is u_t and the relative displacement between the mass and the ground is *u*. All this quantities vary with time and at each instant are related by the following equation:

$$u^t(t) = u(t) + u_g(t) \tag{2.1.1}$$

Considering the free body diagram, it's possible to obtain the equation of dynamic equilibrium:

$$f_I + f_D + f_S = 0 \tag{2.1.2}$$

Where $f_I = m\ddot{u}^t$ is the inertia force, $f_D = c\dot{u}$ is the damping force related to the relative velocity $\dot{u}$ through the damping coefficient and f_S is the resisting force provided by the frame thanks to its stiffness.

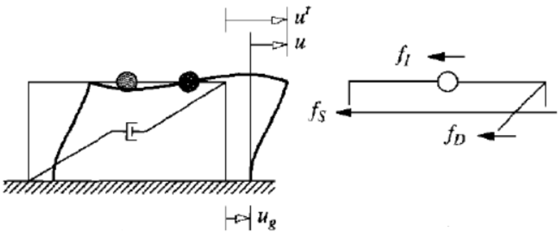

Figure 2-1. Single degree of freedom system.

The force-displacement relation ($f_S - u$) can be both linear, for small deformations, and nonlinear, for larger deformations, as shown in Figure 2-2.

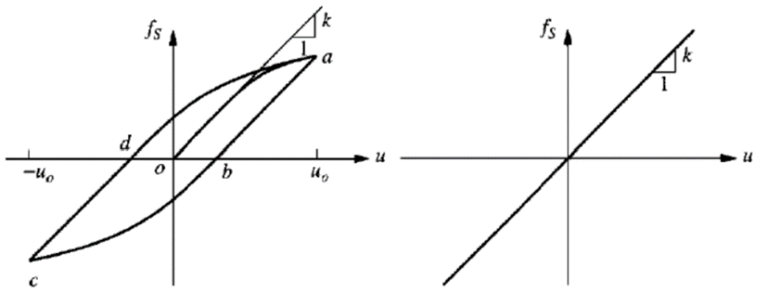

Figure 2-2. Inelastic (left) and elastic (right) force displacement relation.

In case of linear elastic system, the relation between the resisting force and the deformation of the structure is linear:

$$f_s = ku \tag{2.1.3}$$

For an inelastic system, instead, the loading curve changes its shape at the larger amplitudes passing from the elastic field to the plastic one. For this reason the force corresponding to the deformation u is not singular and depends on the deformations 'history and velocity (positive if the force is increasing and negative if the force is decreasing):

$$f_s = f_s(u, \dot{u}) \tag{2.1.4}$$

The study of inelastic systems under dynamic action is extremely important because many structures are designed to enter into the plastic field in order to exhibit a certain energy dissipation thanks to the formation of a force-deformation hysteresis loop.

Considering a linear response, substituting the expression of the forces in eq.(2.1.2) gives

$$m\ddot{u} + c\dot{u} + ku = -m\ddot{u}_g \tag{2.1.5}$$

that is the equation of motion of the structure. The ground motion causes the rise of an inertia force that can be seen as an external force $-m\ddot{u}_g$, called *effective earthquake force*, applied to the structure.

Dividing the eq.(2.1.5) by the mass *m* gives

$$\ddot{u} + 2\zeta\omega_n\dot{u} + \omega_n^2 u = -\ddot{u}_g(t) \tag{2.1.6}$$

where

$$\omega_n = \sqrt{\frac{k}{m}} \tag{2.1.7}$$

is the *natural circular frequency of vibration* and

$$\zeta = \frac{c}{2m\omega_n} \tag{2.1.8}$$

Is the damping ratio.

The eq.(2.1.6) is a second order differential equation and requires two boundary condition, the initial displacement $u(0)$ and the initial velocity $\dot{u}(0)$, in order to obtain the solution $u(t)$ that represent the displacement at each time instant. An elastic system is able to dissipate the seismic energy only by mean of the viscous damping, and subject to a ground motion shows little deformations but high resisting forces.

Considering a nonlinear response, substituting the expression of the forces in eq.(2.1.2) gives

$$m\ddot{u} + c\dot{u} + f_S(u,\dot{u}) = -m\ddot{u}_g \tag{2.1.9}$$

Dividing by *m* the eq.(2.1.9) we obtain the following equation:

$$\ddot{u} + 2\zeta\omega_n\dot{u} + \omega_n^2 u_y \tilde{f}_S(u,\dot{u}) = -\ddot{u}_g(t) \tag{2.1.10}$$

Where ω_n and ζ are the quantities introduced before and

$$\tilde{f}_S(u,\dot{u}) = \frac{f_S(u,\dot{u})}{f_y} \tag{2.1.11}$$

The eq.(2.1.10) can be rewritten in terms of $\mu(t) = u(t)/u_y$ dividing by the yield deformation so it is possible to identify the parameters that influence the ductility factor μ

$$\ddot{\mu} + 2\zeta\omega_n\dot{\mu} + \omega_n^2\tilde{f}_S(\mu, \dot{\mu}) = -\omega_n^2\frac{\ddot{u}_g(t)}{a_y} \tag{2.1.12}$$

Solving this second order differential equation is possible to find the ductility required by the structure at each time instant in order to satisfy the seismic demand. It is easy to understand the importance of the structural ductility because it permits to design structures taking into account lower actions, and for this reason avoiding excessive dimensions of the resisting elements, but higher deformations.

If the bare frame is coupled with a second resisting system, for example with an elastoplastic steel bracing system (BRBs) as it happens in the study case of this thesis, the equation of motion of the dual system is (*Tubaldi et al. 2017)*:

$$m\ddot{u}(t) + c\dot{u} + f_s + f_b = -m\ddot{u}_g \tag{2.1.13}$$

Where f_b is the resisting force of the BRB. Assuming the frame to have a nonlinear behavior with initial stiffness k_f, a yield displacement u_{fy} and a ductility μ_f and using a hysteretic constitutive model for the BRB simplified by an elastoplastic behavior with initial stiffness k_b, a yield displacement u_{by} and a ductility μ_b it is possible to obtain a SDOF model that describes the behavior of a RC frame retrofit with BRBs.

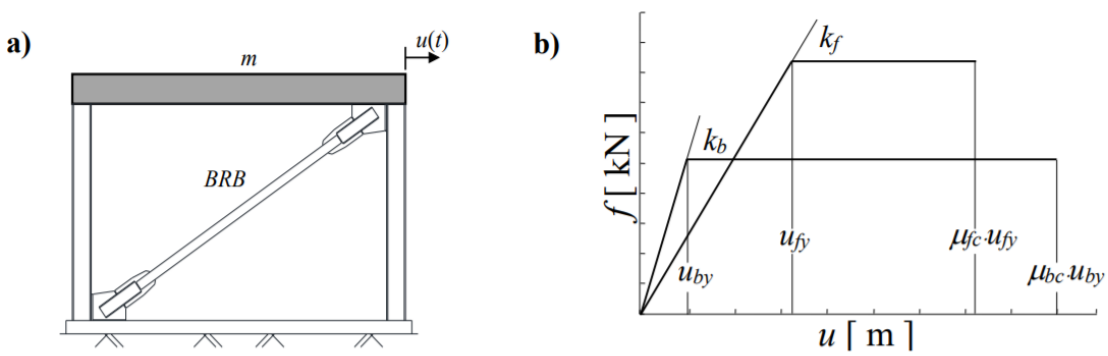

Figure 2-3. (a) SDOF dual system with BRB, (b) Constitutive laws of the dual system.

2.2 Energetic response of the structure

During an earthquake the structure is subject to an input energy from the ground acceleration that is partially accumulated an partially dissipated.

$$E_I(t) = E_A(t) + E_D(t) \tag{2.2.1}$$

E_I is the input energy and it is the work done by the total base shear force at the foundation on the ground displacement. E_A is the mechanical energy accumulated in the system and it is divided into two components, E_S that is the strain energy and E_K that is the kinetic energy.

$$E_A = E_S + E_K \tag{2.2.2}$$

The dissipated energy E_D can be divided into two components depending on the dissipative mechanism.

$$E_D = E_H + E_V \tag{2.2.3}$$

Where E_H and E_V are the energies dissipated respectively by the hysteretic cycles or plastic deformations and by the viscous damping. The presence of the dissipation reduces the elastic stresses on the structures for the same value of the input energy E_I. This permits to design resisting elements with smaller dimensions but showing higher structural damages after the earthquake. For this reason, the damage to the structure can be reduced only decreasing the ductility or the hysteretic energy demand of the structure through passive energy dissipation devices. In this way part of the hysteretic energy and viscous damping energy demand is transferred to the device

$$\begin{aligned} E_V &= E_{V,stucture} + E_{V,device} \\ E_H &= E_{H,stucture} + E_{H,device} \end{aligned} \tag{2.2.4}$$

Using BRBs the reduction in ductility demand is provided by reduced displacements that arise from increased stiffness of the system and from hysteretic energy dissipation within the devices.

2.3 Behavior of existing gravity load designed RC structures

RC buildings represent a great portion of the Italian construction heritage, 60% of them were built before the introduction of the Law n.64 of 1974 that made obligatory the observance of specific technical provision for the seismic zones. For this reason, most of the existing RC buildings does not have an acceptable behavior under seismic action. Together with the fact that 44% of the Italian territory characterized by an high seismic hazard it is clear that the retrofitting or the upgrading of the existing structures is indispensable to prevent the collapse or extended structural damages of the structures. Another problem deals with the evolution of the seismic hazard of the areas of the Italian territory over the years that may cause, for non-recent buildings, the risk of being subject to a higher seismic action than expected in the design phase. For all this reasons, the evaluation of RC building resistant capacity is one of the most important topic of the last years because it permits both to quantify the seismic vulnerability and to choose the best retrofitting solutions for the structure.

The worst response to seismic action has been observed in structures realized before the introduction of the seismic codes that were designed to resist only to gravitational loads. This typology of buildings is characterized by a low ductility and by the lack of a resistance hierarchy that permits to reach a global collapse of the structure after the use of all its plastic resources and avoiding local failure due to brittle mechanism.

Gravity load designed RC buildings realized before the ‘70es are made by resisting frames oriented in one direction only, perpendicular to the direction of the floor structure. This frames are usually composed by emergent beams and rectangular columns designed without taking into account horizontal forces.
The design errors that influence the most the seismic response of these buildings are:

- *Inadequate structure configuration.* The frames are oriented in only one direction and for this reason, the resistance to the seismic action in the orthogonal direction is very low or absent. Moreover, it is very usual to have non-continuous frame in the two main direction.

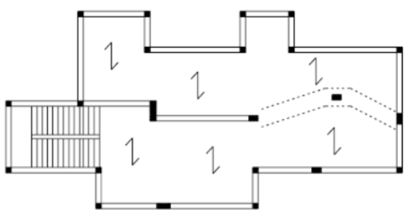

Figure 2-4. Example of inadeqate structure configuration.

- *Absence of in plane regularity.* The presence of an asymmetric distribution of the shear walls, or others stiffer elements as the lift shaft or the stairs, causes a large eccentricity between the center of resistance and the center of mass and the rise of torsional effects.

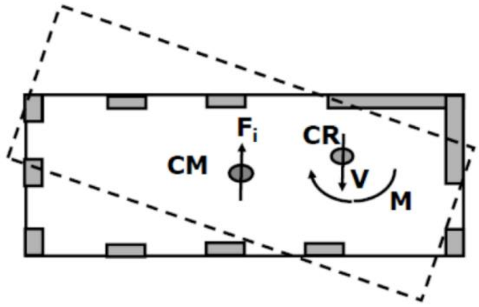

Figure 2-5. Effect of in plane irregularity.

- *Absence of in elevation regularity.* It consists in an irregular distribution of lateral resisting system, both structural and nonstructural (infills), along the elevation of the building. This deficiency causes a concentration of ductility demand in a portion of the structure, usually in a single story, that reaches a local collapse. Some typical case of in elevation irregularity are due to discontinuous load path caused by changing in the vertical disposition of the columns, different heights of the stories and the presence of stiff masonry infills only in the upper floors.

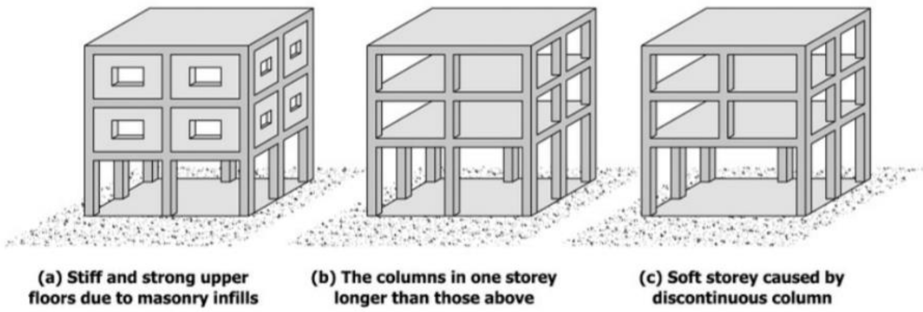

Figure 2-6. Examples of in elevation irregularity.

The so-called soft story shows a significant reduction of lateral stiffness compared to the other stories and for this reason, its deformation is higher than the other one. This problem is most critical when it occurs at the first floor because the shear reach its maximum at this level. If all the stories have the same stiffness, the deflection is distributed equally along the height, otherwise most part of it is concentrated in the soft story.

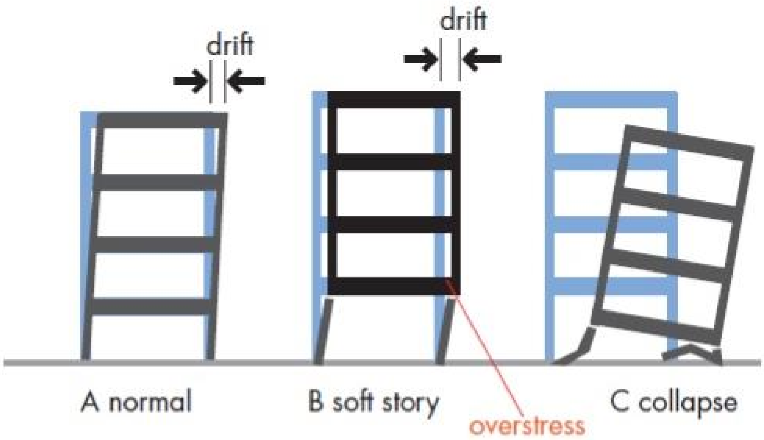

Figure 2-7. Soft storey collapse mechanism.

Typical examples of collapses caused by the presence of soft floors are shown in the following pictures.

Figure 2-8. Example of soft storey mechanism collapse.

Figure 2-9. Example of soft storey mechanism collapse.

- *Lack of rigid diaphragm at floor level.* The presence of a concrete slab at each floor, with an adequate stiffness, is fundamental for the distribution of the seismic forces between the resisting elements. If the thickness of the slab is too small or in presence of a pre-cast floor without an appropriate connection with the structure the result is an excessive in-plan flexibility that causes a bat repartition of the horizontal forces among the vertical elements.

- *Presence of short columns.* The presence of stocky columns influences the repartition of the loads between the resisting elements because the forces are distributed in proportion to the stiffness of the members that is inversely proportional to the cube of the length. For this reason, short columns are subject to higher forces during an earthquake and reach the failure due to shear causing the collapse of the structure. One of the most common cause of this problem is the presence of partially infilled frames because they reduce the effective length of the columns.

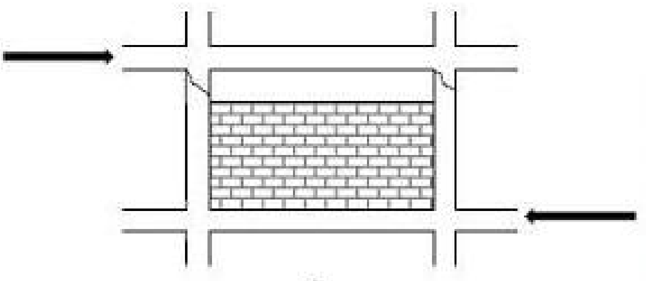

Figure 2-10. Stocky columns due to a partially infilled frame.

- *Inadequate local details.* A proper local detailing of members and connection is necessary to achieve a good strength and ductility in order to prevent brittle failure. The most important regions are the connection between the columns and the beams, where it is expected the formation of the plastic hinges. In case of gravity load designed RC structures the most common deficiencies are:
    - Discontinuous stirrups in beams and columns, with an excessive spacing, that can cause brittle failure due to shear;
    - Incorrect position of steel rebars;
    - Lack of adequate anchorage and overlapping of the longitudinal steel rebars;
    - Eccentricities in beam to column joints;
    - "Strong" beams and "weak" columns that can cause a soft-story mechanism. This design error is very common for gravity load designed RC buildings because the columns were designed to resist only to axial load, without taking into account bending action due to horizontal forces. For this reason the formation of the plastic hinge is localized on the column, with a low amount of longitudinal and transverse steel reinforcement, instead of on the beam.
    - Absence of confinement and discontinuous longitudinal reinforcement in beam to column joints. Beam-column joints should be designed to allow the columns and the beams to maintain their strength and stiffness also after large deformations. A loss of strength or stiffness due to the failure of the joint causes an increase of the lateral displacement and consequently of the second order effects.

2.4 Design procedures according to the seismic codes

New buildings are designed according to the so called *performance based seismic design* (PBSD) introduced by *Pacific Earthquake Engineering Research* (PEER) through the Vision 2000 document of 1995. The intent of PBSD is to provide a method that allows to design, retrofit or upgrade buildings in such a way that they are able to reach certain performances if subjected to certain levels of seismic intensity, i.e. are able to satisfy predetermined "performance objectives ". These performance objectives are related to the amount of damage the building may experience in response to the earthquake and they are described in terms of displacement rather than forces. The goal of the performance based seismic design is to obtain a structure that is capable of reaching a target displacement when it is subject to an earthquake compatible with the design response spectrum. The main performance objectives for structural and nonstructural elements, as defined in the *Prestandard and Commentary for the Seismic Rehabilitation of Buildings* (FEMA 365), are:

- Operational (O)
- Immediate occupancy (IO)
- Life safety (LS)
- Collapse prevention (CP)

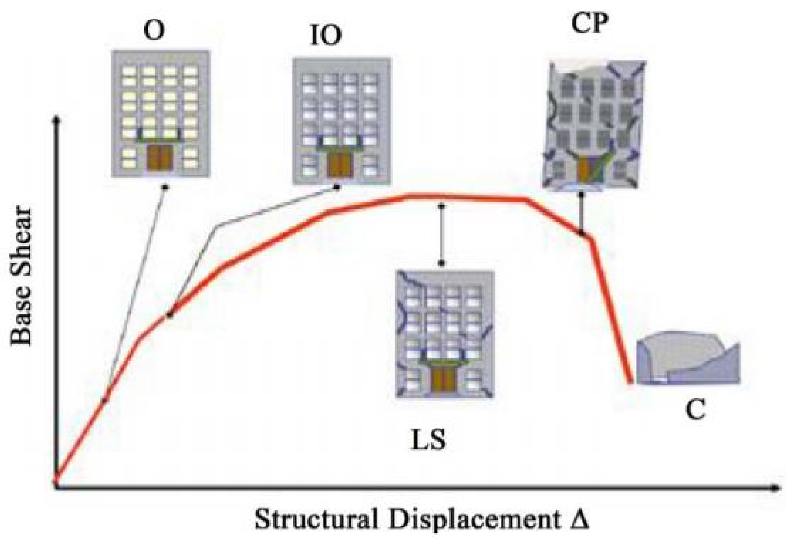

Figure 2-11. Graphical representation of the performance levels according to FEMA 365.

Table C1-2	*Damage Control and Building Performance Levels*			
	Target Building Performance Levels			
	Collapse Prevention Level (5-E)	**Life Safety Level (3-C)**	**Immediate Occupancy Level (1-B)**	**Operational Level (1-A)**
Overall Damage	Severe	Moderate	Light	Very Light
General	Little residual stiffness and strength, but load-bearing columns and walls function. Large permanent drifts. Some exits blocked. Infills and unbraced parapets failed or at incipient failure. Building is near collapse.	Some residual strength and stiffness left in all stories. Gravity-load-bearing elements function. No out-of-plane failure of walls or tipping of parapets. Some permanent drift. Damage to partitions. Building may be beyond economical repair.	No permanent drift. Structure substantially retains original strength and stiffness. Minor cracking of facades, partitions, and ceilings as well as structural elements. Elevators can be restarted. Fire protection operable.	No permanent drift. Structure substantially retains original strength and stiffness. Minor cracking of facades, partitions, and ceilings as well as structural elements. All systems important to normal operation are functional.
Nonstructural components	Extensive damage.	Falling hazards mitigated but many architectural, mechanical, and electrical systems are damaged.	Equipment and contents are generally secure, but may not operate due to mechanical failure or lack of utilities.	Negligible damage occurs. Power and other utilities are available, possibly from standby sources.

Figure 2-12. FEMA 356 performance levels.

Analog performance levels are described in other seismic codes, for example the *"Eurocode 8: Design of structures for earthquake resistance"* (EC 8) or the Italian *"Norme tecniche per le costruzioni"* (NTC).

Target displacement associated with a performance level can be reach only if the structure has a ductile behavior and for this reason, one of the practical applications of the PBSD is the *Capacity Design*. Through this set of design rules, it is possible to program the structural response of the building and to localize the formation of plastic hinges in specific points of the structure, favoring the ductile behavior of the whole building.

The damage control on which the PBSD is based can be achieved introducing nonlinear analysis into the seismic design methodology. The most appropriate approach is combining the nonlinear static (pushover) analysis with the response spectrum approach finding the so-called *performance point* that correspond to the expected state of the structure under the considered earthquake. One of the most used method is the capacity spectrum method that is based on the comparison of the capacity curve obtained from the pushover analysis with the demand curve of the earthquake expressed in form of a design spectrum. The two curves are plotted in the spectral acceleration vs spectral displacement domain.

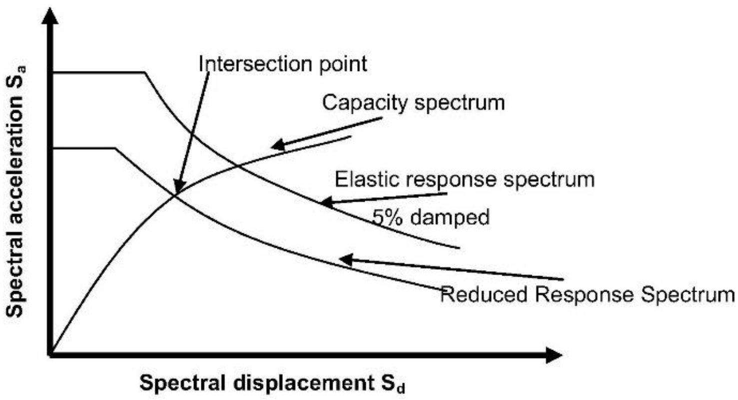

Figure 2-13. Capacity spectrum method.

The intersection of the capacity spectrum with the demand spectrum is the performance point.

The seismic upgrading of an existing RC building, that is the aim of this thesis, has been performed in such a way, following the PBSD philosophy through the N2 method developed by *P. Fajfar* (1999) that is a variant of the capacity spectrum method based on inelastic spectra.

Chapter 3

3 Seismic response control systems

3.1 Earthquake protective systems

Earthquake protective systems were first proposed about a century ago but have been used in designing or retrofitting structures only in the last decades. The aim of these devices is to prevent or divert a portion of the seismic energy from entering into the main structure in order to minimize the structural and nonstructural damages. There are three types of seismic control systems:

- *Passive seismic control*. These protective systems works reducing the input energy or increasing the dissipated energy. The earthquake input motion, without any additional energy source, activates them.
- *Active seismic control*. These systems provide seismic protection imposing forces that counterbalance the earthquake induced actions. They requires an energy source, motion sensors and a computerized control to work.
- *Hybrid seismic control*. It is a combination of passive and active control that requires less energy and costs compared to full active systems.

The adjective "passive" emphasizes the fact that these techniques reduce the seismic response of the structure without adapting interactively to the earthquake, as it happens instead in the case of "active" devices, through the application of actions that counteract the inertia forces. Passive systems are the best known and the most used even if in some countries code provisions are very onerous and causes a strong disincentive to their use.

The seismic retrofitting of a building located in L'Aquila, which is the aim of this thesis, has been done using BRBs that belong to the passive control category.

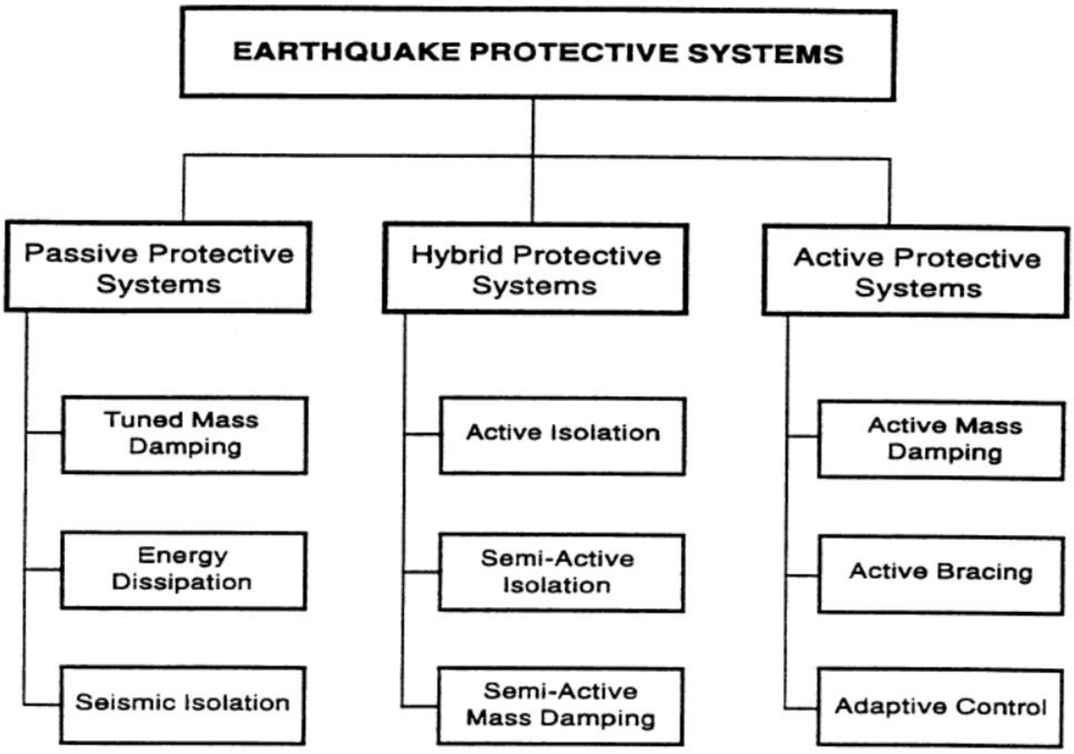

Figure 3-1. Earthquake protective systems.

3.2 Passive seismic control techniques

The control of the structural response through passive protective systems can be use both for retrofitting existing structures and for designing new ones as an alternative to the conventional design methods. In this way it is possible to obtain structures that are able to satisfy the performance objectives required by the performance based seismic design.

Passive control systems include:

- Seismic base isolation;
- Energy dissipation devices;
- Tuned mass dampers.

Each one of them works in a different way, modifying the terms of the of the energy balance equation.

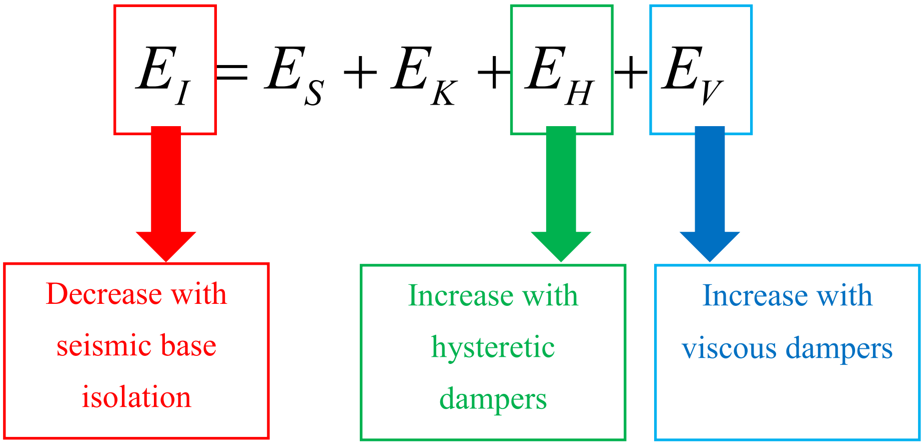

3.2.1 Seismic base isolation

Base isolation is one of the most popular way to protect a structure against earthquake actions. Seismic isolators are devices characterized by a high axial stiffness (in vertical direction) and a low lateral stiffness (in horizontal direction) that are placed under the structure, isolating it from the shaking ground. The basic principle of seismic base isolation is to increase the natural time period of the structure thanks to the lower stiffness of the isolators, reducing the pseudo-acceleration and consequently the earthquake-induced force but increasing the deformation of the isolation system.

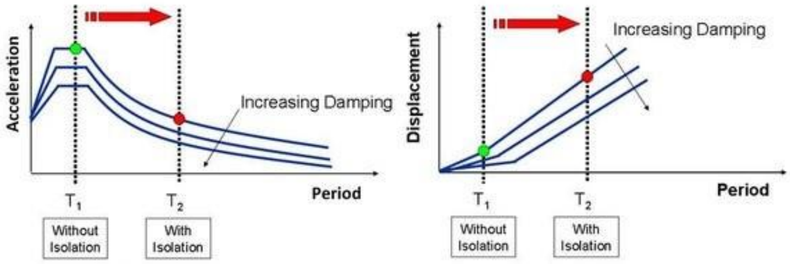

Figure 3-2. Influence of the base isolation.

The most common isolators are elastomeric devices made of rubber with reinforcing steel plate that increase the axial stiffness, called high dumping rubber bearing (HDR). These devices provides also a certain damping thanks to the hysteretic cycles developed by the material. The natural damping of the only rubber is quite low so additional damping is provided by the introduction of a plumb core that increase the energy dissipation through yielding.

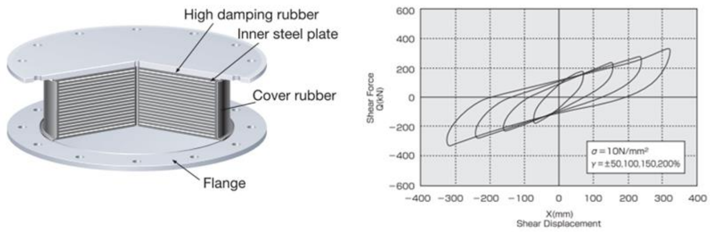

Figure 3-3. Typical HDR isolator and its hysteretic behavior.

Another important typology of seismic isolators are the friction pendulum (FP) bearings. These devices permits the supported structure to moves with small pendulum motions thanks to their concave shape and provides energy dissipation by friction.

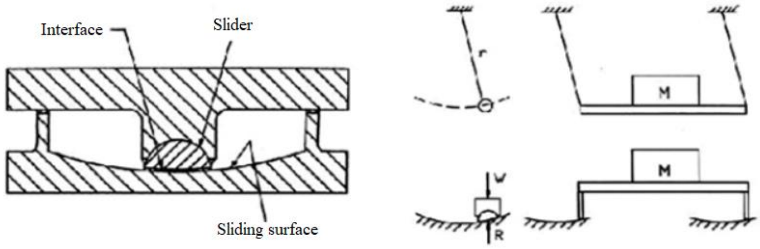

Figure 3-4. Friction pendulum bearing.

3.2.2 Energy dissipation devices

Energy dissipation devices are mechanical systems, incorporated within the structural frame of the building, designed to dissipate a portion of the earthquake input energy converting it into thermal energy. The seismic input energy is the same of the structure without the protective system, unlike the seismic isolation that reduces the energy entering the system, but it is dissipated through the yielding or the deformation of particular devices instead of the structure. In this way, it is possible to avoid an excessive damage on the structural frame after an earthquake reducing the seismic demand. The effect of this type of devices can be seen as an increasing of the damping ratio ζ that lowers the response spectrum both in accelerations and in displacements, leaving the natural period of the bare frame unchanged.

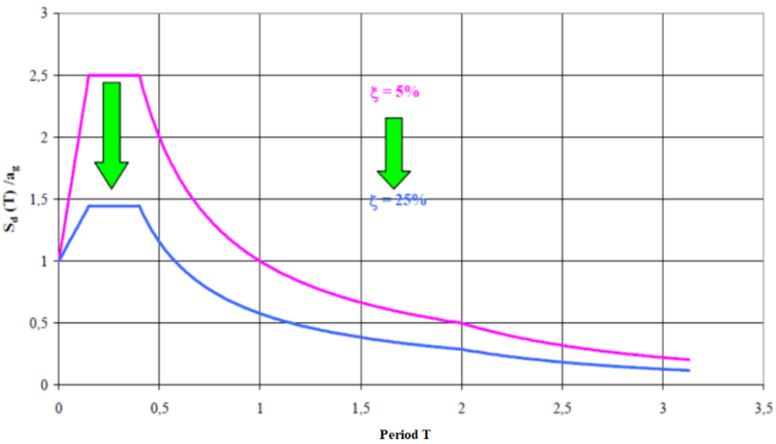

Figure 3-5. Influence of the damping on the elastic design spectrum.

These dampers increase also the strength and the stiffness of the coupled structure shifting the natural period towards lower values and increasing consequently the spectral acceleration and the inertial forces. For this reason, it is necessary to design accurately the distribution of the braces and their geometry in order to obtain the desired behavior of the structure, avoiding excessive concentration of stiffness.

Numerous passive energy dissipation devices are available and they are classified in two main categories:

- *Rate-dependent devices.* The resisting force depends on the rate of change of displacement (the relative velocity) along the damper. Their behavior is described using viscoelasticity models. Viscoelastic fluids dampers usually have a very low stiffness in the range of frequencies that includes the natural frequency of the structure and for this reason they do not change the fundamental period of the system, unlike viscoelastic solid dampers that exhibit a certain stiffness that affects the response of the structure.

- *Rate-independent devices*. The resisting force does not depend on the rate of change of displacement along the damper but only on the magnitude of the displacement. Their behavior is described using nonlinear hysteretic models. Example of these devices are the metallic and friction dampers and they both increase the stiffness of the coupled system.

Table 1

	Viscous Fluid Damper	**Viscoelastic Solid Damper**	**Metallic Damper**	**Friction Damper**
Basic Construction			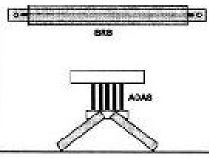	
Idealized Hysteretic Behavior	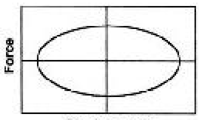	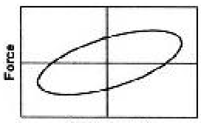	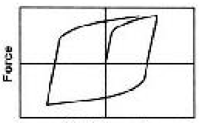	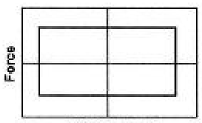
Idealized Physical Model	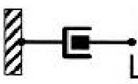	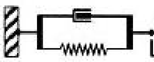		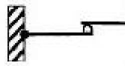
Advantages	- Activated at low displacements - Minimal restoring force - For linear damper, modeling of damper is simplified. - Properties largely frequency and temperature-independent - Proven record of performance in military applications	- Activated at low displacements - Provides restoring force - Linear behavior, therefore simplified modeling of damper	- Stable hysteretic behavior - Long-term reliability - Insensitivity to ambient temperature - Materials and behavior familiar to practicing engineers	- Large energy dissipation per cycle - Insensitivity to ambient temperature
Disadvantages	- Possible fluid seal leakage (reliability concern)	- Limited deformation capacity - Properties are frequency and temperature-dependent - Possible debonding and tearing of VE material (reliability concern)	- Device damaged after earthquake; may require replacement - Nonlinear behavior; may require nonlinear analysis	- Sliding interface conditions may change with time (reliability concern) - Strongly nonlinear behavior; may excite higher modes and require nonlinear analysis - Permanent displacements if no restoring force mechanism provided

Viscous fluid dampers

These dampers are composed by a hollow cylinder filled with fluid and a piston. As the piston head is pushed into the cylinder the fluid is forced to flow through holes placed on the piston head generating differential pressure that produce high resisting forces. The friction between the fluid particles and the piston head provides energy dissipation in form of heat.

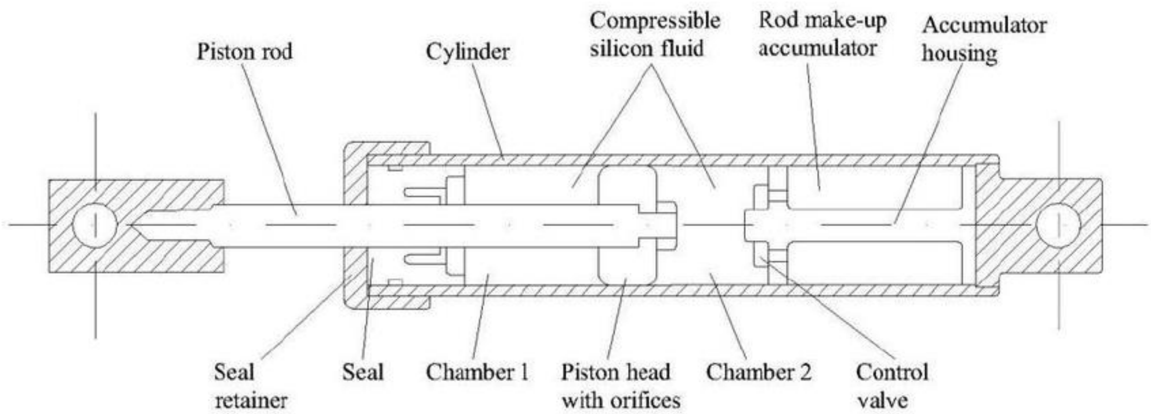

Figure 3-6. Viscous fluid damper.

Maxwell's model that consists in a damper placed in series with a spring describes the behavior of these devices.

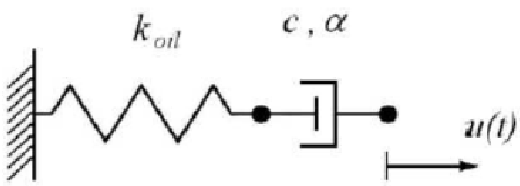

Figure 3-7. Maxwell's model.

The following constitutive law characterizes the damper:

$$F = cv^{\alpha} \tag{3.2.1}$$

where c is the damping coefficient, v is the relative velocity and α a coefficient that depends on the piston geometry. The stiffness of the spring k_{oil} depends on the geometry and on the compressibility of the fluid.

Figure 3-8 shows the force-velocity relation of a viscous damper for different values of the coefficient α.

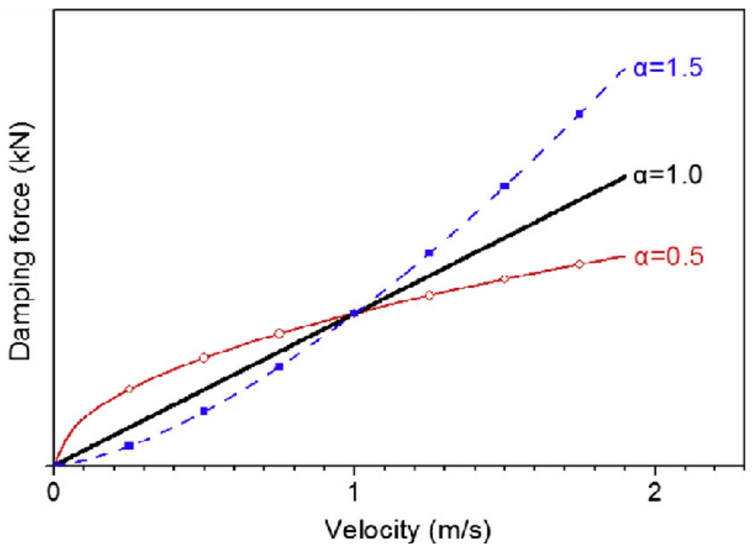

Figure 3-8. Force-velocity viscous damper relationship.

Viscoelastic solid dampers

Viscoelastic solid dampers consists of a solid elastomeric layer placed between steel plates attached to the structure through diagonal braces. The relative displacement between the steel plates causes a shear deformation of the viscoelastic material that dissipates energy developing heat.

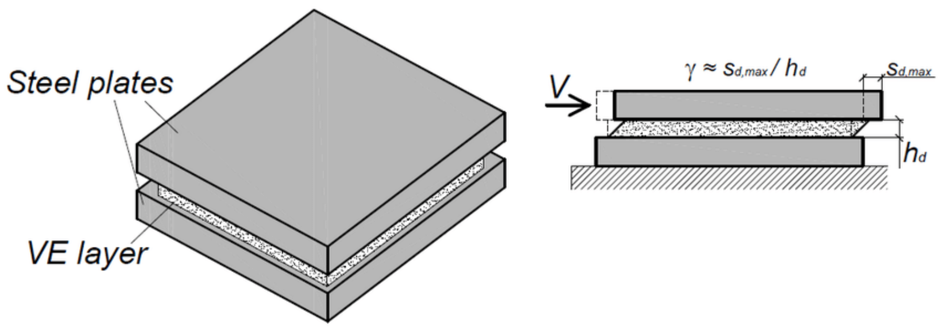

Figure 3-9. Viscoelastic solid damper.

Voigt’s model that consists in a spring placed in parallel with a viscous dashpot describes the behavior of viscoelastic solid dampers.

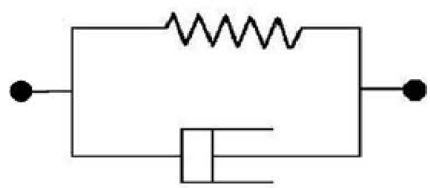

Figure 3-10. Voigt’s model.

The constitutive law of the damper is

$$F = ku + cv \tag{3.2.2}$$

Where k is the stiffness of the damper, u the relative displacement between the plates, c the damping coefficient and v the velocity.

Friction dampers

These dampers dissipates energy through friction developed between the interfaces of two steel plates. One common configuration, known as Pall cross-bracing friction damper (*Pall and Marsh* 1982), consist of cross bracing connected in the center to a rectangular damper as can be seen in Figure 3-11. Under lateral loads two braces goes in compression, two in tension and the rectangular damper deform into a parallelogram dissipating energy through friction at the bolted joints.

The constitutive law of this type of damper is described by Coulomb’s friction model

$$F = \mu N \tag{3.2.3}$$

Where μ is the coefficient of dynamic friction and N the normal force at the sliding interface.

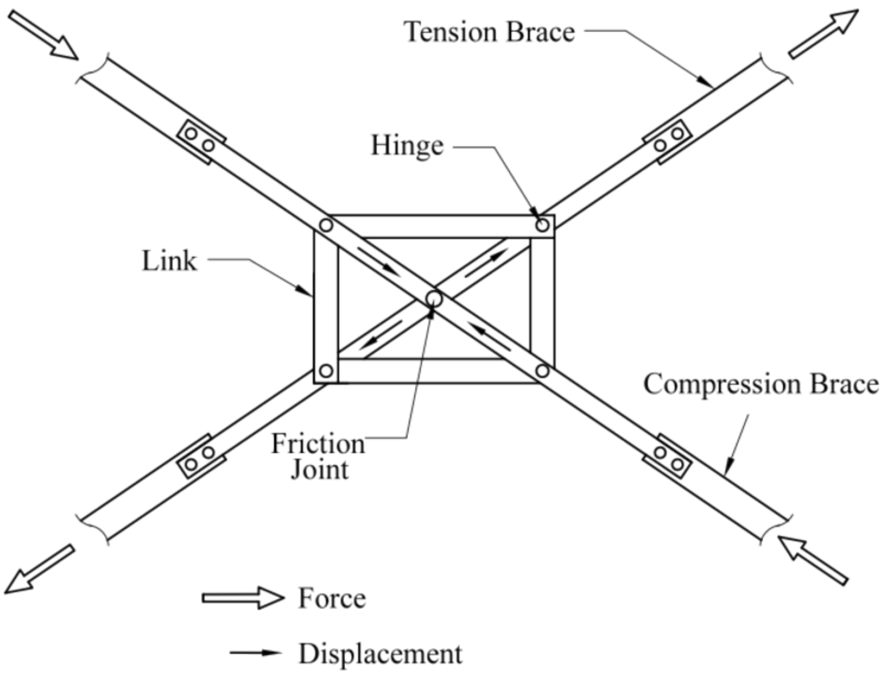

Figure 3-11. Pall cross-bracing friction damper.

Metallic dampers

The most common typology of metallic dampers are the buckling restrained braces (BRBs). These steel braces are composed by a steel core placed inside a steel tube filled with a concrete-like material. The confinement provided by the concrete prevent the buckling of the steel core in compression so the damper can yield both in tension and in compression with similar behavior. The energy induced in the structure by the earthquake is dissipated thanks to inelastic behavior of the core material that produces a large hysteretic loop.

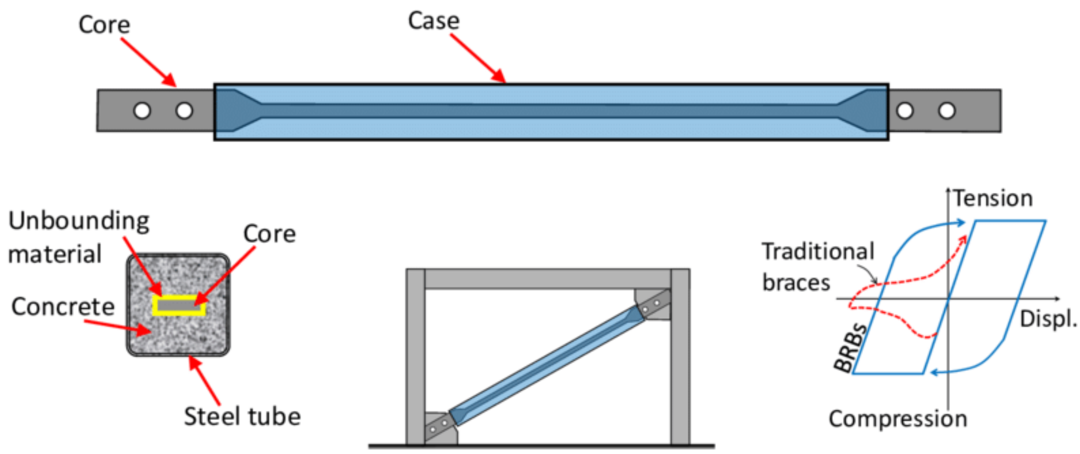

Figure 3-12. Typical BRB composition, section, disposition and tension displacement law.

Various mathematical models can describe the hysteretic behavior of BRBs. One of the most known is the Bouc-Wen model (Wen 1976) but more sophisticated constitutive models have been developed in the last years taking into account all the particularities of the BRBs' behavior. The BRBs system designed for retrofitting the existing RC building located in L'Aquila in the study case of this thesis has been modelled in Opensees using the elastoplastic model developed by *Zona and Dall'Asta* (2011). This model is described in details in chapter 4.

Another typology of metallic dampers are the added damping an stiffness (ADAS), consisting in a series of steel plates placed between the top of a chevron bracing system and the floor level. The floor level displaces laterally respect to the chevron bracing inducing shear forces and bending moments into the steel plates. The geometry of the plates is such to have a uniform flexural stress distribution over the height of the plate and so uniformly distributed inelastic action. The hysteretic behavior is similar to that of a BRB damper.

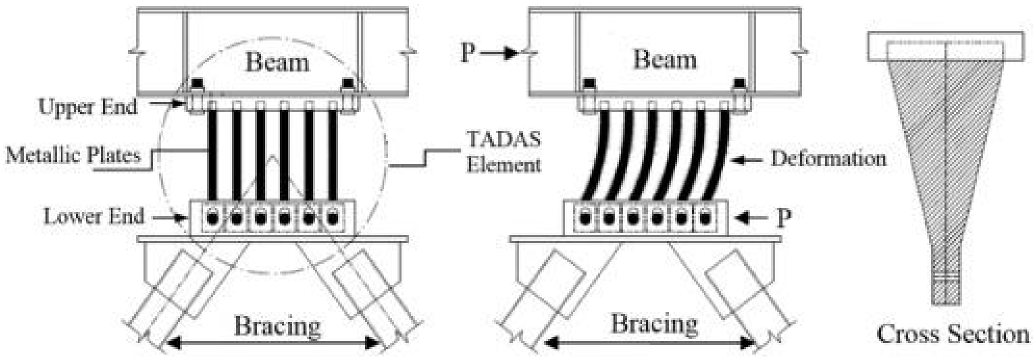

Figure 3-13. Typical ADAS damper.

Chapter 4

4 Energy dissipation through hysteretic devices (buckling restrained braces)

4.1 Influence of hysteretic cycles on the energy dissipation

As seen in chapter 3 the input energy generated from the shaking ground is dissipated both by yielding and viscous damping. The terms of the energy balance equation can be obtained integrating the equation of motion of an inelastic SDOF system

$$\int_0^u m\ddot{u}(t)du + \int_0^u c\dot{u}(t)\,du + \int_0^u f_s(u,\dot{u})du = -\int_0^u m\ddot{u}_g(t)\,du \tag{4.1.1}$$

The right side represent the total input energy

$$E_I = -\int_0^u m\ddot{u}_g(t)\,du \tag{4.1.2}$$

While the terms on the left side represent the energy absorbed by the structure and dissipated. The first integral of eq.(4.1.1) is the kinetic energy of the mass associated with its relative motion

$$E_K(t) = \int_0^u m\ddot{u}(t)du = \frac{m\dot{u}^2}{2} \tag{4.1.3}$$

The second term is the energy dissipated by viscous damping

$$E_D = \int_0^u c\dot{u}(t)\,du \tag{4.1.4}$$

The third term is the sum of the strain energy

$$E_S(t) = \frac{\left[f_S(t)\right]^2}{2k} \tag{4.1.5}$$

and the energy dissipated through the hysteretic cycles

$$E_H = \int_0^u f_s(u,\dot{u})du - E_S \tag{4.1.6}$$

The eq.(4.1.1) becomes

$$E_I(t) = E_K(t) + E_D(t) + E_S(t) + E_H(t) \tag{4.1.7}$$

In Chopra (1995) *Dynamics of structures* the results of a test performed on two SDF systems subjected to a ground motion recorded in El Centro (California) during the Imperial Valley earthquake of May 18 1940 are shown. The firs SDF system is linearly elastic with natural period $T = 0.5$ and damping ratio $\zeta = 0.05$ while the second is elastoplastic with the same elastic properties and a normalized yield strength $\bar{f}_y = 0.25$. The effect of the yielding and so of the hysteretic cycles is evident looking at the time variation of the dissipated energy.

In both cases, the structure dissipates the input energy but in the elastoplastic system, the energy dissipated by viscous damping is smaller than the elastic system thanks to the presence of the hysteretic loops provided by yielding.

The presence of yielding, or hysteretic, energy indicates a demand on the structure that causes damages and permanent deformations. The aim of adding energy dissipation devices to new or existing structures is to dissipate a consistent part of the earthquake-induced energy through their plasticization, reducing the contribution of the main structure and so limiting structural and nonstructural damages. This solution permits to avoid the evacuation of the building and so business interruption involving lower repair costs, even if it is necessary to substitute these devices after a severe earthquake.

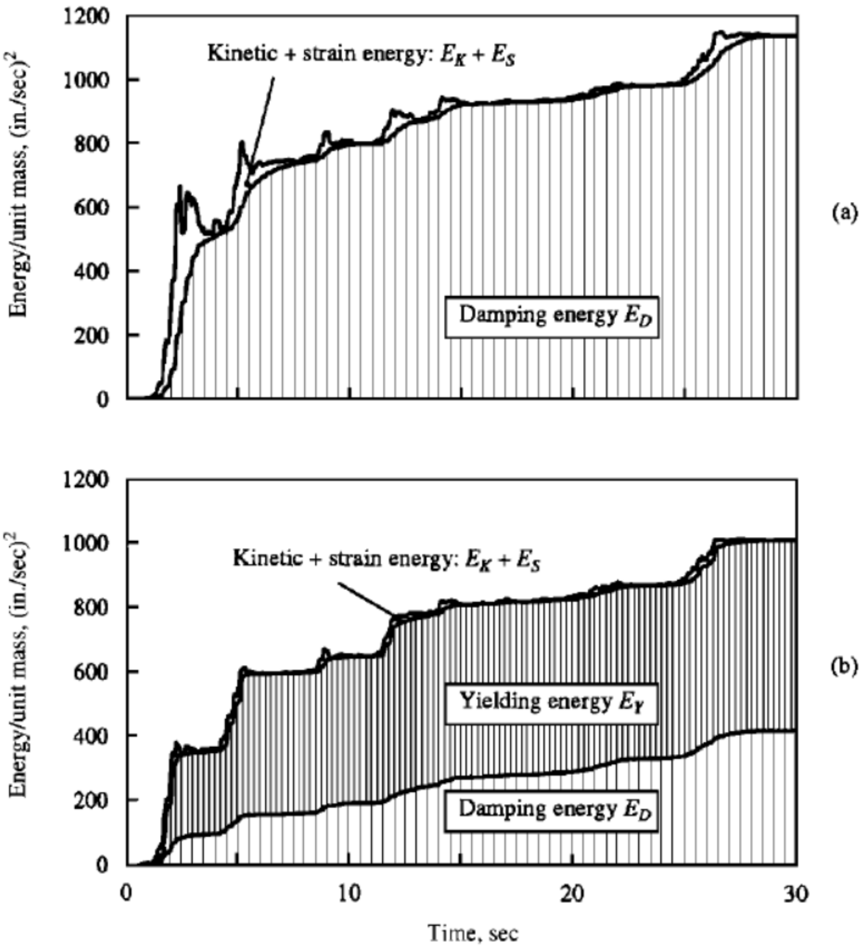

Figure 4-1. Time variation of energy dissipated by viscous damping and yielding, and of kinetic plus strain energy for a linear system (a) and an elastoplastic system (b).

4.2 Buckling restrained Braces (BRBs)

The L'Aquila earthquake (M_w=6.3) of April 6 2009 that affected the central regions of Italy highlighted that numerous RC existing building designed to resist only to gravity load located in areas with high seismic hazard do not have a proper behavior under lateral loads, exhibiting low lateral stiffness, strength or ductility. This problem has made necessary to develop some retrofitting strategies that are able to improve the performance of the structures without excessive costs. Numerous experimental tests and numerical simulations have shown that one some the best solutions for retrofitting or upgrading multi-storey framed RC existing building are dissipative unbounded or buckling restrained braces (*Di Sarno et al., 2009).*

The most used structural systems in seismic regions are moment frame and braced frame. Compared to a moment frame a braced frame offers a higher stiffness for lateral drift control but it is affected by the buckling of the compressed brace that decrease the capacity of dissipate energy. For this reason, in the past years an alternative solution to the conventional concentric braced frame has been developed. Buckling restrained braces (BRBs) are hysteretic dampers that differ from normal concentric steel braces because the they can yield both in tension and compression without being affected by buckling. This typology of dissipative devices has been developed recently, in fact the first attempts to create a brace that can show plastic deformation also in compression without buckling started during the 80's in Japan (*Watanabe et al., 1988*), leading to the first implementation in a building in 1988. This technology was transferred to the US at the end of the 90's and applied to the seismic rehabilitation of RC building (*Brown et al., 2001; Tremblay et al., 1999).*

Figure 4-2. Retrofitting of Wallace F. Bennett Federal Building Salt Lake City by means of BRB (Brown 2001).

The comparison between the behavior of a BRB and a conventional brace is evident looking at Figure 4-3 and Figure 4-4.Figure 4-3. Behavior of a conventional brace and a BRB under lateral loads.

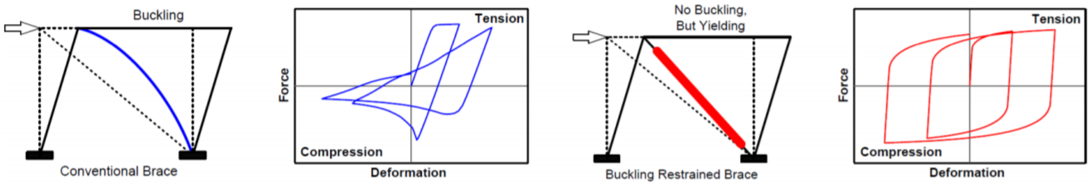

Figure 4-3. Behavior of a conventional brace and a BRB under lateral loads.

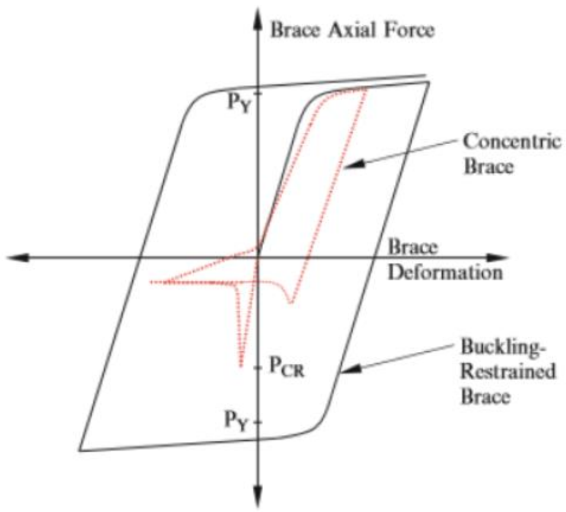

Figure 4-4. Comparison between the force-deformation relationship of a BRB and a concentric brace.

A BRB has a stable force-deformation law during tension and compression cycles while a concentric brace shows an instable behavior in compression caused by buckling. After the buckling, the brace loses its strength and it is no more able to provide stiffness to the frame. Moreover low compression cycle capacity leads to a lower energy dissipation compared to a BRB because the hysteretic loop is smaller.

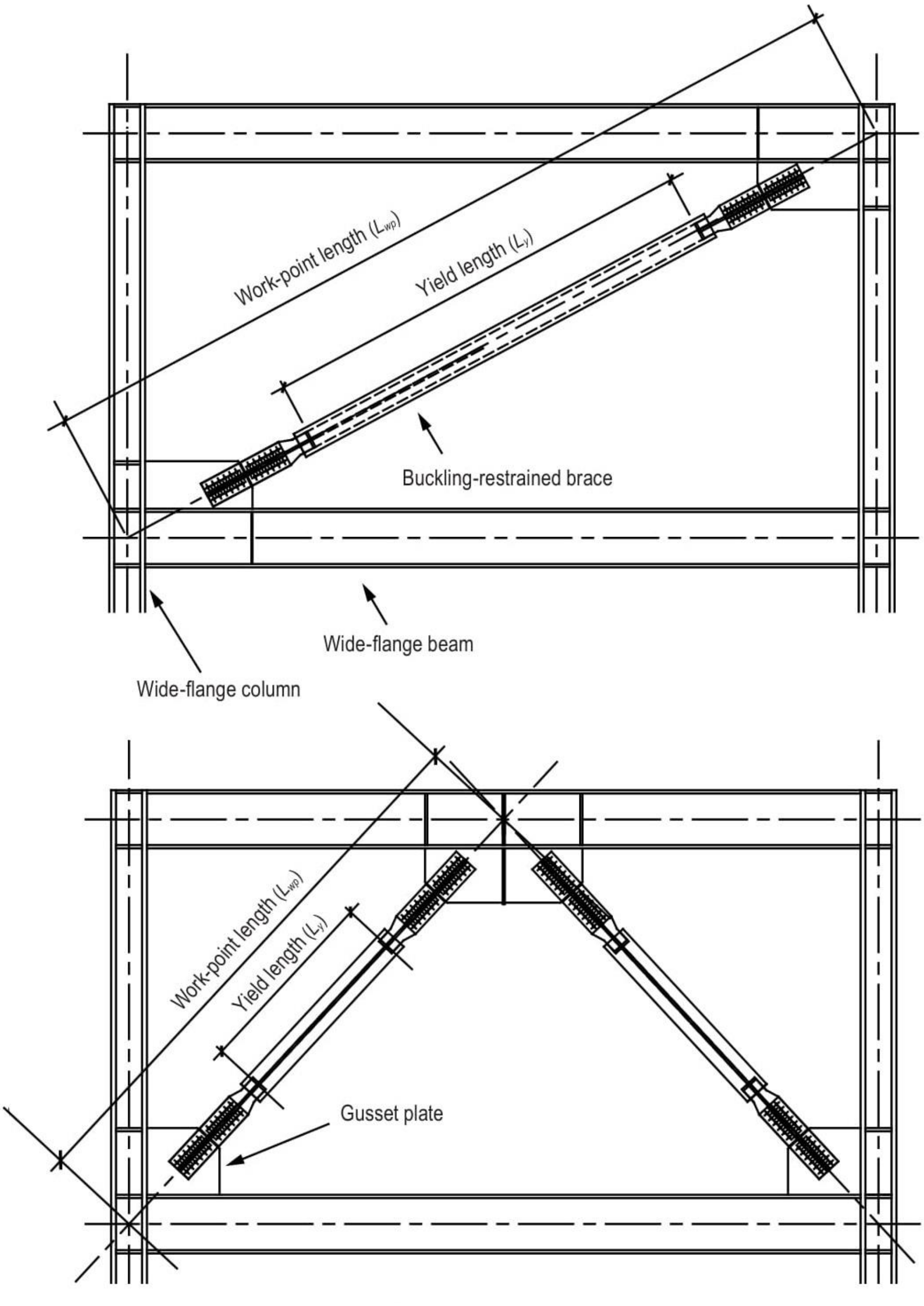

Figure 4-5. Typical BRB configurations in a steel frame.

4.2.1 Composition and characteristics of a BRB

A buckling restrained brace is composed of a ductile steel core that can yield both in tension and compression placed inside a steel chasing filled with mortar or concrete that is necessary to prevent the buckling of the core. Between the steel core and the mortar is placed an unbounding material or a small gap to prevent the transfer of the axial force and to permit the lateral expansion of the steel core in compression due Poisson effect.

The components of a BRB are:

- *Restrained yielding segment*. It is the core of the BRB, with rectangular or cruciform cross section. It is supposed to yield both in tension and compression under cyclic loads and for this reason it is better to use mild steel with high ductility.
- *Restrained nonyielding segment*. An extension of the yielding segment with a larger section in order to remain in elastic field. It is surrounded by mortar as the core.
- *Unrestrained nonyielding segment*. An extension of the restrained nonyielding segment that comes out from the casing and it connects the brace to the frame.

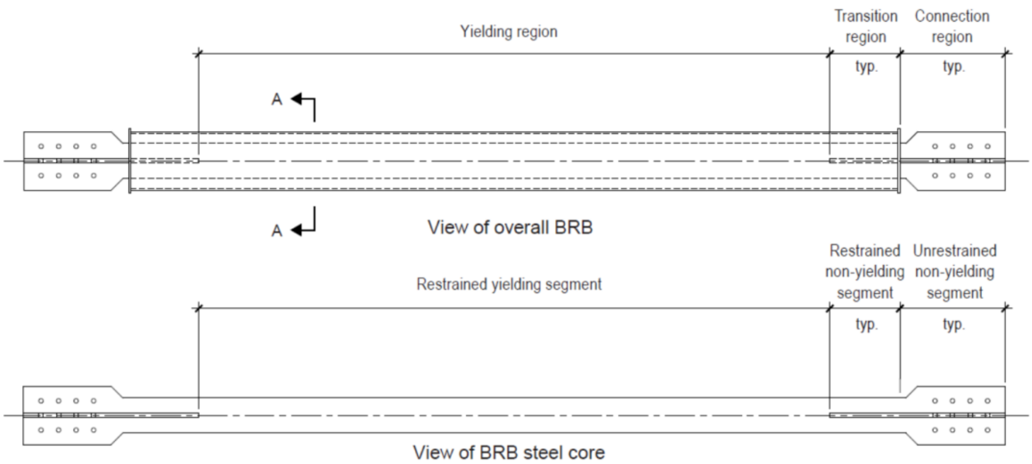

Figure 4-6. Common BRB assembly.

- *Unbounding material.* A special material necessary to minimize or eliminate the transfer of shear force between the steel core and the mortar in order to avoid the rise of axial forces on the buckling restrain mechanism. Sometimes this layer of unbounding material is absent and the friction is avoided thanks to a small gap that needs to be sufficiently large to allow the expansion of the steel core in compression but not too large to avoid an excessive curvature of the buckled segment.

- *Buckling restraining mechanism.* This part of the BRB is composed of mortar and a steel casing and prevent the buckling of the core.

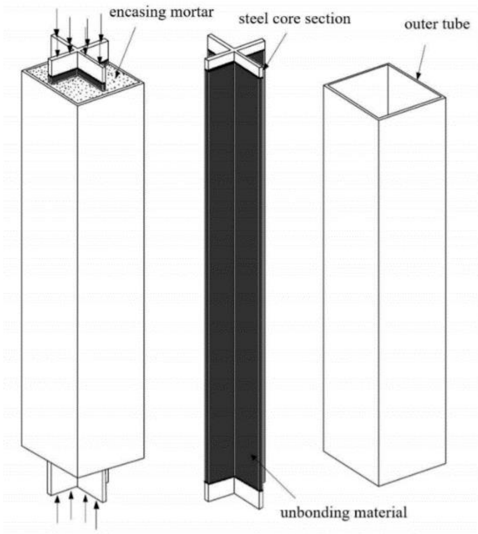

Figure 4-7. Typical unbounded BRB.

The strength and the stiffness of the BRB depends on the lengths and the sections of the three segment that compose the brace.

$$K_e = \frac{EA_y A_t A_c}{A_t A_c L_y + 2A_y A_c L_t + 2A_y A_t L_c} \tag{4.2.1}$$

where A_y , A_t , A_c and L_y , L_t , L_c are the cross sections and lengths respectively of the yielding segment, restrained non-yielding segment and unrestrained non-yielding segment.

The steel chasing should not resist to any significant axial load but is designed with a sufficient flexural stiffness in order to avoid buckling using the criterion suggested by *Watanabe et al.* (1988)

$$\frac{P_e}{P_y} \geq 1.0 \tag{4.2.2}$$

where $P_e = \pi^2 EI_{sc} / L_{sc}$ is the elastic buckling strength of the chasing and P_y the yield strength of the restrained yielding segment. Knowing the work-point length L_{sc} is possible to obtain the moment of inertia of the steel chasing and so defining the geometry. The effect of the mortar increase the flexural stiffness (*Chen et al.* 2001) but it is conservatively neglected. *Watanabe et al.* (1988) also suggest taking into account the effect of cyclic strain hardening that increase the compressive strength of the diagonal by 30% and adding a safety factor in the numerator the eq.(4.2.2) becomes

$$\frac{0.9P_e}{1.3P_y} \geq 1 \Rightarrow \frac{P_e}{P_y} \geq 1.5 \tag{4.2.3}$$

According to numerous experimental tests BRB exhibit stable hysteretic behavior and so an high energy dissipation capacity. *Iwata et al.* (2000) performed experimental tests on four types of specimens with different restraining mechanism. Three of them (1, 2 and 3) had the same core plate and yield stress of 262.6 N/mm^2 while the fourth had a different geometry of the core and a yield stress of 289.1 N/mm^2.

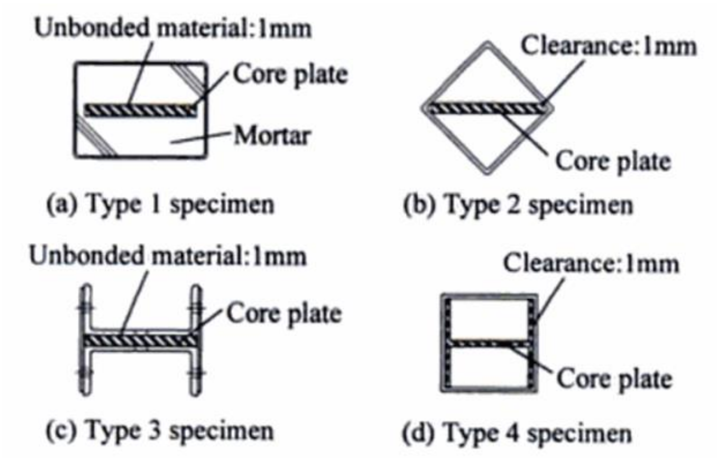

Figure 4-8. Sections of the four specimen tested by Iwata et al. (2000).

The tests were performed applying increasing deformations in tension and compression reaching pre-established levels of strain until 3%. Each load after yielding was applied twice in order to determine the stability of the loop and after the reaching of the 3% strain the test continued with the same maximum deformation until the failure of the specimen. The results are shown in Figure 4-9.

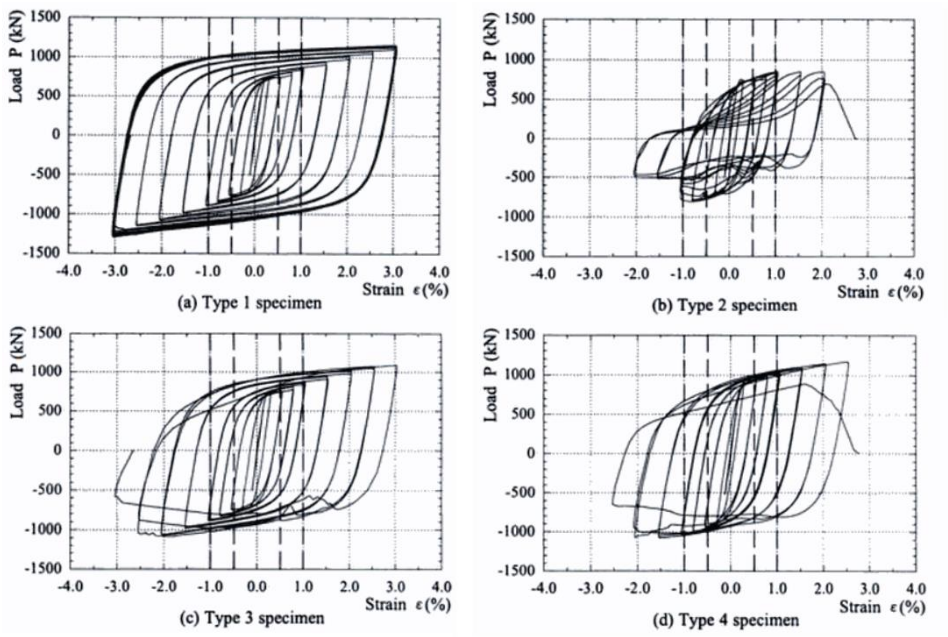

Figure 4-9.Results of the tests performed by Iwata et al. (2000).

Specimen 2 and 4 does not perform as expected because of the absence of the mortar that prevent buckling while specimen 3 failed because the restraining effect was lower than the mortar. The only specimen that showed very stable hysteretic cycles until 3% of strain, which corresponds to a ductility ratio of 24 was the number 1.

Black et al. (2002) obtained similar results performing tests on BRBs applying a relative displacement derived from the inter-story drift of an idealized five-story building. The buckling restrained braces had a yield stress of 280 N/mm^2 and behaved stably a 3% inter-story drift reaching a ductility ratio of 20.

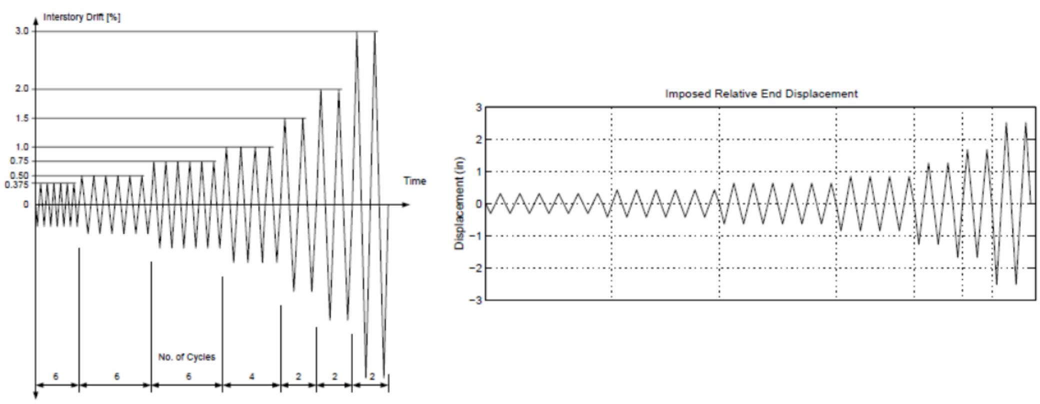

Figure 4-10. Loading history used for spring 1999 test specimens (Black et al. 1999)

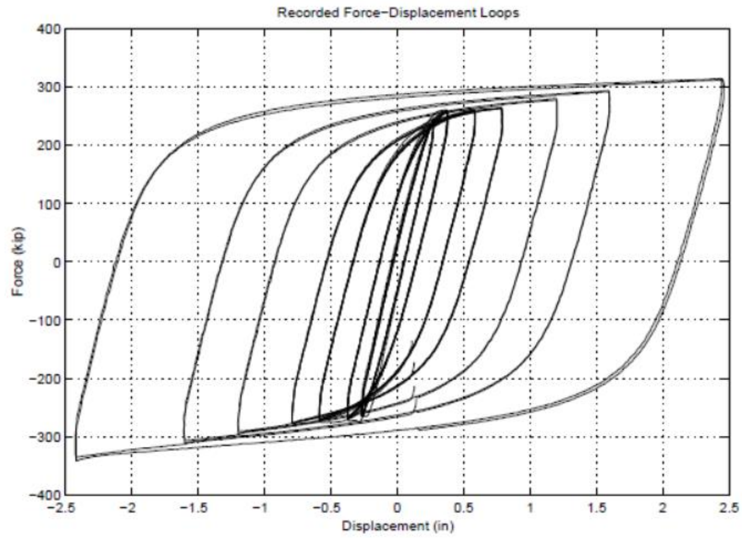

Figure 4-11. Recorded force-displacement loops under loading history (Black et al. 1999).

Higher ductility ratio are also possible, in fact *Yamaguhci et al.* (2000) carried out experiments on low-strength steel BRB (F_y=96 N/mm^2) reaching a maximum ductility of 30. All these tests prove that BRBs have high ductility capacity and stable hysteretic loops and for this reason are suitable for dissipating large amount of energy and so for applications in seismic field.

4.2.2 Advantages and disadvantages of BRB

The advantages of a BRBF respect to a moment resisting frame and a CBF are:

- High elastic lateral stiffness that reduces inter-storeys drifts, especially at low-level seismic input.
- Stable and large hysteretic behavior, avoiding the buckling of the compressed brace, under high-level seismic input.
- Easy connection to the structural system by means of bolted or pinned connection to gusset plate
- Simple modelling of cyclic behavior for nonlinear analysis.
- Design flexibility because strength and stiffness can be chosen inside a wide range and tuned to reach the desired behavior.
- Concentration of the damage on the brace, which can be replaced after the earthquake, rather than on the main structural system.
- Does not require structural members and foundation strengthening.

The disadvantages of this structural system are:

- Lack of recentering mechanism.
- Lack of criteria for detecting and replacing damaged braces.
- Wide range of yield stress of steels commonly used for the core of the BRB and ductility proprieties that are affected by the geometry and the material type of the core.
- Large permanent deformations under high-level seismic action.

4.2.3 Reduced length buckling restrained brace

A classical BRB, as the ones tested and implemented in structures during the first years after the development of this technology, is made of a single dissipative member which length extends between two beam to column joints. The ratio between the length of the yielding core and the total length for a classical BRB goes from 0.5 to 0.8. In the last years, after 2000, several tests have been performed on BRBs with a small length of the yielding segment, that goes from 0.2 to 0.4 the total length of the brace.

Reducing the length of the BRB brings numerous advantages such as simple replaceability, lower weight, easier assembly inside the frame and less costs compared to a normal heavy BRB. This new typology of BRB is called reduced length buckling restrained braces (RLBRB) and it consists in a brace divided into two members placed in series. One is the proper BRB that shows plastic deformations in tension and compression and the other is an over-strengthened brace designed in order to remain into elastic field.

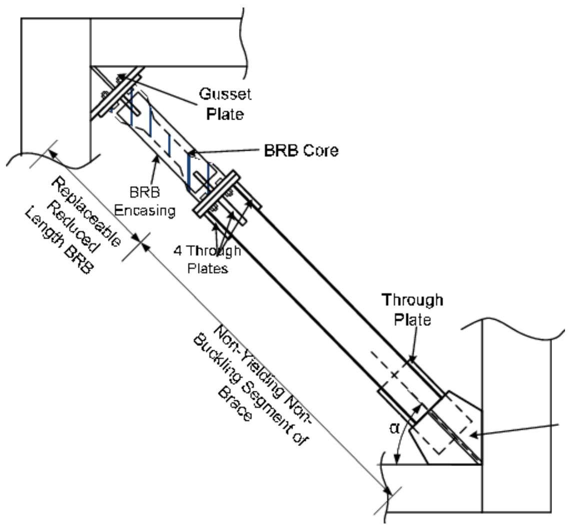

Figure 4-12. Reduced length BRB disposition in a frame.

The strain level for conventional BRB is usually limited to 1-2% as reported in *Razavi et al.* (2011) even if several tests show that the behavior is stable also for higher strain amplitude. The plastic strain of a BRB is inversely proportional to its yielding segment length so reducing the size of core leads to an increase of the ductility capacity of the hysteretic damper.

The reduction of the length of the yielding segment has a benefic effect also on the reduction of the friction force between the core and the restraining mechanism that depends on the contacts point and total length.

RLBRB needs to be checked against global buckling of the brace that derives from the reduction of the encasing length. In fact, as the restrained segment becomes smaller compared to the unrestrained part of the brace the critical load that cause global buckling decrease respect to the buckling load of the classical BRB. Another important effect on the decreasing of the buckling load is given by the position of the weak segment inside the brace. *Mirghaderi et al*. (2008) studied these problems and the results are shown in the following figure.

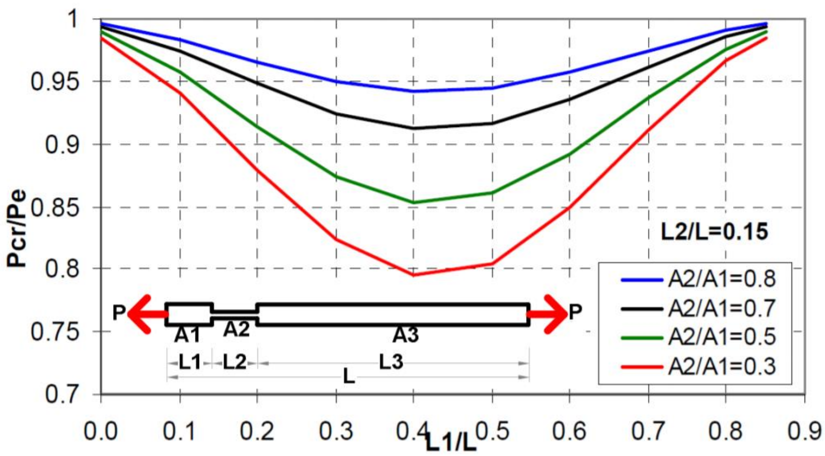

Figure 4-13. Change in critical buckling load (Mirghaderi et al. 2008).

P_e is the buckling load of the original BRB, without the reduced-length core, and P_{cr} is the global buckling load of the RLBRB. If the weak segment is positioned near the center of the diagonal, the decrease of the critical load is maximum. The best choice for the position of the yield core is near the end of the brace because it causes the minimum drop of the buckling load with regard to the original state.

4.3 Seismic retrofitting of reinforced concrete structures with BRB

It is evident from the results of the numerous tests that BRB have a large and stable hysteretic behavior under cyclic loads if they are well designed in order to prevent the buckling of the inner steel core with an appropriate restraining mechanism. For this reason this typology of hysteretic dampers are suitable for applications in seismic design or retrofitting because they absorb and dissipate a large amount of the energy induced in the structure by the earthquake inhibiting the formation of plastic hinges on the structure.

The first applications of BRBs systems regards steel structures, as well as the first laboratory tests performed on steel frames, but they can be applied also in existing RC structure showing the same improvement of the structural response under seismic actions. An example of seismic retrofit of an existing RC structure with no seismic provisions by *Di Sarno* and *Manfredi* (2009) was performed on two sample frames. These frames were realized for investigate through experimental tests and numerical simulations the effectiveness of BRBs as innovative retrofitting strategy.

4.3.1 Experimental tests on retrofitted RC frame

During the experiments, two identical, full-scale multi-storey, RC frames were built and tested. One was tested with no type of additional reinforcement and used as a benchmark system while the other was retrofitted with BRBs.

Figure 4-14. Full-scale sample frames (Di Sarno et al. 2009).

The foundations consist of a 6 by 7m, 50cm thick, shallow RC mat. The structures combine two 2.55m bays in one direction and a single 4.40m bay in the orthogonal direction. The interstorey heights are 3.50m and 3.44m for the first and second floor respectively, resulting in a total height of 7.65m. The beams are 30x50cm deep and the columns have a square section of 30x30cm. The frames were designed with structural deficiencies, typical of the gravity load designed structures, i.e. smooth bars (f_{ym}=330N/mm^2), intermediate concrete compression strength (f_{cm}=19N/mm^2), hooks and stirrups with large spacing.

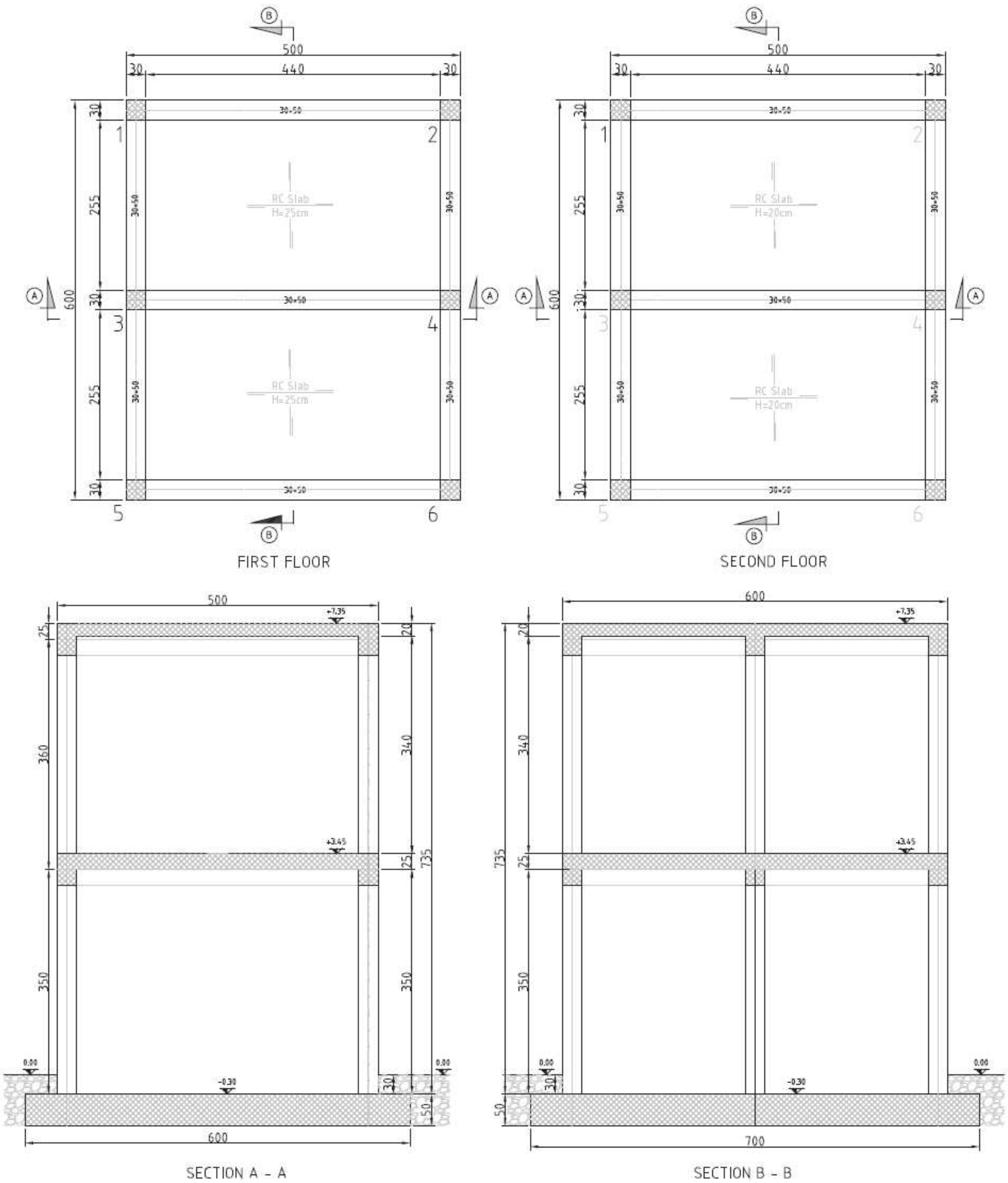

Figure 4-15. Plans and sections of the RC structures used for the tests (Di Sarno et al. 2012).

Two different types of RLBRB were used for the retrofitting, one for the ground floor and one for the first floor. The RLBRB at the ground floor was composed by a yielding segment with a yield force of F_y=75kN and a maximum of $F_{y,max}$=90kN, an elastic stiffness k_{el}=90KN/mm and a maximum displacement d=±15mm, connected to a tubular pipe of diameter 80mm and thickness 7.2mm. The RLBRB at the first floor was composed by a yielding segment with a yield force of F_y=40kN and a maximum of F_{max}=55kN, an elastic stiffness k_{el}=90kN/mm and a maximum displacement d=±14mm, connected to a tubular pipe of diameter 80mm and thickness 7.4mm.

Sensors for vibration measurement, including accelerometers with tolerance of $1x10^{-6}$ g, were applied on the corners of the two floors of the full-scale RC structures in order to collect data at a frequency of 1000Hz for the estimation of the modal shape of the system. The deformation of the steel bars of the foundation, columns and beams was monitored using 61 strain gauges while the deformations of the beam-to-column joints were registered by means of displacement transducers.

The external action were applied to the structure at the two floor level using hydraulic jacks connected to a steel truss used as a reaction which deformation was monitored through displacement transducers.

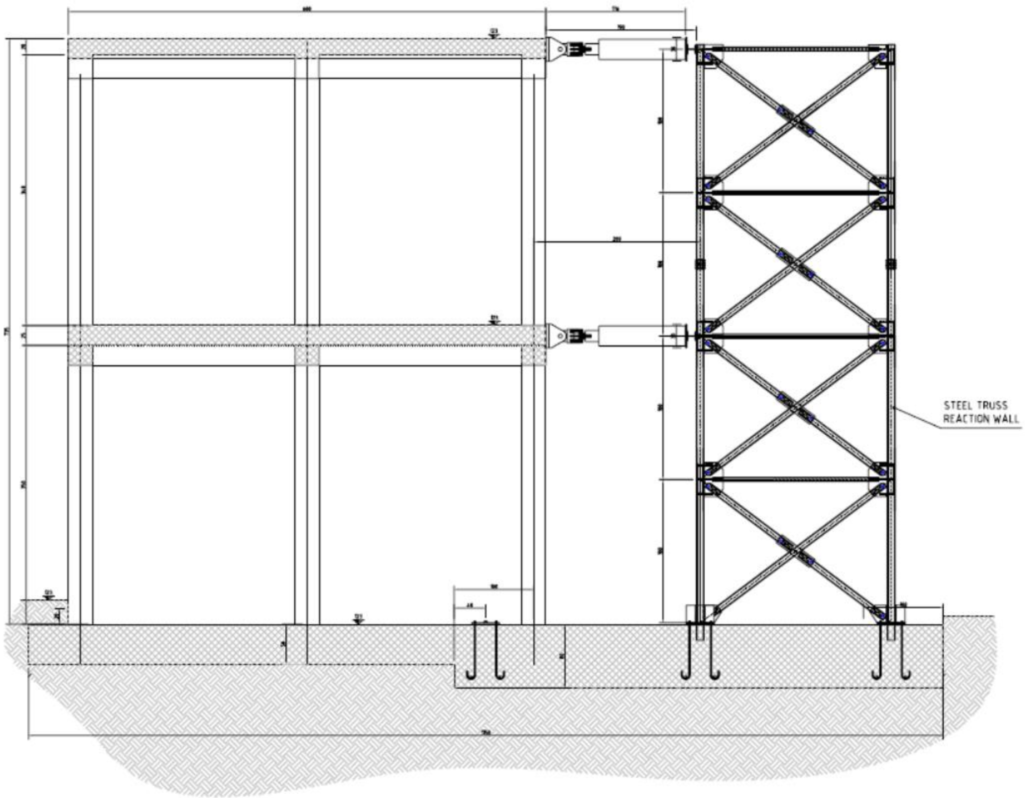

Figure 4-16. Test set up for pushover loading (Di Sarno et al. 2009).

The experiments began with preliminary dynamic tests in order to evaluate the periods of vibration and the equivalent damping of the structures. These tests were performed also after the application of the lateral loads so it was possible to evaluate the stiffness reduction. The period of vibration of the unretrofitted frame before and after the execution of the loading tests are shown in Figure 4-17 and it is evident that the damage of the structure caused an increasing of the periods of all the first six modes of about 50%.

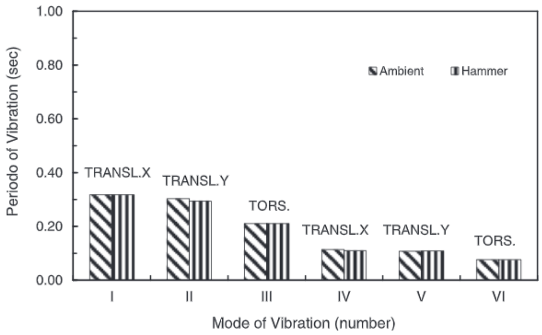

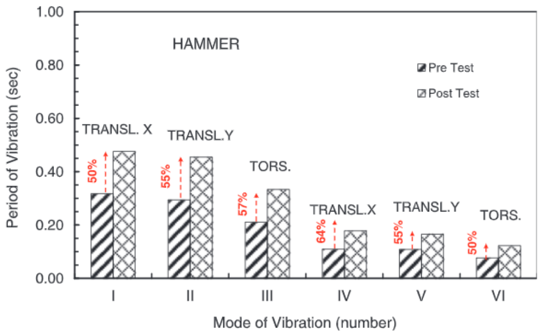

Figure 4-17. Periods of vibration of the unretrofitted frame.

The equivalent viscous damping relative to the fundamental mode was found by means of impulsive (transient) waveforms generated by instrumented impact hammer and using the logarithmic decrement method. Mean value of the damping ratio obtained from the tests is 3% with a standard deviation of 0.2%.

The frames were subjected to monotonic and cyclic incremental lateral loading (pushover) in order to simulate the effect of the forces inducted on the structure by the earthquake.

Under monotonic lateral load pattern the bare frame experienced large inelastic deformations reaching a maximum roof drift of 2.2% (158mm) and a maximum base shear of 123.7kN. At ultimate displacement, the structure was affected by high damages that caused a rapid deterioration of strength and stiffness. These damages were localized at the top and the bottom of the ground floor columns.

Figure 4-18. Damage observed in the bare frame (Di Sarno et al. 2012).

In the retrofitted system BRBs provided energy dissipation saving the structure from the development of significant yielding on the elements. The pushover curve reached an ultimate displacement of 80mm relative to a drift of 1% when the BRB reached the design axial displacement and the total base shear is of 220kN.

The cyclic lateral loading pattern consisted in the application of a reverse loading at 69.5mm (0.95% top drift), 84mm (1.15% top drift) and the maximum 158.5mm (2.16% top drift) roof displacements for the unretrofitted frame. For the retrofitted frame the reverse loads were applied, instead, at 23.4mm (0.32% top drift), 55mm (0.75% top drift) and the maximum displacement of 80mm (1.09% top drift). From the results of the experimental tests is clear that the retrofitted system exhibit a better seismic performance for both serviceability and ultimate limit state because the bare frame remains into the elastic field until the collapse of the system and the energy dissipation is provided by the BRBs instead of the structure. The cyclic response of the two full-scale samples is shown in Figure 4-19.

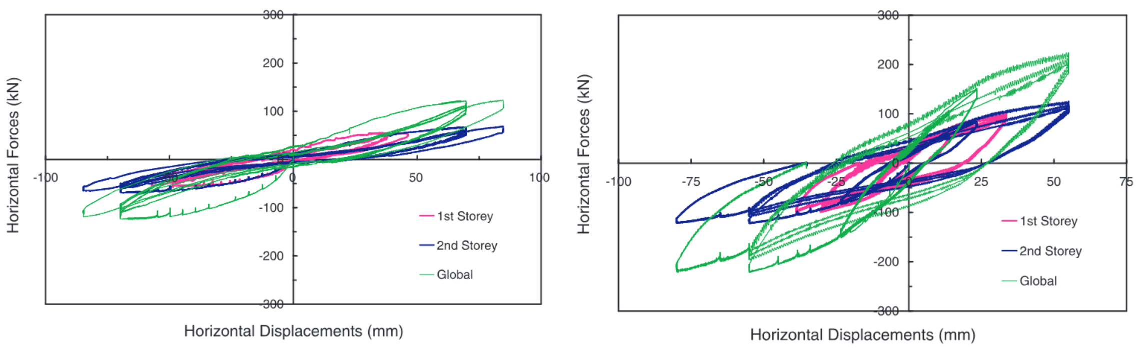

Figure 4-19. Cyclic response of the unretrofitted (left) and retrofitted (right) structure (Di Sarno et al. 2009).

The total energy dissipated by the two frames at the first and the second floor is compared in Figure 4-20 and it is evident the increasing of the hysteretic loops in the retrofitted structure.

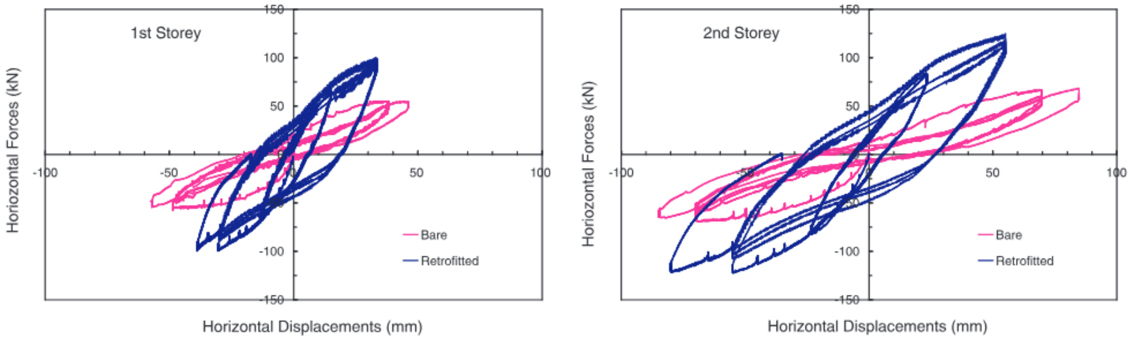

Figure 4-20. Comparison of the hysteretic response at the first (left) and second (right) storey.

4.4 Elastoplastic model for steel buckling restrained braces

The description of the global behavior of a BRB requires the definition of an appropriate model because it does not replicate exactly the behavior of the steel core material. Numerous experimental tests, in fact, pointed out a significant role of isotropic hardening and a tension compression asymmetry due principally to friction between the core and the restraining mechanism that increase the resisting force in compression of 10-15% respect to that in tension. Other important features that an appropriate model for the BRB behavior should have are the possibility to compute explicitly the plastic component of the deformation, necessary for the evaluation of the cumulative plastic ductility (CPD) used for BRB verification according to specific capacity models, and the smoothness of the transition between the elastic and plastic branch.

Various cyclic models have been used through the years to represent the BRB behavior in finite elements models. Some of these are:

- Bilinear elastoplastic models with higher strength in compression than in tension and post yielding stiffness set to 0 or 0.05 the elastic stiffness;
- Trilinear force-deformation model taking into account the effect of isotropic hardening;
- Bouc-Wen smooth law;
- Menegotto-Pinto smooth law with kinematic and isotropic hardening;

Each one of these models has some benefits but none of them is able to provide all the features described before.

A model that addresses all the requirements have been developed by *Zona and Dall'Asta* (2011) and it is based on a rheological scheme consisting of a spring in series with a friction slider in parallel with a second spring as shown in Figure 4-21.

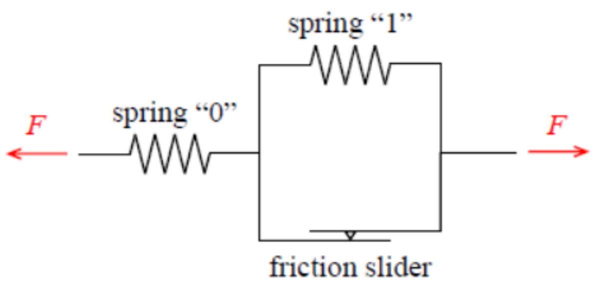

Figure 4-21. Elastoplastic rheological scheme.

This elastoplastic constitutive model is able to provide the evolution of the response once that the external deformation history $\delta(t)$ is assigned. The stiffness k_0 of the spring 0 is equal to the model initial elastic stiffness while the stiffness k_1 of the spring 1 is the post yielding stiffness. It is necessary to introduce an internal variable to describe the internal changing in the system and this variable is the deformation of the elastic-friction component $\delta_1(t)$, i.e. the plastic deformation. The material state is described by the couple of $\delta(t)$ and $\delta_1(t)$. Various quantities can be obtained starting from these variables.

The deformation increment and the force increment of the spring 0 are:

$$\dot{\delta}_0(t) = \dot{\delta}(t) - \dot{\delta}_1(t) \tag{4.4.1}$$

$$\dot{F}(t) = \dot{F}_0(t) = k_0 \dot{\delta}_0(t) \tag{4.4.2}$$

The force increment and the increment of the cumulative plastic deformation are:

$$\dot{F}_1(t) = k_1 \dot{\delta}_1(t) \tag{4.4.3}$$

$$\dot{\mu}(t) = \left|\dot{\delta}_1(t)\right| \tag{4.4.4}$$

The increment of the yield force $\dot{F}_y(t)$ caused by the isotropic hardening is related to the cumulative plastic deformation $\mu(t)$ and depends on the initial yield force F_{y0}, on the maximum yield force $F_{y,\max}$ and on a positive non-dimensional constant δ_r that controls the rate of the isotropic hardening (if higher the isotropic hardening is lower)

$$\dot{F}_y(t) = \left(F_{y,\max} - F_{yo}\right)\exp\left(-\frac{\mu(t)}{\delta_r}\right)\frac{\dot{\mu}(t)}{\delta_r} \tag{4.4.5}$$

Integrating this equation is possible to obtain the evolution of the yield force $F_y(t)$.
Finally the evolution in time of the internal variable $\dot{\delta}_1(t)$ is

$$\dot{\delta}_1(t) = \operatorname{sgn}\left(F(t)\right)\left|\frac{F(t) - F_1(t)}{F_y(t)}\right|^{\alpha}\left|\dot{\delta}(t)\right| \quad if \quad F(t)\dot{\delta}(t) > 0 \tag{4.4.6}$$

$$\dot{\delta}_1(t) = 0 \quad otherwise \tag{4.4.7}$$

α is a positive non-dimensional constant that controls the transition between the elastic and the plastic branch (a lower values gives a smoother transition).

Since the response of the BRB is different in tension and compression the model can be improved considering different values of $F_{y,\max}$, δ_r and α in the two case. Als the stiffness k_0 and k_1 can be different in tension and compression.

The parameters that influence the elasto-plastic model can be calibrated in order to obtain a numerical approximation of the results of experimental tests. For example the results of the tests performed by *Iwata et al.* (2000), that are described in subparagraph 4.2.1, can be well predicted using this model assigning to the parameters the values shown in Table 2.

Table 2

Case	$\frac{F_{ymax}^-}{F_{ymax}^+}$	$\frac{F_{ymax}^+}{F_{y0}}$	δ_r^+	δ_r^-	α^+	α^-	$\frac{k_1^+}{k_0^+}$	$\frac{k_1^-}{k_0^-}$
A1	1.12	1.65	0.20	0.15	0.6	0.4	0.01	0.01
A2	1.12	1.65	0.20	0.15	1.2	0.2	0.01	0.01
A3	1.12	1.65	0.45	0.15	0.6	0.4	0.01	0.01
Merritt et al.	1.12	1.67	0.20	0.15	0.6	0.4	0.01	0.01
Iwata et al.	1.08	1.65	0.80	0.80	0.6	0.4	0.01	0.01
Tremblay et al.	1.18	1.33	0.20	0.10	0.9	0.9	0.01	0.04
Clark et al.	1.12	1.29	0.80	0.80	0.6	0.6	0.01	0.01
Chou and Chen	1.08	1.43	0.50	0.40	0.6	0.6	0.01	0.02

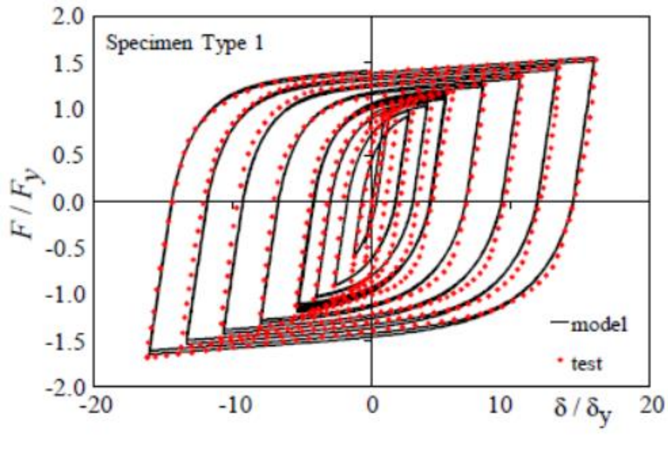

Figure 4-22. Comparison between model prediction and experimental tests performed by Iwata et al. (2000)

The same comparison has been done also with the results of the tests performed by *Tremblay et al.* using a deformation history that contains a portion of the cyclic path with non-zero mean strain.

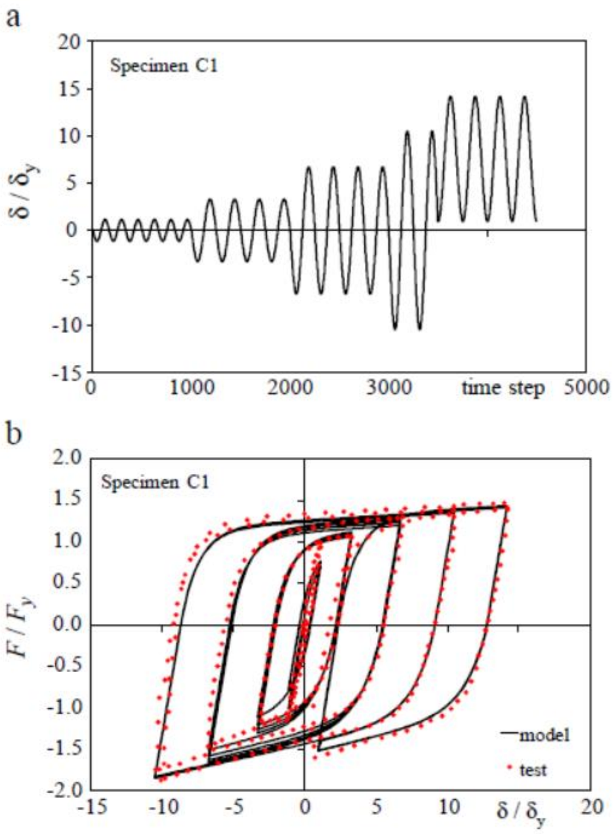

Figure 4-23. Deformation history (a) and comparison between model prediction and experimental results of Tremblay et al. (2004).

Chapter 5

5 Design method for retrofitting existing RC frame with elasto-plastic dissipative braces (BRB)

Dissipative braces are very efficient devices for designing new buildings or retrofitting existing ones in order to improve the seismic response. In this chapter is presented a design method for these devices, based on elastic-plastic or viscoelastic behavior, which takes into account the energy dissipation provided both by the bare frame and by the dampers. In this specific case, the focus is on elastic-plastic devices considered as buckling restrained braces (BRBs).

As explained in chapter 4 BRBs are metallic dampers that can yield both in tension and compression without being affected by buckling thanks to a restraining mechanism made by a steel casing filled with mortar that surround the steel core. A very common solution in the retrofitting of existing RC structure consists in the application of these devices with a reduced length inside a diagonal, placed in series with an over-strengthened steel brace.

The introduction of the BRB system increase the stiffness and the strength of the retrofitted structure together with the dissipative capacity thanks to the large hysteretic loops of the metallic dampers.

The design method used in this thesis is based on the concept that the modal shape of the first translational vibration mode in the direction of the reinforcing system of the coupled structure (BRB system + RC frame), in the case of regular inelastic frame behavior, coincides with the first translational vibration mode of the bare frame. The design procedure, after the choosing of the deformed shape, is based on nonlinear static analysis (pushover) of the frame and on the reduction of the capacity curve of the structure to that of an equivalent SDOF system. The evaluation of the equivalent SDOF system of the retrofitted structure is based on the capacity spectrum method (*Freeman* 1998), and more precisely on its variation, the N2 method (*Fajfar* 2000), in order to achieve performance point that satisfy a certain limit state under a certain level of seismic action. The N2 method is based on the representation on the acceleration-displacement plan of the capacity curve of the SDOF system against the inelastic response spectrum, rather than the elastic one.

After the evaluation of the equivalent SDOF system is necessary to design the distribution of the BRB along the height of the building in order to obtain a modal response of the retrofitted structure that coincides with the response of the bare frame as anticipated before.

5.1 BRB modelling

The overall characteristics of the dissipative brace depend on the characteristics of both components placed in series, the damper and the over-strengthened steel brace. Referring to the properties of the dissipative brace with the subscript c they are:

- K_c : stiffness of the dissipative brace;
- F_c : yielding force of the dissipative brace;
- μ_c : ductility of the dissipative brace;
- L_c : overall length of the dissipative brace (diagonal of the frame).

The properties of the BRB are indicated with the subscript 0 and are:

- K_0 : stiffness of the elastic branch of the BRB;
- F_0 : yielding force of the BRB;
- μ_0 : ductility of the BRB;
- L_0 : length of the BRB;
- A_0 : cross sectional area of the BRB steel core.

From these it is possible to derive other quantities such as the yielding displacement $\delta_{0y} = F_0 / K_0$ and the ultimate displacement $\delta_{0u} = \mu_0 \delta_{0y}$ of the damper. Generally the range of F_0 is quite wide and it depends from the cross section of the steel core while the values of stiffness are more restrictive and they depends both from the cross sectional area and from the length of the device.

Finally, the properties of the elastic part of the brace are indicated with the subscript b:

- K_b : stiffness of the elastic steel brace;
- L_b : length of the elastic steel brace;
- A_b : cross sectional area of the elastic steel brace.

The stiffness of the steel tube is proportional to its cross sectional area, according to $K_b = EA_b/L_b$, where E is the steel elastic modulus and $L_b = L_c - L_0$.

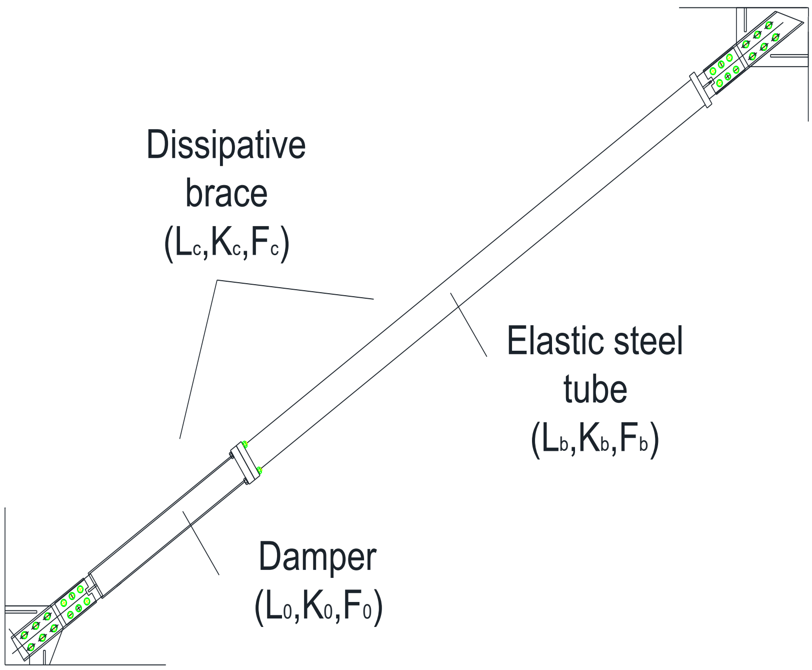

Figure 5-1. Representation of the dissipative brace.

Thanks to the fact that the BRB is placed in series with the elastic brace it is possible to obtain the properties of the overall brace starting from the properties of the two members. Equaling the yielding strength of the BRB with that of the brace gives:

$$F_c = F_0 \tag{5.1.1}$$

$$K_c = \frac{K_b K_0}{K_b + K_0} \tag{5.1.2}$$

$$\mu_c = \frac{K_0 + K_b \mu_0}{K_b + K_0} \tag{5.1.3}$$

Since the steel tube has to remain into the elastic field it is necessary to design its transverse section in order to guarantee a certain overstrength with respect to the yielding strength of the BRB. Introducing a safety coefficient γ_{ov} (usually equal to 1.2) the yielding strength of the elastic steel tube should be $F_b \geq \gamma_{ov} F_0$. Although instability cannot occur on the device, by definition, it is however necessary to check the global buckling of the diagonal in the presence of a compressive action $\gamma_{ov} F_0$. If the damper device is very short compared to the length of the diagonal this verification can be determinant, imposing an inferior limit for the steel tube cross sectional area.

Usually the design procedure of dissipative braces requires to obtain a certain elasto-platic behavior of the diagonal, described by assigned value of K_c, μ_c and F_c for each brace. Choosing the ductility μ_0 of the dissipative devices it is possible to derive the stiffness of the BRB and of the elastic connecting arm in order to achieve the desired behavior by means the following relations:

$$K_0 = K_c \frac{\mu_0 - 1}{\mu_c - 1} \tag{5.1.4}$$

$$K_b = \frac{K_0}{K_0 / K_c - 1} \tag{5.1.5}$$

The yielding strength of the BRB is equal to the yielding strength of the diagonal as anticipated in eq.(5.1.1).

The overall ductility μ_c is lower than the ductility μ_0 of the device and it may be interesting to observe how the requests for the stiffness of the components change variating the ratio μ_c / μ_0. In Figure 5-2 and Figure 5-3, the trends of the ratios between the stiffness of the two members of the brace and the stiffness of the overall diagonal, variating the ductility ratio, are shown. The graphs refers to a ductility of the device $\mu_0 = 20$. Increasing the ductility ratio in order to obtain the maximum value of ductility, equal to that of the dissipative device, requires that the stiffness of the BRB must approach the stiffness of the overall brace while the stiffness of the elastic member increase exponentially. The introduction of excessive ductility ratios (above 0.7-0.8) often leads to large connecting arms and may not be convenient for both economic and constructive reasons. On the other hand, the introduction of low values of the ductility ratio can cause problems in the design of the members of the brace. In this case, the stiffness required by the BRB becomes high while the stiffness of the connecting arm becomes small and may no longer be compatible with the demand for overstrength or stability.

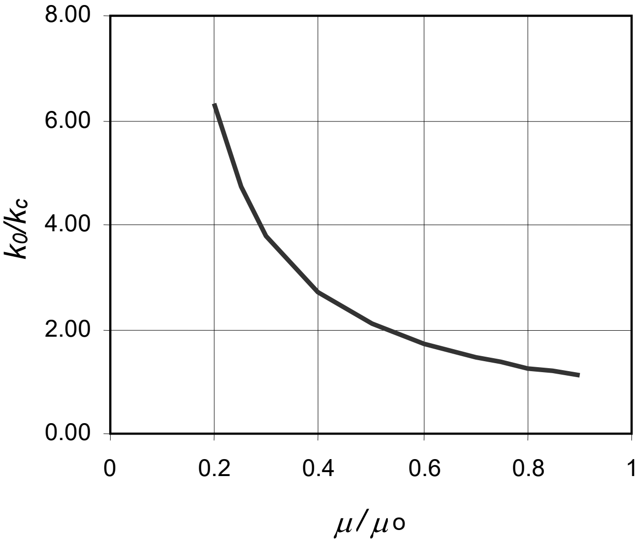

Figure 5-2. Variation of BRB stiffness respect to the ductility ratio.

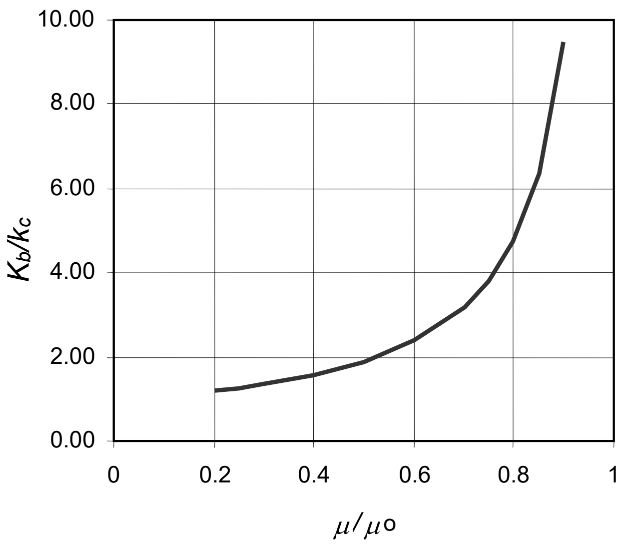

Figure 5-3. Variation of elastic arm stiffness respect to the ductility ratio.

5.2 Design of the BRB system

To design the BRB system it is necessary to reduce the behavior of the multiple degrees of freedom (MDOF) system that represent the RC bare frame into an equivalent SDOF system. In this way, the capacity curve of the equivalent SDOF system can be compared with the seismic demand represented by the response spectrum in the acceleration-displacement plan and the additional resistance and stiffness offered by the bracing system can be easily evaluated as a function of the seismic intensity.

The design of the bracing system starts establishing, as a design parameter, the behavior that the retrofitted structure will show along its height. When defining the deformation along the height, different choices can be made depending on the type of structure to be protected (steel pendulum structure, newly constructed frame structure, existing frame structure). In case of existing RC structures, if the behavior along the height is regular, without localization of displacement demand in the inelastic field (no soft storey mechanism) it is reasonable to assume as the objective displacement of the coupled system the deformed shape of the first vibration mode. Because of this choice the two parallel resisting system deform in the same way according to the selected vibration mode, at least until the frame remains elastic.

Focusing on the case of RC frame with regular behavior in height, the objective displacement shape coincides with the first vibration mode of the bare frame and for this reason the displacements are defined with exception of a multiplicative constant. The absolute displacement of the first vibration mode are U^i while the relative interstorey displacements are $\Delta^i = U^i - U^{i-1}$. It is convenient to refer to the normalized distributions of relative and absolute displacements obtained by dividing the quantities for the displacement of the last floor, usually taken as control point in the push-over analyses. Therefore, the normalized relative displacements are

$$\delta^i = \Delta^i / U^n \tag{5.2.1}$$

And the normalized absolute displacement

$$u^i = U^i / U^n \tag{5.2.2}$$

The distribution of the shear forces at the different levels of the structure can be obtained from equilibrium:

$$V^n = \omega^2 m^n u^n \tag{5.2.3}$$

$$V^i = V^{i+1} + \omega^2 m^i u^i \tag{5.2.4}$$

where ω is the circular frequency of the first vibrational mode. The distribution of the shear is defined with exception of a multiplicative constant that is the square of the circular frequency of the first mode. Once a modal deformation has been chosen, only the "shape" of the floor shear is identified, which can be described by the relative shear obtained dividing by the base shear of the structure V^1.

$$v^i = V^i / V^1 \tag{5.2.5}$$

This vector depends only on the modal shape and does not change with the variation of the circular frequency of the structure. A distribution of the stiffness along the floors can be obtained from the ratio between shear and inter-storey displacements.

$$K^i = V^i / \Delta^i \tag{5.2.6}$$

It is necessary to highlight that these stiffness do not correspond to the real stiffness of each floor but represent a distribution of the stiffness along the height that is function of the shear and inter-storey displacement. Normalizing these components respect to the base stiffness gives:

$$k^i = K^i / K^1 \tag{5.2.7}$$

The choice of controlling the deformation of the first mode is an effective design criterion if the first vibration mode is dominant in the dynamic behavior of the system into the linear field and if it is sufficiently representative of the maximum displacements in height. If the elastic limit of the system is distributed in height proportionally to the floor shears, it will be possible to have a contemporary and homogeneous plasticization at the various levels with a benefit for the overall ductility of the structure.

In case of existing RC structure retrofitted by means of dissipative braces the stiffness and the strength to horizontal actions is provided by the existing frame and by the dissipative bracing system. If the existing frame has a sufficiently regular behavior in height, it is reasonable to design the dissipative system to be placed in parallel assuming, as the objective deformation, the deformation of the first mode of the existing frame. The retrofitted structure will maintain the same deformed shape even after the introduction of the dissipative bracing system. In case of existing RC frame without a regular behavior in height, due to the presence of a soft storey, it is reasonable to design the dissipative system to be placed in parallel with the existing frame by setting a deformation distribution able to delay the plasticization of the weaker storey. The main problem consists in identifying a suitable deformation. In a simplified way it is possible to perform the classical push-over analysis with a load pattern proportional to the forces of inertia of the first mode and observing the concentration of the plasticizations at a certain level, is assigned by attempts a distribution of forces that reduce the shear at the soft plane. If the new distribution is effective, a more homogeneous distribution of the plasticizations and a ultimate displacement greater than the initial one should be observed. The corresponding distribution of displacements in the elastic field can be adopted as a new objective deformation.

In conclusion, once that the deformation shape of the first mode, described by the relative displacements vector δ^i, is chosen, the associated quantities u^i, m^*, Γ are known, and the relative ratios between the shears v^i and the storey stiffness k^i are fixed. The only value that remains indeterminate is a proportionality parameter of the stiffness K^1 or, alternatively, of the shears V^1. This parameter will be determined according to the procedure explained in the following subparagraphs.

5.2.1 Evaluation of the system capacity curve.

The capacity curve of the bare frame is obtained by means of a pushover analysis. This nonlinear static analysis is performed subjecting the structure to a monotonically increasing load pattern of lateral forces. These forces should represent the inertial forces experienced by the structure during a ground shaking and their increment causes various structural elements to yield sequentially. Through this analysis is possible to obtain a nonlinear force-displacement relation of the MDOF system that represent the real structure. The selection of the lateral load pattern is one of the most important parameter for the analysis because it influence the result that is not univocal and for this reason one practical solution is to use two different load patterns and then envelope the results. The N2 method (*Fajfar* 2000) is based on the execution of the pushover analysis using a vector of the lateral loads **P** determined as

$$\mathbf{P} = p\mathbf{\Psi} = p\mathbf{M\Phi} \tag{5.2.8}$$

where **M** is the diagonal mass matrix, $\mathbf{\Phi}$ is the assumed displacement shape and p controls the magnitude of the lateral load. It is evident that the applied load and the displacement shape are directly dependent, unlike other pushover analysis approach. From eq.(5.2.8) follows that the force applied to the i-th level is proportional to the displacement at the floor level and to the mass of the floor.

$$P_i = pm_i\Phi_i \tag{5.2.9}$$

This approach has a physical explanation because if the assumed displacement shape coincides with the displacement of the structure during ground shaking, the distribution of the loads is equal to the distribution of the effective earthquake forces.

In the N2 approach, the seismic demand is determined by means of inelastic response spectra that are referred to a single degree of freedom system and for this reason is necessary to transform the capacity curve of the MDOF system into the capacity curve of an equivalent SDOF system. In order to do that it is necessary to consider the equation of motion of a MDOF system along the load direction.

$$\mathbf{M\ddot{U}} + \mathbf{R} = \mathbf{M1}a \tag{5.2.10}$$

U and **R** are vectors that represents the displacements and the resisting force of the structure, while a is the ground acceleration. Assuming the displacement shape $\mathbf{\Phi}$ constant in time and equal to the first translational modal shape of the structure in the considered direction, normalized in order to have the component at the top equal to 1, the displacement vector **U** is defined as

$$\mathbf{U} = \mathbf{\Phi}D_t \tag{5.2.11}$$

where D_t is the top displacement and it is a function of the time.

From statics it follow that the resisting forces are equal to the applied load

$$\mathbf{P} = \mathbf{R} \tag{5.2.12}$$

Introducing the previous equations in the eq.(5.2.10) and multiplying for $\mathbf{\Phi}^\mathbf{T}$ gives

$$\mathbf{\Phi}^{\mathrm{T}}\mathbf{M}\mathbf{\Phi}\ddot{d}_t + \mathbf{\Phi}^{\mathrm{T}}\mathbf{M}\mathbf{\Phi}p = -\mathbf{\Phi}^{\mathrm{T}}\mathbf{M}\mathbf{1}a \tag{5.2.13}$$

Multiplying and dividing the left hand side with $\mathbf{\Phi}^{\mathbf{T}}\mathbf{M1}$ it is possible to obtain the equation of motion of the equivalent SDOF system.

$$m^*\ddot{d}^* + F^* = -m^*a \tag{5.2.14}$$

where m^* is the equivalent mass of the SDOF system

$$m^* = \mathbf{\Phi}^{\mathrm{T}}\mathbf{M}\mathbf{1} = \sum m_i\Phi_i \tag{5.2.15}$$

and d* and F* are the displacement and the force of the equivalent SDOF system obtained dividing D_t and the base shear of the model V

$$V = \sum P_i = \mathbf{\Phi}^{\mathrm{T}}\mathbf{M}\mathbf{1}p = p\sum m_i\Phi_i = pm^* \tag{5.2.16}$$

for the so called modal participation factor indicated with the constant Γ

$$\Gamma = \frac{\mathbf{\Phi}^{\mathrm{T}}\mathbf{M}\mathbf{1}}{\mathbf{\Phi}^{\mathrm{T}}\mathbf{M}\mathbf{\Phi}} = \frac{\sum m_i\Phi_i}{\sum m_i\Phi_i^2} = \frac{m^*}{\sum m_i\Phi_i^2} \tag{5.2.17}$$

In this way

$$d^* = \frac{d_t}{\Gamma} \tag{5.2.18}$$

$$F^* = \frac{V}{\Gamma} \tag{5.2.19}$$

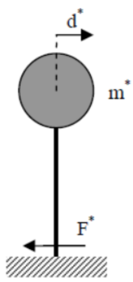

Figure 5-4. Equivalent SDOF system.

It is important to highlight that the transformation of both displacement and forces from the MDOF system to the equivalent SDOF system happens dividing for the same constant Γ and for this reason the relation that is at the base of the capacity curve is the same for the two systems. This can be seen changing the scale of both axes and noticing that the initial stiffness of the SDOF system remains the same of that of the MDOF system.

After the reduction of the capacity curve of the MDOF system to that of a SDOF system it is necessary to determine a simplified elasto-plastic force-displacement relationship. In order to do that numerous procedures have been developed during the years and some of these are implemented in the most famous codes.

Eurocode 8 (CEN 2004) suggest a bilinear fit, with an elastic-perfectly plastic behavior, based on the equivalence of the areas above and below the bilinearized curve. This approach is similar to that of the original N2 method (*Fajfar and Fischinger* 1988) and requires the fitting of the curve up to the point of the formation of a plastic mechanism. The yield force F_y^*, that represents also the ultimate strength of the idealized system, is equal to the base shear force at the formation of the plastic mechanism and the slope of the elastic branch, representing the stiffness, is determined in order to equalized the areas.

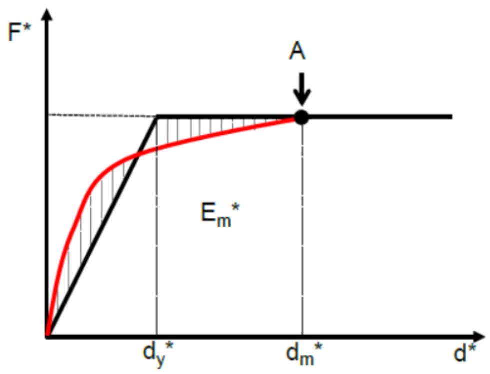

Figure 5-5. Fitting procedure according to EC8 (2004).

Based on this assumption the yield displacement of the idealized SDOF system d_y^* is given by:

$$d_y^* = 2\left(d_m^* - \frac{E_m^*}{F_y^*}\right) \tag{5.2.20}$$

where E_m^* is the deformation energy up to the formation of the plastic mechanism and coincides with the area under the SDOF capacity curve.

Other procedures that takes into account post yielding behavior (hardening or softening) can be found in FEMA documents (FEMA 273 1997; FEMA 365 2000; FEMA 440 2005). According to FEMA 365 the bilinearized curve has an initial slope calculated for a base shear force equal to 60% of the nominal yield strength and a post-yielding slope that can be positive or negative, evaluated through the balancing of the areas up to the target displacement δ_t. FEMA 440 provides the same fitting method with some additional rules that regards the softening behavior. The softening slope α_e is necessary for the evaluation of the minimum value of the decreasing strength after the reaching of the peak of the curve that avoid dynamic instability.

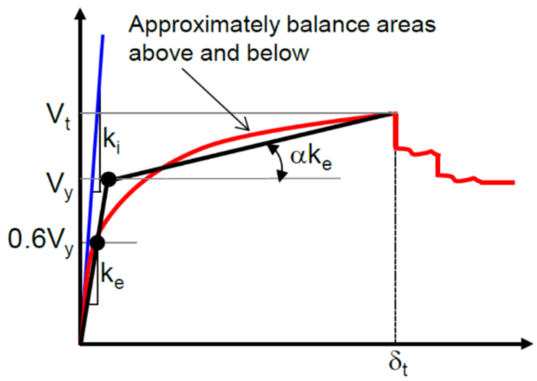

Figure 5-6. Fitting procedure according to FEMA 365(2000).

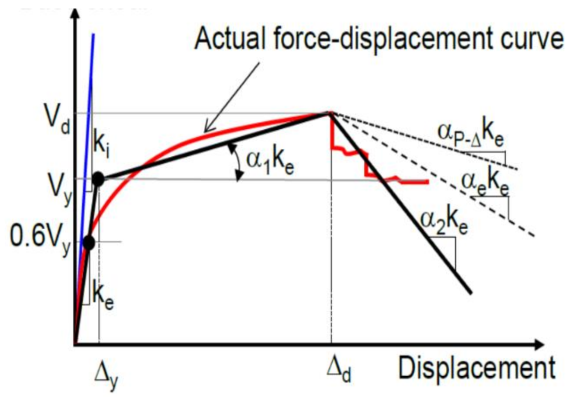

Figure 5-7. Fitting procedure according to FEMA 440.

In the Italian guidelines for the application of the NTC 2008 code (CS.LL.PP. 2008; 2009) is suggest an elastoplastic fit for the capacity curve that takes into account also a limited softening behavior up to a degradation of the maximum base shear equal to the 15%. This approach is based on the 60% rule for the initial stiffness as well as the FEMA documents but considers a post-yielding branch with zero slope. This plateau of the bilinearized capacity curve can be extended up to the point in which is reached a 15% degradation of the maximum strength. The yielding force F_y^* is found equalizing the area under the capacity curve of the SDOF system with that of the fitting curve.

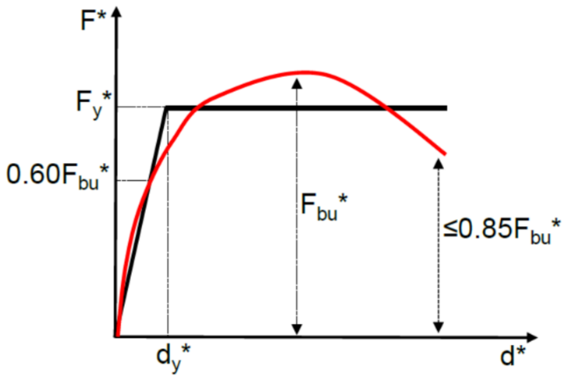

Figure 5-8. Bilinearization according to Italian seismic code (CS.LL.PP 2008)

The result of this choice is that the plateau of the fitting curve is always lower than the maximum shear strength of the exact capacity curve. If the structural model can not display any softening branch in its capacity curve the criterion becomes equal to the Fema provisions.

Since the N2 method requires that the post-yielding stiffness of the fitting curve is equal to zero, the fitting procedure propose by the Italian seismic code is suitable for this purpose. For this reason, this is the fitting procedure used in the study case of this thesis. The request of a null post-yielding stiffness is due to the fact that the reduction factor R_μ applied to the elastic demand spectrum is defined as the ratio of the required elastic strength to the yield strength and so the influence of a moderate strain hardening is incorporated in the demand spectra (*Fajfar* 2000).

Once that a simplified elasto-plastic force-displacement relationship has been found it is possible to obtain the elastic period of the idealized SDOF system by means of the eq.(5.2.21)

$$T^* = 2\pi \sqrt{\frac{m^* d_y^*}{F_y^*}} \tag{5.2.21}$$

where F_y^* and d_y^* are the yield strength and displacement.

The capacity diagram is than transformed into the acceleration-displacement format dividing the forces F^* by the equivalent mass m^* of the SDOF system in order to obtain the accelerations

$$S_a = \frac{F^*}{m^*} \tag{5.2.22}$$

Another fundamental parameter that can be obtained from the bilinearized capacity curve is the ductility μ of the elastic perfectly-plastic system given by the ratio between the ultimate displacement d_u^* and the yield displacement d_y^*.

$$\mu = \frac{d_u^*}{d_y^*} \tag{5.2.23}$$

5.2.2 Evaluation of the seismic demand by means of inelastic spectra

The seismic demand is usually defined using an elastic pseudo-acceleration spectrum S_{ae} that consists in the representation of the spectral accelerations as a function of the natural period T of the structure, considered as an elastic SDOF system. From the elastic spectrum is possible to obtain the inelastic demand spectrum refereed to an inelastic SDOF system by means of the N2 method that is based on the application of a reduction factor that relates the elastic spectrum with the inelastic one.

The elastic spectrum can be represented into the acceleration-displacement format deriving the spectral displacement with the equation:

$$S_{de} = \frac{T^2}{4\pi^2} S_{ae} \tag{5.2.24}$$

where S_{ae} and S_{de} are the are the values of the spectral accelerations and displacements corresponding to a period T and a fixed viscous damping ratio, usually considered equal to 5% for a common structure. In Figure 5-9 is represented a typical smooth elastic acceleration spectrum normalized to a peak ground acceleration of 1.0 g and the corresponding elastic displacement spectrum.

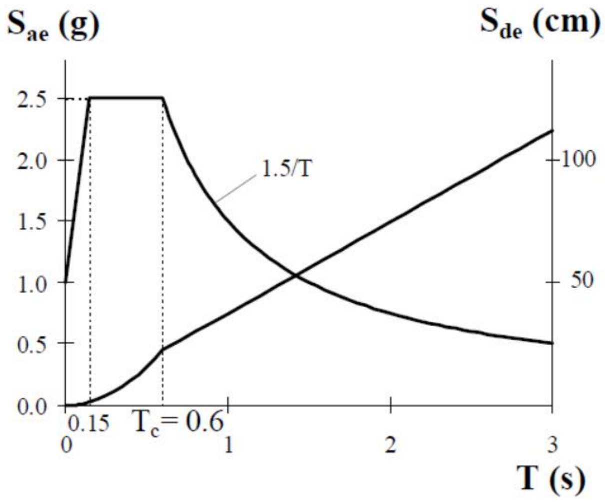

Figure 5-9. Typical elastic acceleration (S_{ae}) and displacement (S_{de}) spectrum.

The two spectrum can be plotted together in the acceleration-displacement format as shown in Figure 5-10

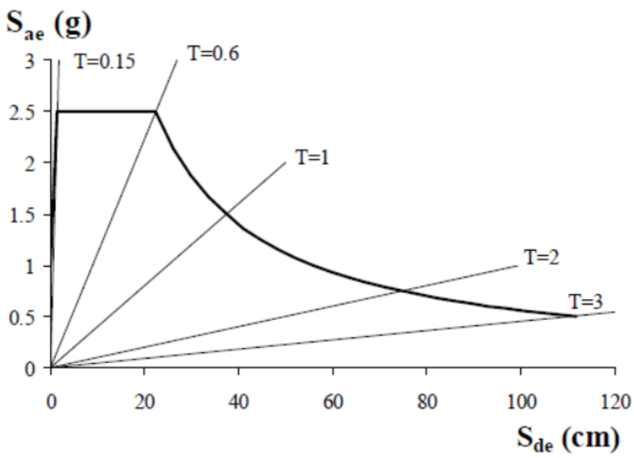

Figure 5-10. Spectrum in AD format

For an inelastic SDOF system with a bilinear elasto-perfectly-plastic force-deformation relationship the two acceleration and displacement spectra can be determined with the following relations (*Vidic et al.* 1994)

$$S_a = \frac{S_{ae}}{R_\mu} \tag{5.2.25}$$

$$S_d = \frac{\mu}{R_\mu} S_{de} = \mu \frac{T^2}{4\pi^2} S_a \tag{5.2.26}$$

where μ is the ductility factor introduced by the eq.(5.2.23) and R_μ is a reduction factor that depends on the ductility and so on the hysteretic energy dissipation provided by the structure.

This reduction factor R_μ in the N2 method assume the following values proposed by *Vidic et al.* (1994):

$$R_\mu = (\mu - 1)\frac{T}{T_0} + 1 \qquad T \le T_0 \tag{5.2.27}$$

$$R_\mu = \mu \qquad T > T_0 \tag{5.2.28}$$

$$T_0 = 0.65\mu^{0.3} T_C \le T_C \tag{5.2.29}$$

T_C is the characteristic period of the ground motion and corresponds to the period of transition between the constant acceleration segment and the constant velocity segment of the spectrum. It roughly corresponds to the period that maximize the seismic energy introduced in the structure. The eq.(5.2.27) and (5.2.28) can be plotted into a graph (Figure 5-11) showing the variation of the reduction factor R_μ with the ductility μ and the period T. In medium and long period range the displacement of the inelastic system is the same of the corresponding elastic system because the reduction factor is constant and equal to μ according to eq.(5.2.28) and substituting it into eq.(5.2.26) gives $S_d = S_{de}$. Simplified values for R_μ can be obtained setting $T_0 = T_C$ and this approach, in case of low ductility demand, is conservative for short period structure.

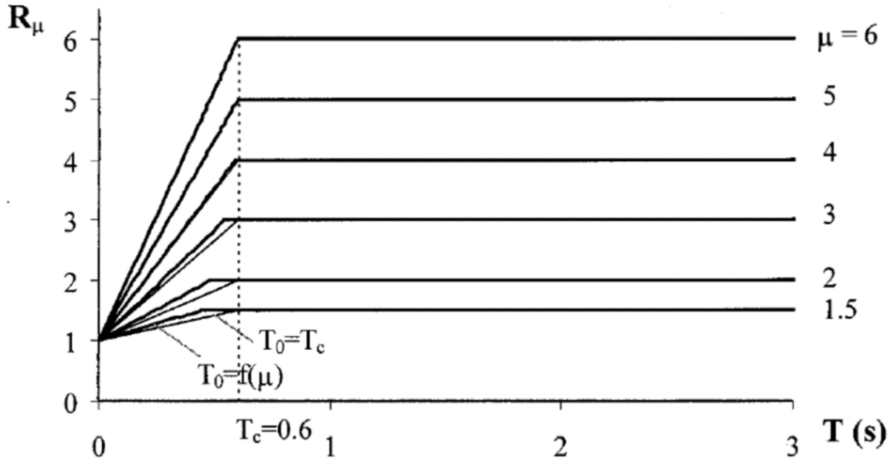

Figure 5-11. Ductility dependant reduction factor R_μ (Fajfar 1999).

Applying the reduction factor to the elastic acceleration-displacement response spectrum of the Figure 5-10 by means of the eq.(5.2.25) and (5.2.26) it is possible to obtain the inelastic spectrum for a fixed value of ductility μ as shown in Figure 5-12.

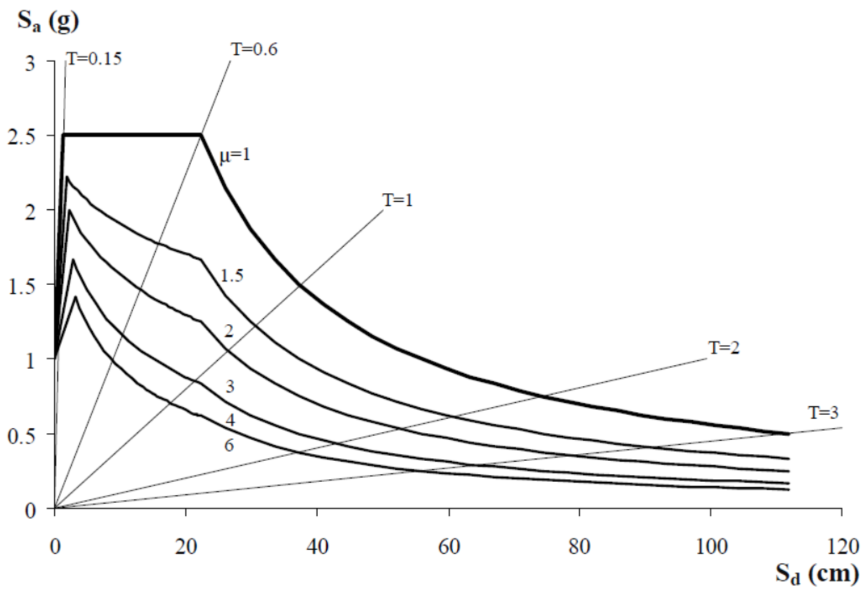

Figure 5-12. Inelastic spectra for different values of ductility.

5.2.3 Definition of the coupled SDOF equivalent system

Once that the capacity of the bare frame and the seismic demand are known is possible to plot the two curves into the same acceleration-displacement plan and check graphically if the capacity curve is able to reach the performance point intersecting the inelastic response spectrum.

If the structure is not able to reach the performance point is necessary to design the characteristics required to the dissipative bracing system in order to retrofit the existing structure. The dissipative bracing system may be represented by an equivalent elastic-perfectly plastic SDOF system, as well as the bare frame, with a base shear V_d^1 and a ductility μ_d. The coupled system is still a an elastic-perfectly plastic SDOF system but the base shear is

$$V^1 = V_f^1 + V_d^1 \tag{5.2.30}$$

where V_f^1 is the base shear of the bare frame and the ductility

$$\mu = \frac{\mu_d \mu_t \left(V_t^1 + V_d^1\right)}{V_t^1 \mu_d + V_d^1 \mu_t} \tag{5.2.31}$$

is obtained by applying the areas equivalence criterion.

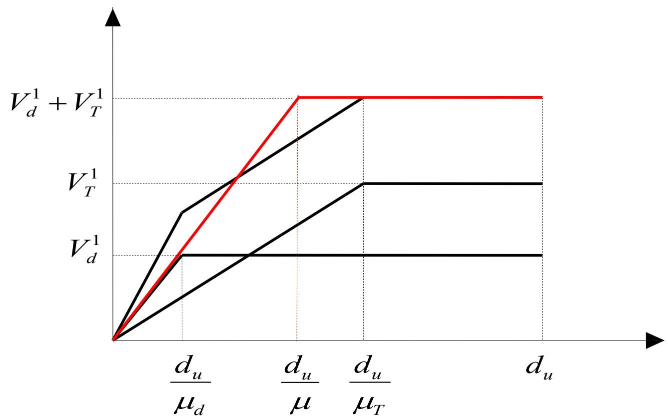

Figure 5-13. Design capacity curve of the coupled system (frame + BRB system).

The equivalent SDOF system of the retrofitted structure can withstand a maximum acceleration of

$$a^* = V^1 / m^*\Gamma \tag{5.2.32}$$

With a maximum displacement

$$d_u^* = d_u / \Gamma \tag{5.2.33}$$

The values of m^* and Γ remain unchanged even after the introduction of the bracing system.

The capacity curve of the coupled system must be compared with the demand requests by the design earthquake that is described by means of the inelastic spectrum obtained for a value of ductility μ (ductility of the coupled system). If the capacity curve intersects the inelastic spectrum at its ultimate displacement the performance point is reached.

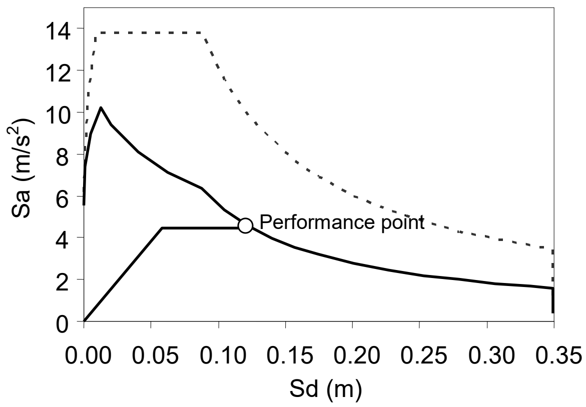

Figure 5-14. Comparison between capacity and demand.

The design consists in determining, in a first step, the base shear V_d^1 of the dissipation system to be placed in parallel with the frame. This parameter can be chosen by a comparison between the capacity of the retrofitted system and the seismic demand varying the value of V_d^1 until the capacity curve intersect the demand curve at the ultimate frame displacement.

This design parameter is not sufficient to describe the contribution of the elastic-plastic dissipative system and it is necessary to decide a priori a value μ_d for the ductility of the bracing system. This value coincides with the ductility of each single brace and must be compatible with that of the hysteretic devices adopted and therefore lower than μ_0. Adopting higher values of μ_d causes a higher overall ductility of the coupled system and lower base shear. On the other hand, as explained in paragraph 5.1, when approaching the limit value of the ductility μ_0 of the dissipative devices, the request for stiffness of the connecting arms leads to over dimensioning the diagonals with increasing in terms of costs and difficulties related to the compatibility of the diagonals with the existing building. The choice of an optimal value of ductility μ_d depends therefore on different factors and varies according to the different design cases. In case of retrofitting of existing RC buildings, it has been observed that the shear at the base is not much reduced for values higher than 5-6 while the dimensions to be assigned to the links start to grow rapidly.

Once that both the value of the base shear V_d^1 and of the ductility μ_d have been decided it follows that the associated stiffness of the dissipative system at the first floor is

$$K_d^1 = \frac{\mu_d V_d^1}{d_u^* \delta^i} \tag{5.2.34}$$

where d_u^* is the ultimate displacement of the capacity curve of the coupled system, coinciding with the ultimate displacement of the capacity curve of the bare frame.

5.2.4 Distribution in height of the base shear and stiffness of the BRB system

Once that the base shear at the elastic limit of the dissipative bracing system is known it is possible to obtain the distribution of the shears V_d^i carried by the braces at the i-th floor by means of the eq.(5.2.5)

$$V_d^i = V_d^1 v^i \tag{5.2.35}$$

The same philosophy is applied for the distribution of the stiffness that must be provided by the dissipative braces at each floor using the eq.(5.2.7)

$$K_d^i = K_d^1 k^i \tag{5.2.36}$$

Substituting to K_d^i the eq.(5.2.34) gives

$$K_d^i = \frac{\mu_d V_d^1}{s_u} k^i \tag{5.2.37}$$

Following this criterion leads to obtain a deformed shape of the first translational vibrating mode in the direction of the bracing system that is equal to the first translational modal shape of the unretrofitted structure in the same direction. This is a direct consequence of the distribution in height of the resisting shear forces and stiffness provided by the bracing system that is the same of the bare frame.

5.2.5 In plane distribution of the braces and design of the components

After that V_d^i and K_d^i for each floor are known it is necessary to proceed with the repartition of these values for each brace inside the single plane choosing the number of braces and their position in order to minimize the torsional effects that can rise. It is a good solution to use more than two braces for each floor in order to limit the axial stress transmitted by the braces to the adjacent columns.

Once that the shear forces and the stiffness to be provided by each brace are obtained it is possible to evaluate the yielding force and the stiffness of each brace. The effectiveness of the braces depends on their inclination and so on the dimension of the frames in which they are placed. The yielding force F_c of the brace is obtained dividing the shear resisting force of the single brace by the cosine of its inclination angle α.

$$F_c^i = \frac{V_d^i}{\cos(\alpha)} \tag{5.2.38}$$

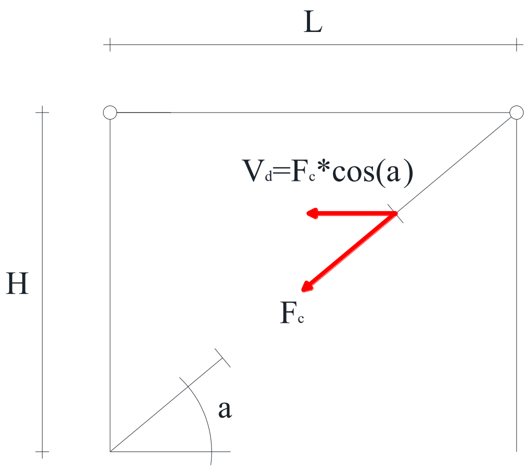

Figure 5-15. Geometric relation between the horizontal shear force and the axial yielding force of the diagonal.

The axial stiffness K_c of the diagonal can be derived from the horizontal stiffness of the braced frame K_d by means of simple geometrical considerations.

$$K_d = \frac{V_d}{\delta} = \frac{F_c \cos(\alpha)}{\delta} \tag{5.2.39}$$

$$K_c = \frac{F_c}{\delta \cos(\alpha)} \tag{5.2.40}$$

$$K_c = \frac{K_d}{\cos^2(\alpha)} \tag{5.2.41}$$

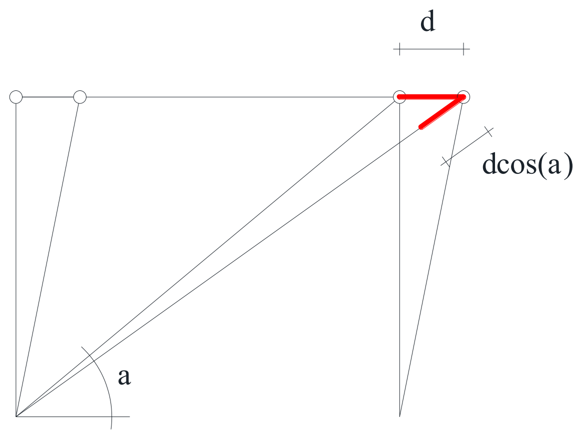

Figure 5-16. Geometrical relation between the horizontal displacement of the frame and the axial displacement of the brace.

Finally, once that the yielding force and the axial stiffness of the overall diagonal are known, it is possible to proceed with the design of the characteristics of the two components of the brace, the dissipative BRB and the elastic connection arm.

In order to obtain the stiffness K_0 and K_b of the two members by means of the eq.(5.1.4) and (5.1.5) it is necessary to set a priori another design parameter that is the ductility μ_0 of the dissipative device. The overall ductility of a single brace μ_c, as anticipated before in subparagraph 5.2.3, is equal to the ductility μ_d assigned to the bracing system.

The cross sectional area of the BRB steel core is obtained dividing the yield force of the device F_0 , equal to the yield force of the overall diagonal according to eq.(5.1.1), by the yielding stress $f_{y,0}$ of the material chosen for the steel core.

$$A_0 = \frac{F_0}{f_{y,0}} \tag{5.2.42}$$

The length of the BRB is obtained in order to have an axial stiffness of the dispositive equal to K_0.

$$L_0 = \frac{EA_0}{K_0} \tag{5.2.43}$$

where E is the elastic modulus of the steel.

The design of the elastic steel tube that connects the BRB to the opposite joint of the frame begins finding the length $L_b = L_c - L_0$, where L_c is the length of the diagonal of the frame. Knowing the length, the stiffness K_b and the elastic modulus of the material is possible to obtain the area

$$A_b = \frac{K_b L_b}{E} \tag{5.2.44}$$

And finally the yielding force of the connecting arm

$$F_b = A_b f_{y,b} \tag{5.2.45}$$

where $f_{y,b}$ is the yielding stress of the steel used for the connecting arm.

The connecting arm can be realized using different steel profiles but the more used are I-beam or hollow structural section (HSS) . In this case, considering a circular hollow section it is necessary to choose the thickness t_b of the profile and the radius r_b is obtained with eq.

$$r_b = \frac{A_b}{2\pi t_b} \tag{5.2.46}$$

The connecting arm needs to be checked against buckling comparing the force acting on the brace, equal to the yielding force of the BRB, with the critical buckling load $N_{b,Rd}$ obtained using the Eurocode 3 formulation

$$N_{b.Rd} = \frac{\chi \cdot A_b \cdot f_{y,b}}{\gamma_{M1}} \tag{5.2.47}$$

where χ is the reduction factor for the relevant buckling mode

$$\chi = \frac{1}{\Phi + \sqrt{\Phi^2 - \bar{\lambda}^2}} \leq 1.0 \tag{5.2.48}$$

This reduction factor depends on

$$\Phi = 0,5\left[1 + \alpha\left(\bar{\lambda} - 0,2\right) + \bar{\lambda}^2\right] \tag{5.2.49}$$

and on the non-dimensional slenderness $\bar{\lambda}$

$$\bar{\lambda} = \sqrt{\frac{Af_y}{N_{cr}}} \tag{5.2.50}$$

The relevant bucking mode for this type of element with circular hollow section is the flexural instability so the elastic critical force is $N_{cr} = \pi^2 EI_b / L_b^2$. Substituting this value in eq.(5.2.50) gives

$$\bar{\lambda} = \frac{\lambda}{\lambda_1} \tag{5.2.51}$$

where the slenderness λ of the connecting arm is given by the ratio between the length of the member and the radius of inertia of the circular section

$$\lambda = \frac{L_b}{\rho} \tag{5.2.52}$$

And λ_1 is the value of slenderness that separates the plastic collapse from the instability collapse

$$\lambda_1 = \pi \sqrt{\frac{E}{f_{y,b}}} \tag{5.2.53}$$

The value of the imperfection factor α of the eq.(5.2.49) depends on the bucking curve associated to the section and to the bucking axis. In case of circular hollow section the bucking can happens along any axis and according to tables 6.1 and 6.2 of the EC8 the value of α for this particular case is 0.21

Cross section		Limits	Buckling about axis	Buckling curve: S 235 S 275 S 355 S 420	Buckling curve: S 460
Hollow sections		hot finished	any	a	a_0
		cold formed	any	c	c

Figure 5-17. Table 6.2 of the EC8.

Buckling curve	a_0	a	b	c	d
Imperfection factor α	0,13	0,21	0,34	0,49	0,76

Figure 5-18. Table 6.1 of the EC8.

5.2.6 Verification of the retrofitted structure

Once that the design procedure of the BRB system is finished it is necessary to check if the response of the retrofitted structure agrees with the design expectations. In order to do that the BRB system needs to be added to the model of the structure and a nonlinear static (pushover) analysis is performed. If the capacity curve of the retrofitted model intersect the demand spectrum the retrofitting of the structure is verified.

To obtain a more realistic behavior of the retrofitted structure under a shaking ground it is also possible to perform nonlinear dynamic (time history) analysis according to NTC 2018 (2018) or EC8 (1998). It is possible to use artificial or recorded ground motion that must have a response spectrum consistent with the elastic response spectrum.

Chapter 6

6 Case study: Seismic upgrading of an existing RC building by means of BRBs

The aim of this thesis consists in the retrofitting of an existing RC building located in L'Aquila by means of hysteretic devices. Buckling restrained braces (BRB), whose characteristics have been described in chapter 4, are used as dissipative devices for the retrofitting of the structure.

The building was built in 1984 and so it presents some typical problematics of the RC structures built before the introduction of modern seismic codes as the fact that has been designed only for gravity load and the lack of seismic details of the reinforcements.

In order to improve the behavior of the structure under seismic actions for limiting the damages on structural and nonstructural elements it is necessary to retrofit the structure by means of passive control techniques.

6.1 Description of the Building

The building is realized in reinforced concrete (RC) and is composed of five storeys, that from now will be referred with numbers from 0 (ground floor) to 4 (last floor) with an height of 2.8 m at floor 0 and 3 m at the remaining floors.

The plan configuration consists in two bays whit different length of 5.5 m and 5.05 m in one direction (from now referred as Y). In the orthogonal direction (from now referred as X) the frame system is composed by three frames, two of them have seven bays with different lengths of 3.9 m, 3.225 m and 2.95 m while the other one is composed by six bays with different lengths of 3.9 m and 4.7 m. The resisting mechanism of the frames is parallel to Y direction and the structural direction of the floors, which has a thickness of 20 cm, is parallel to X direction.

The columns of the frames have rectangular section with dimensions of 35x60 cm at floor 0 and 30x60 at the remaining floors with the longer side in Y direction, according to the fact that the resisting mechanism of the frame is explicated along this way. The columns that support the stair landing have the same rectangular section of 25x60 cm at each floor with the longer side also in direction Y. At the center of the building is present an elevator surrounded by three columns with rectangular section of 80x30 cm and the longer side is parallel to the X direction.

The beams along the frames in Y direction are deep beams with rectangular section of 35x50 cm at the first elevation and 30x50 cm at the remaining floors, except for the beams of the stairs that are 25x50 cm. In X direction the beams are deep beams along the perimetral frames with rectangular sections of 30x50 cm at the first elevation and 25x50 cm at the remaining, while along the internal frame are flat beams with rectangular section of 20x60 cm.

The building is symmetric along X direction with respect to the central axis. Along Y direction the structure is not symmetric due to the different length of the bays and to the presence of the lifts on one side and of the elevator near the center of the building.

Figure 6-1. Frontal view of the building.

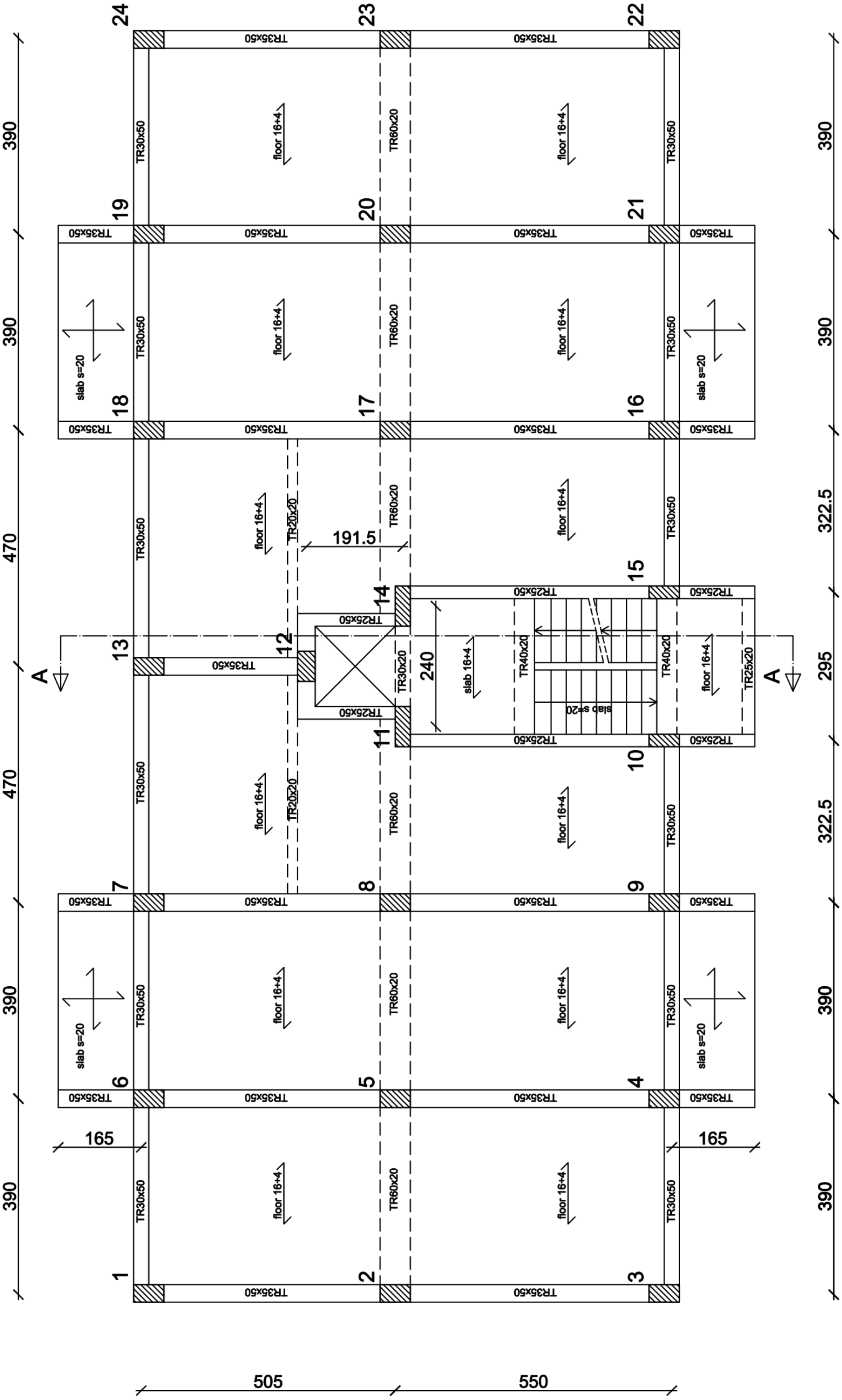

Figure 6-2. Beams layout of the first floor (H=2.8m)

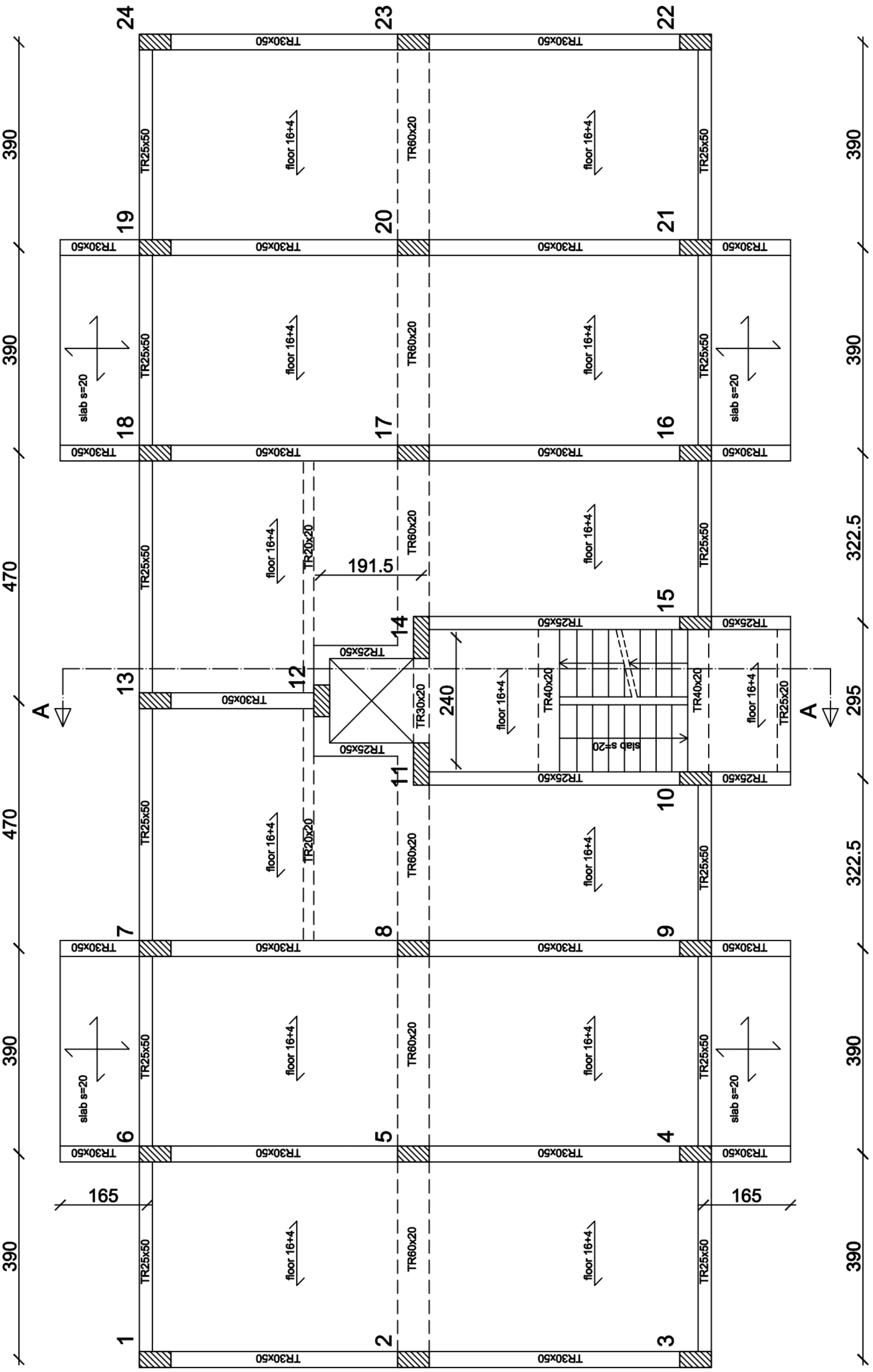

Figure 6-3. Beams layout of floors 2, 3, 4 (H=5.8, 8.8, 11.8).

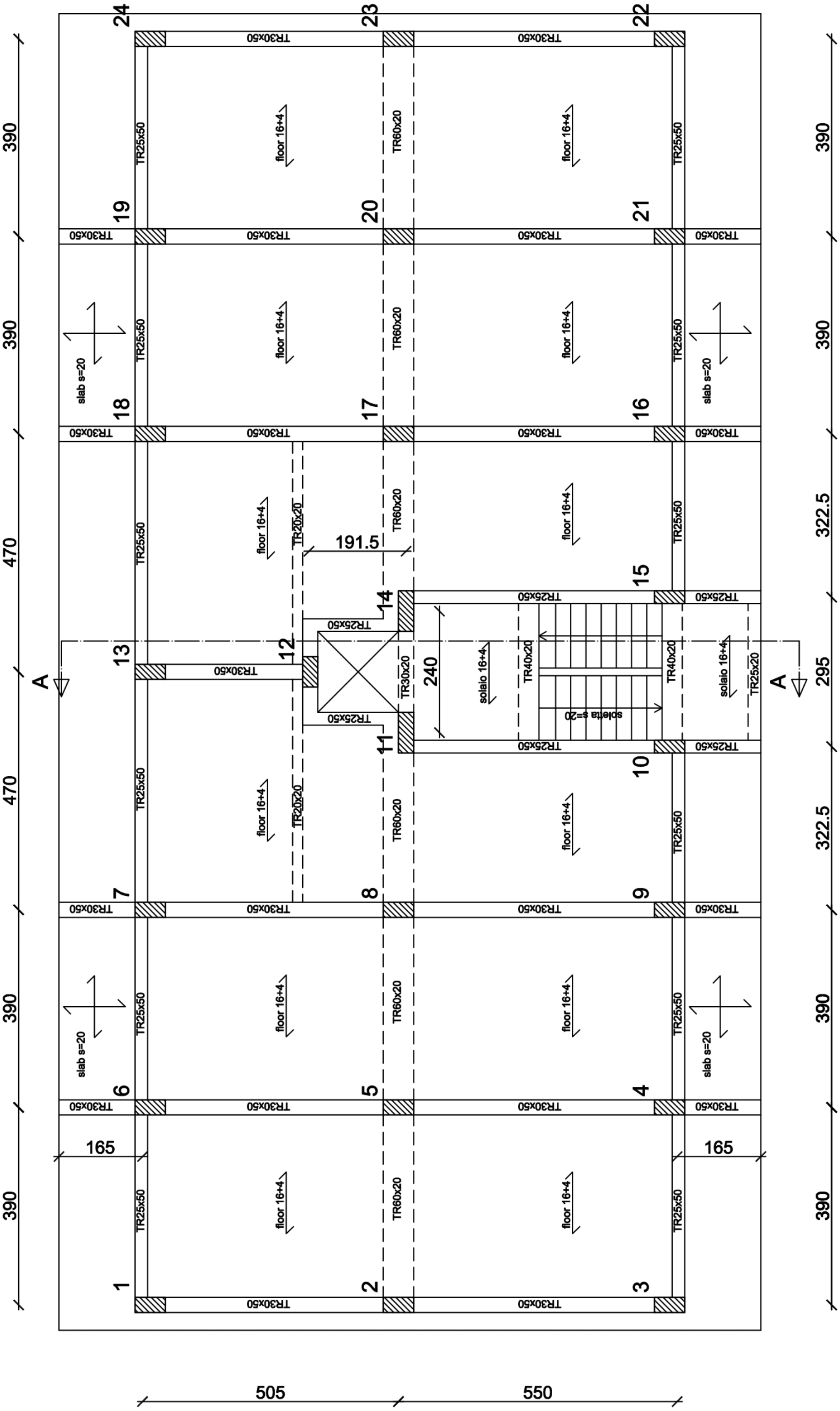

Figure 6-4. Beams layout of the fifth floor (H=14.8m).

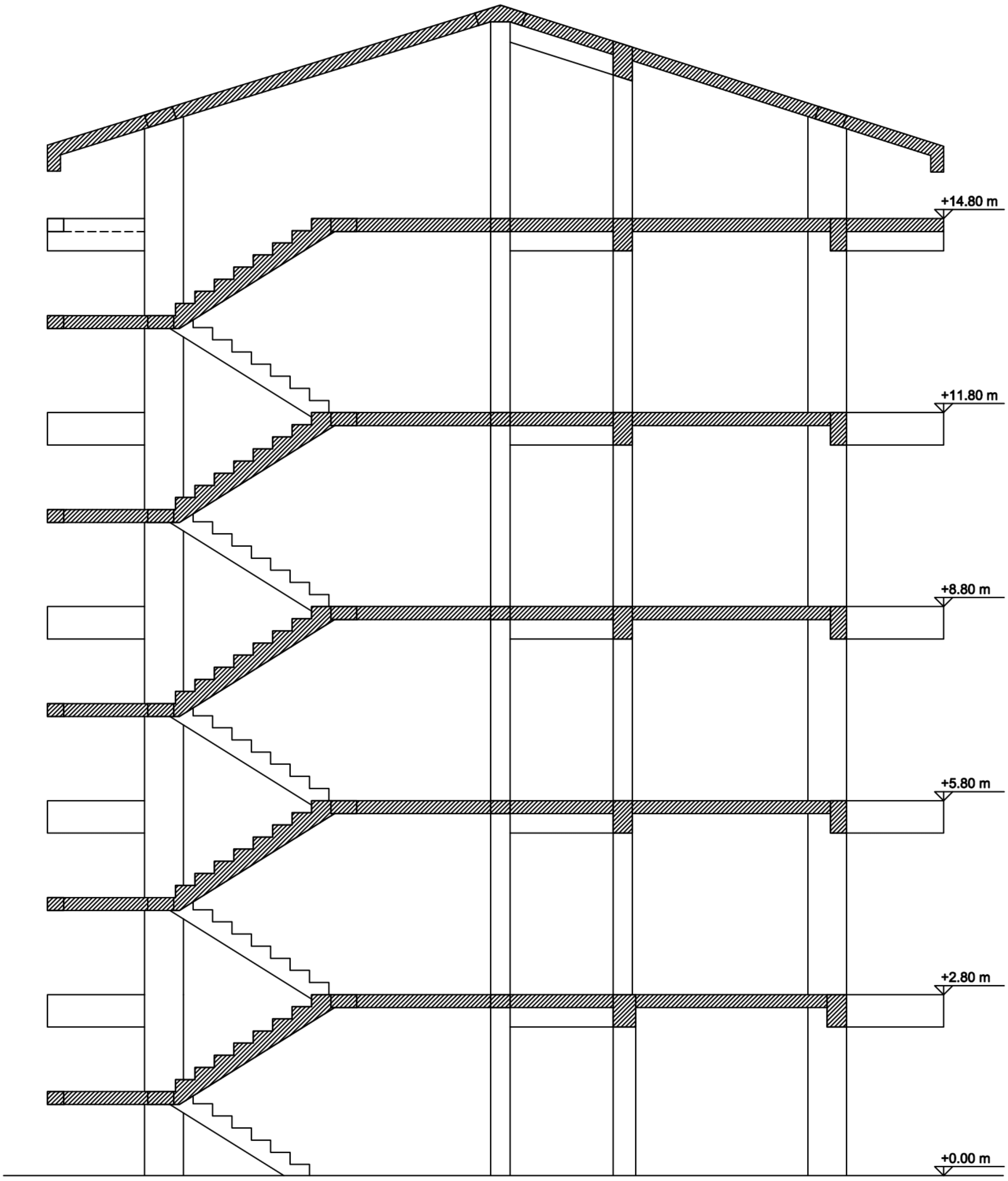

Figure 6-5. Section A-A of the building.

The sections of the columns with the particular of the reinforcements are shown Table 3 while the section of the beams with their reinforcement are summarized in Table 4 and Table 5.

Table 3

	COLUMNS					
	1,2,3,4,5,6,7,8,9,12,13,16 17,18,19,20,21,22,23,24		10,15		11,14	
Floor 0	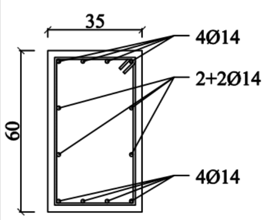		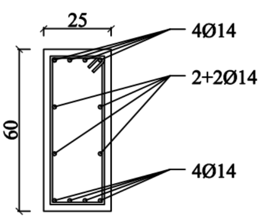		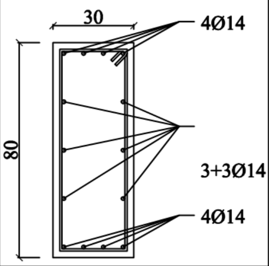	
	Stirrups	Ø8/15	Stirrups	Ø8/10	Stirrups	Ø8/15
	Longitudinal bars	12Ø14	Longitudinal bars	12Ø14	Longitudinal bars	14Ø14
Floor 1, 2	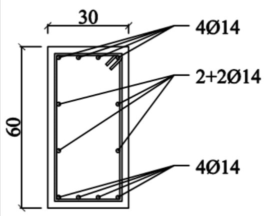		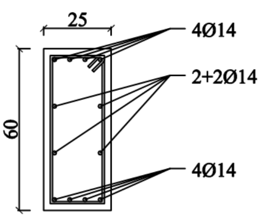		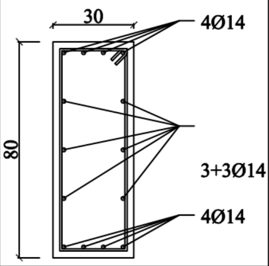	
	Stirrups	Ø8/15	Stirrups	Ø8/10	Stirrups	Ø8/15
	Longitudinal bars	12Ø14	Longitudinal bars	12Ø14	Longitudinal bars	14Ø14
Floor 3, 4	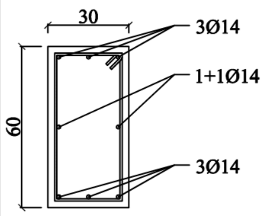		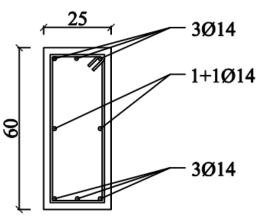		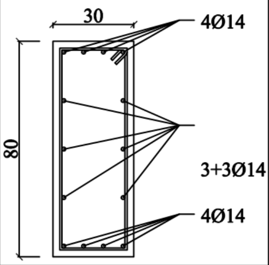	
	Stirrups	Ø8/15	Stirrups	Ø8/10	Stirrups	Ø8/15
	Longitudinal bars	8Ø14	Longitudinal bars	8Ø14	Longitudinal bars	14Ø14
Attic	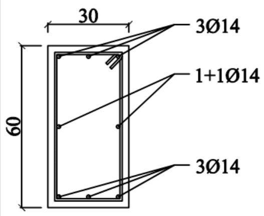		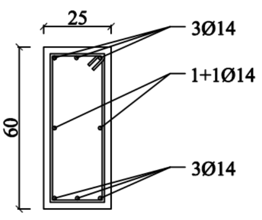		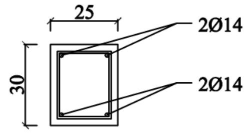	
	Stirrups	Ø8/15	Stirrups	Ø8/10	Stirrups	Ø8/10
	Longitudinal bars	8Ø14	Longitudinal bars	8Ø14	Longitudinal bars	8Ø14

Table 4

FLOOR 1 BEAMS						
SPAN	**SECTION**	**B**	**H**	**UPPPER BARS**	**LOWER BARS**	**STIRRUPS**
Column A - Column B		[cm]	[cm]	[mm]	[mm]	[mm]
1-2 5-6 7-8 18-17 19-20 24-23 2-3 5-4 8-9 17-16 20-21 23-22	A	35	50	8φ14	4φ14	8φ/250
	B	35	50	8φ14	4φ14	8φ/250
10-11 15-14	A	25	50	6φ14	4φ14	8φ/250
	B	25	50	6φ14	4φ14	8φ/250
12-13	A	35	50	6φ14	4φ14	8φ/250
	B	35	50	6φ14	4φ14	8φ/250
11-12 14-12	A	25	50	3φ14	2φ14	8φ/150
	B	25	50	3φ14	2φ14	8φ/150
1-6 3-4 24-19 22-21	A	30	50	6φ14	5φ14	8φ/250
	B	30	50	7φ14	5φ14	8φ/250
6-7 4-9 19-18 21-16	A	30	50	7φ14	5φ14	8φ/250
	B	30	50	7φ14	5φ14	8φ/250
7-13 18-13	A	30	50	7φ14	3φ14	8φ/250
	B	30	50	7φ14	3φ14	8φ/250
2-5 5-8 23-20 20-17 8-11 17-14	A	60	20	5φ14	5φ14	8φ/200
	B	60	20	5φ14	5φ14	8φ/200
9-10 16-15	A	30	50	7φ14	5φ14	8φ/250
	B	30	50	7φ14	6φ14	8φ/250
11-14	A	30	20	3φ14	3φ14	8φ/250
	B	30	20	3φ14	3φ14	8φ/250

Table 5

FLOOR 2,3,4,5 BEAMS						
SPAN	**SECTION**	**B**	**H**	**UPPPER BARS**	**LOWER BARS**	**STIRRUPS**
Column A - Column B		[cm]	[cm]	[mm]	[mm]	[mm]
1-2 5-6 7-8 18-17 19-20 24-23 2-3 5-4 8-9 17-16 21-21 23-22	A	30	50	8φ14	4φ14	8φ/250
	B	30	50	8φ14	4φ14	8φ/250
10-11 15-14	A	25	50	6φ14	4φ14	8φ/200
	B	25	50	6φ14	4φ14	8φ/200
12-13	A	30	50	6φ14	4φ14	8φ/250
	B	30	50	6φ14	4φ14	8φ/250
11-12 14-12	A	25	50	3φ14	2φ14	8φ/150
	B	25	50	3φ14	2φ14	8φ/150
1-6 3-4 24-19 22-21	A	25	50	6φ14	4φ14	8φ/250
	B	25	50	6φ14	4φ14	8φ/250
6-7 4-9 19-18 21-16	A	25	50	6φ14	4φ14	8φ/250
	B	25	50	6φ14	4φ14	8φ/250
7-13 18-13	A	25	50	6φ14	3φ14	8φ/250
	B	25	50	6φ14	3φ14	8φ/250
2-5 5-8 23-20 20-17 8-11 17-14	A	60	20	5φ14	5φ14	8φ/200
	B	60	20	5φ14	5φ14	8φ/200
9-10 16-15	A	25	50	6φ14	4φ14	8φ/250
	B	25	50	6φ14	4φ14	8φ/250
11-14	A	30	20	3φ14	3φ14	8φ/250
	B	30	20	3φ14	3φ14	8φ/250

The loads applied on the structure are shown in Table 6

Table 6

ANALYSIS OF THE LOADS					
	G1 [kN/m²]	**G2 [kN/m²]**	**G2 [kN/m]**	**Q [kN/m²]**	**S [kN/m²]**
Typical floor [h=0.16+0.04 m]	2.4	3.4	-	2	-
Attic floor [h=0.16+0.04 m]	2.4	2.2	-	2	-
Attic slab [h=0.20 m]	5	2.2	-	2	-
Roof [h=0.16+0.04 m]	2.4	1.2	-	-	0.8
Roof slab [h=0.20m]	5	1.2	-	-	0.8
Balcony slab [h=0.20 m]	5	1.5	-	4	-
Stair landing floor [h=0.16+0.04 m]	2.4	1.96	-	4	-
Stair ramp slab [h=0.20 m]	5	3.75	-	4	-
External infill [h=2,5 m]	-	2.5	6.25	-	-
Ext. infill with openings [h=2,5 m]	-	2	5	-	-
Ext. attic infill [h=1,5 m]	-	2.5	3.75	-	-
Ext. attic infill with op. [h=1,5 m]	-	2	3	-	-
Stairs and int. infill [h=2,5 m]	-	2	5	-	-
Stairs and int. infill with op.[h=2,5m]	-	1.6	4	-	-

where

- G1 are the permanent structural loads
- G2 are the permanent nonstructural loads
- S is the snow load

In addition to these loads it is necessary to take into account also the weight of the beams and of the columns that is classified as a permanent structural load G1.

According to NTC2018 the inertial effect of the seismic action shall be evaluated taking into account the masses associated with all the gravity loads that appear in the combination

$$G_1 + G_2 + \sum_j \psi_{2j} Q_j \tag{6.1.1}$$

where ψ_{2j} is the combination coefficient for the variable action j. This coefficient is applied to the variable load of the floor with value 0.3 and to the variable loads of balconies and stairs with the value of 0.6 according to the prescription of NTC2018.

The values of the concrete parameters are summarized in Table 7 where f_{cm} is the medium compressive strength, E_c is the elastic modulus of the undamaged concrete and $E_{c,fess}$ is the elastic modulus of the cracked concrete.

Table 7

CONCRETE PARAMETERS			
	f_{cm} [N/mm^2]	**E_c [N/mm^2]**	**E_{c_fess} [N/mm^2]**
FLOOR 0 COLUMNS	22.4	28021.87	21016.40
FLOOR 1 COLUMNS	18.4	26416.06	19812.04
FLOOR 2 COLUMNS	18.4	26416.06	19812.04
FLOOR 3 COLUMNS	24.4	28750.12	21562.59
FLOOR 4 COLUMNS	24.4	28750.12	21562.59
FLOOR 5 COLUMNS	24.4	28750.12	21562.59
BEAMS	18.4	26416.06	13208.03
AVERAGE VALUE	**21.6**	**27717.80**	**20788.35**

In the realization of the model the average values have been used and the confinement of the concrete has been taken into account.

The steel used for the reinforcements is a Fe B44k and its parameters are shown in Table 8.

Table 8

STEEL PARAMETERS			
f_{ym} [N/mm^2]	**E_s [N/mm^2]**	**f_u [N/mm^2]**	**A [%]**
430.7	206000	540	>12

The building is situated in L'Aquila municipality, which geographical coordinates are

- Lon. = 13.394°
- Lat. = 42.366°

and so in seismic zone 2, characterized by a value of peak ground acceleration (PGA) on a rigid soil with probability of exceedance of 10% in 50 years between 0.15 and 0.25 g, according to the Italian seismic classification of the territory. The variation of the parameters a_g, F_0, and T_C^* ,necessary for the construction of the response spectrum, in function of the return period is shown in Table 9.

Table 9

T_R [years]	a_g [g]	F_0 [-]	T_C^* [s]
30	0.079	2.400	0.272
50	0.104	2.332	0.281
72	0.122	2.318	0.289
101	0.142	2.304	0.296
140	0.164	2.301	0.309
201	0.191	2.315	0.318
475	0.261	2.364	0.347
975	0.334	2.400	0.364
2475	0.452	2.458	0.384

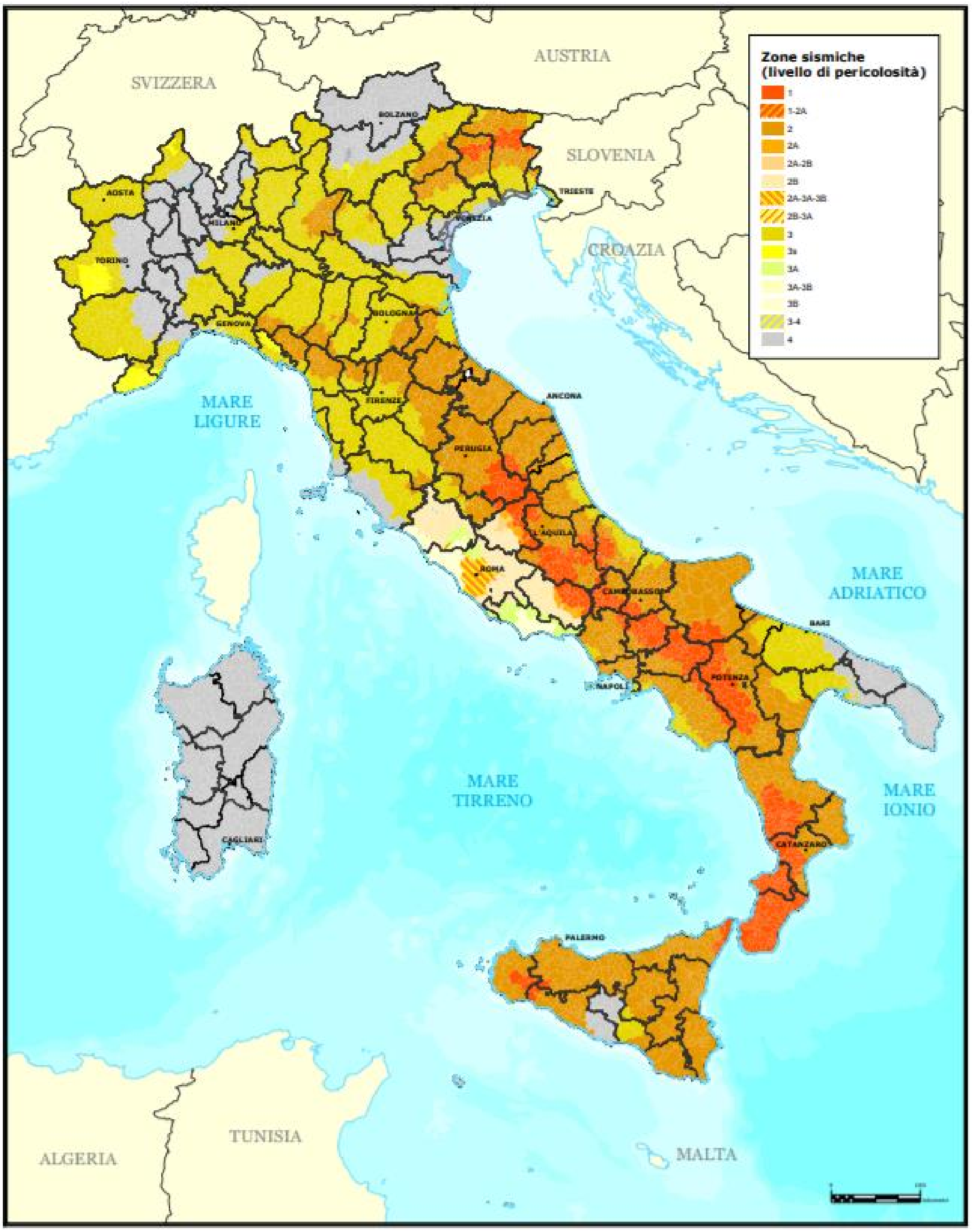

Figure 6-6. Seismic classification of the italian territory in 2015.

The soil is a ground type D according to the classification, shown in Figure 6-7, of the EC8 and NTC2018.

Ground type	Description of stratigraphic profile	Parameters		
		$v_{s,30}$ (m/s)	N_{SPT} (blows/30cm)	c_u (kPa)
A	Rock or other rock-like geological formation, including at most 5 m of weaker material at the surface.	> 800	–	–
B	Deposits of very dense sand, gravel, or very stiff clay, at least several tens of metres in thickness, characterised by a gradual increase of mechanical properties with depth.	360 – 800	> 50	> 250
C	Deep deposits of dense or medium-dense sand, gravel or stiff clay with thickness from several tens to many hundreds of metres.	180 – 360	15 - 50	70 - 250
D	Deposits of loose-to-medium cohesionless soil (with or without some soft cohesive layers), or of predominantly soft-to-firm cohesive soil.	< 180	< 15	< 70
E	A soil profile consisting of a surface alluvium layer with v_s values of type C or D and thickness varying between about 5 m and 20 m, underlain by stiffer material with v_s > 800 m/s.			
S_1	Deposits consisting, or containing a layer at least 10 m thick, of soft clays/silts with a high plasticity index (PI > 40) and high water content	< 100 (indicative)	–	10 - 20
S_2	Deposits of liquefiable soils, of sensitive clays, or any other soil profile not included in types A – E or S_1			

Figure 6-7. Classification of ground types according to EC8.

The topographical category is T1 according to NTC2018.

The importance class of the building, according to EC8, is II and the description is present in Table 10. The importance classes of EC8 are the same of the “classi d’uso” of the Italian code NTC2018.

Table 10

IMPORTANCE CLASS ACCORDING TO EC8	
CLASS IMPORTANCE	**BUILDINGS**
I	Buildings of minor importance for public safety, e.g. agricultural buildings, etc.
II	Ordinary buildings, not belonging in the other categories.
III	Buildings whose seismic resistance is of importance in view of the consequences associated with a collapse, e.g. schools, assembly halls, cultural institutions etc.
IV	Buildings whose integrity during earthquakes is of vital importance for civil protection, e.g. hospitals, fire stations, power plants, etc.

Each importance class is associated with an importance factor (in the Italian code is called C_U) that can be found in the nation annex for each country. In Italy the importance factor ("coefficient d'uso") for a building of class II is

$$C_U = 1$$

The seismic actions are evaluated for each structure in relation to a reference period V_r which is obtained, for the different construction types, multiplying the nominal life V_n by the importance factor C_U. The nominal life V_n is intended as the number of years for which the structure, subject to ordinary maintenance, must be used for its original purpose. The nominal life for an ordinary structure is 50 years so the reference period is

$$V_R = V_N C_U = 50 \ years \tag{6.1.2}$$

In conclusion, the parameters for the evaluation of the elastic response spectrum for the building site are summarized in Table 11.

Table 11

PARAMETERS FOR THE EVALUATION OF THE ELASTIC SPECTRA						
Long.	**Lat.**	**V_n**	**C_U**	**V_R**	**Ground category**	**Topographical Category**
13.3944°	42.366°	50	1	50	D	T1

The NTC2018 includes four limit states:

- Stato Limite di Operatività (SLO);
- Stato Limite di Danno (SLD);
- Stato Limite di salvaguardia della Vita (SLV);
- Stato Limite di prevenzione del Collasso (SLC).

SLO and SLD are called serviceability limit states and describe the limit for which the structure must maintain its functions. SLV and SLC are the ultimate limit state and are related to the ultimate resistance that the structure must guarantee after an earthquake. Each one of these limit state is related to a probability of exceedance P_{Vr} in the reference period V_r as shown in Table 12.

Table 12

Limit state		$\mathbf{P_{Vr}}$
Serviceability	SLO	81%
	SLD	63%
Ultimate	SLV	10%
	SLC	5%

The four elastic response spectrum, in accelerations and displacements, in the site of the building for the different limit state are shown in the following figure and in the following tables are present the parameters necessary for the realization of the spectra.

Table 13

SLO												
INDEPENDENT PARAMETERS							**DEPENDENT PARAMETERS**					
a_g [g]	**F_0**	**T_C* [s]**	**S_s**	**C**	**S_T**	**q**	**S**	**η**	**T_B [s]**	**T_C [s]**	**T_D [s]**
0.079	2.399	0.272	1.800	2.396	1.000	1.000	1.800	1.000	0.217	0.652	1.916

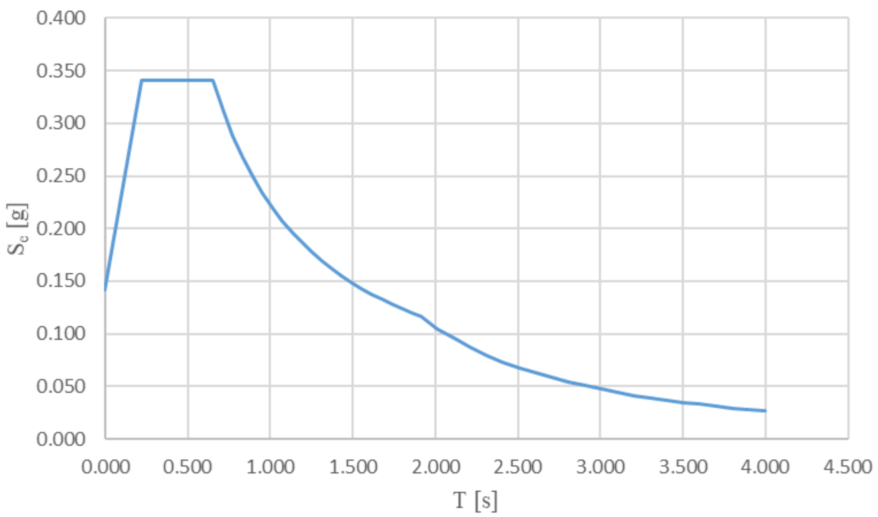

Figure 6-8. Elastic response spectrum in accelerations (SLO).

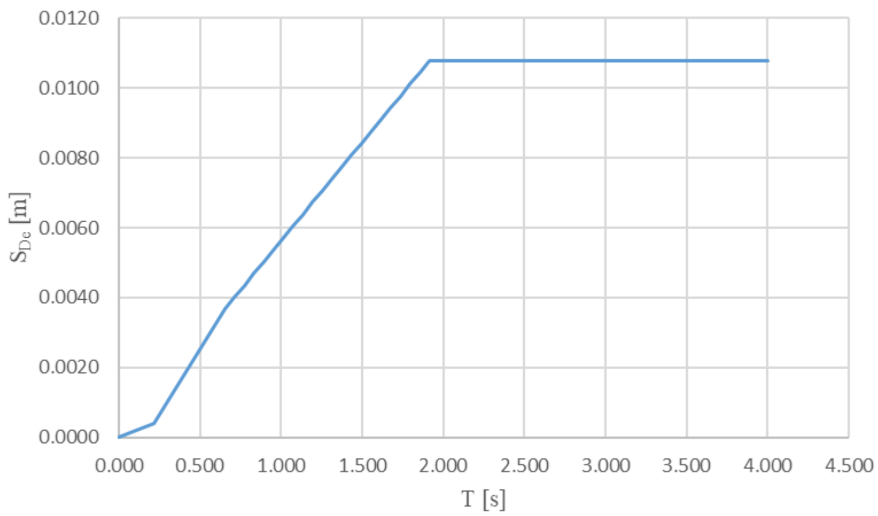

Figure 6-9. Elastic response spectrum in displacements (SLO).

Table 14

SLD											
INDEPENDENT PARAMETERS							**DEPENDENT PARAMETERS**				
a_g [g]	**F_0**	**T_C* [s]**	**S_s**	**C**	**S_T**	**q**	**S**	**η**	**T_B [s]**	**T_C [s]**	**T_D [s]**
0.104	2.332	0.281	1.800	2.358	1.000	1.000	1.800	1.000	0.221	0.663	2.017

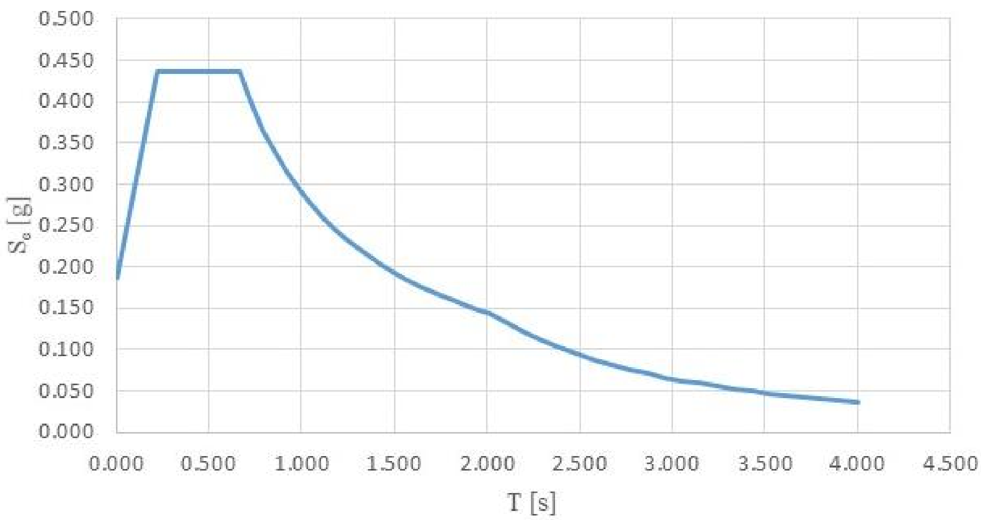

Figure 6-10. Elastic response spectrum in accelerations (SLD).

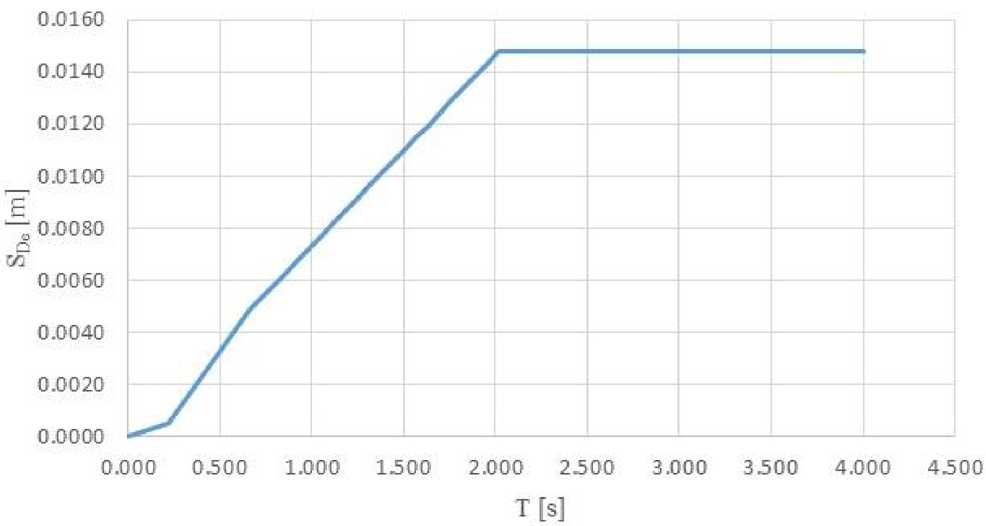

Figure 6-11. Elastic response spectrum in displacements (SLD).

Table 15

SLV											
INDEPENDENT PARAMETERS							**DEPENDENT PARAMETERS**				
a_g [g]	**F_0**	**T_C* [s]**	**S_s**	**C**	**S_T**	**q**	**S**	**η**	**T_B [s]**	**T_C [s]**	**T_D [s]**
0.261	2.364	0.347	1.476	2.124	1.000	1.000	1.476	1.000	0.245	0.736	2.643

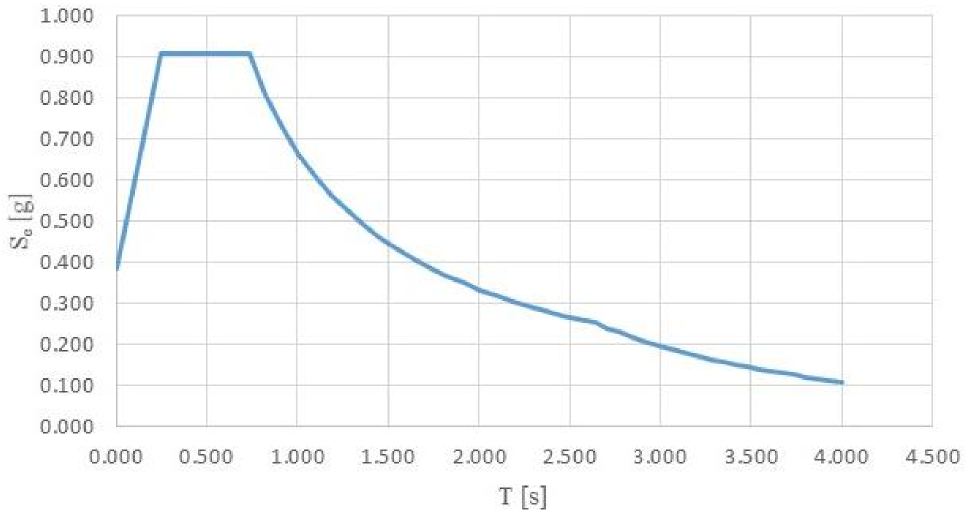

Figure 6-12. Elastic response spectrum in accelerations (SLV).

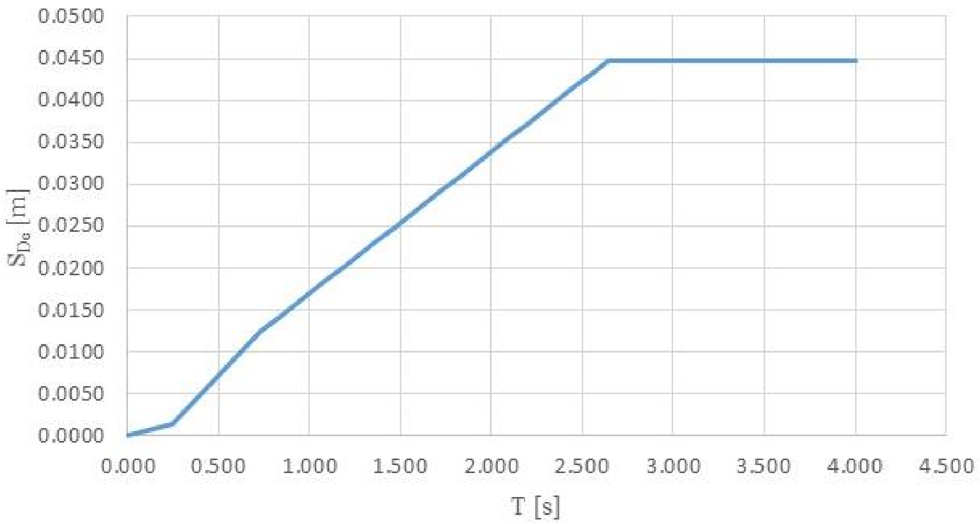

Figure 6-13.Elastic response spectrum in displacements (SLV).

Table 16

SLV											
INDEPENDENT PARAMETERS							**DEPENDENT PARAMETERS**				
a_g [g]	**F_0**	**T_C* [s]**	**S_s**	**C**	**S_T**	**q**	**S**	**η**	**T_B [s]**	**T_C [s]**	**T_D [s]**
0.334	2.400	0.364	1.198	2.072	1.000	1.000	1.198	1.000	0.251	0.754	2.936

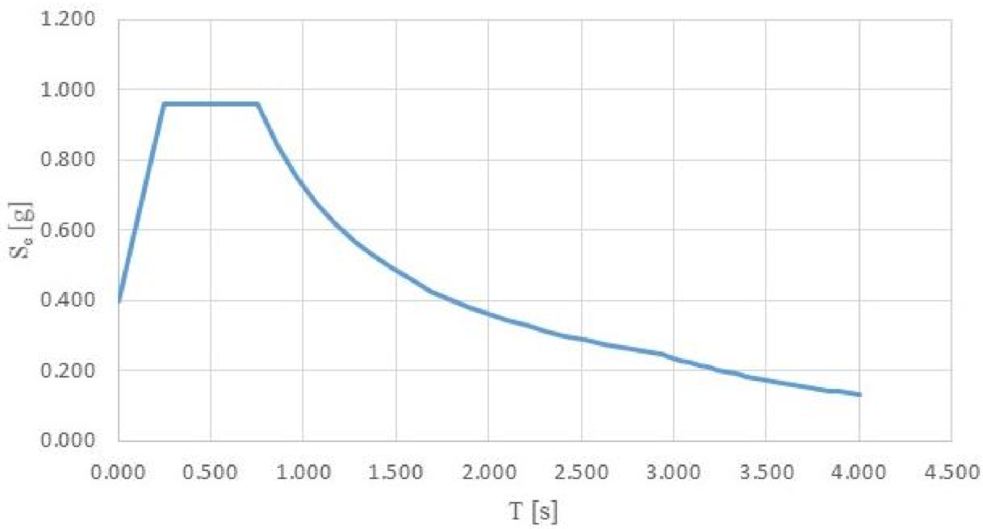

Figure 6-14. Elastic response spectrum in accelerations (SLC).

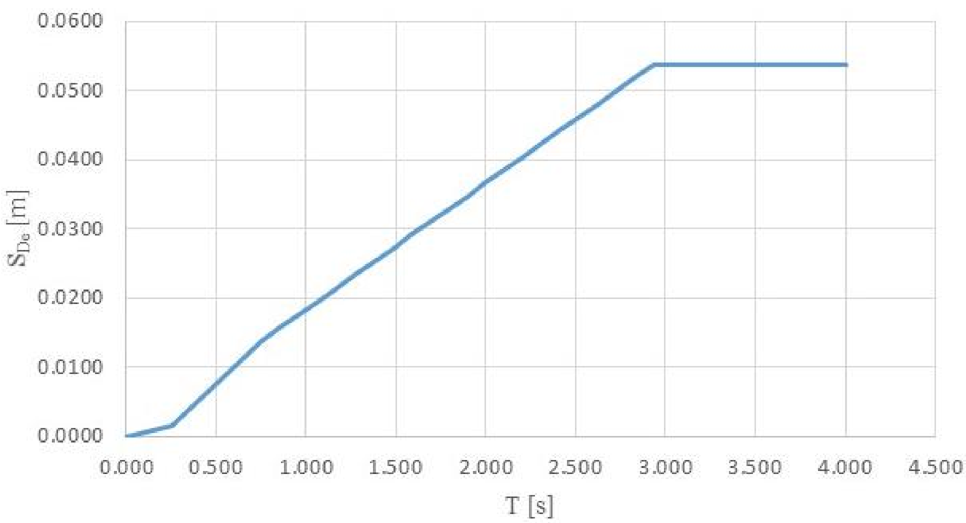

Figure 6-15. Elastic response spectrum in displacements (SLC).

6.2 Realization of the finite element model

The finite element model of the building and the nonlinear analysis were realized using the object-oriented, open source software framework OpenSees (*McKenna* 2000) (Open System for Earthquake Engineering Simulation). This software was created at the Pacific Earthquake Engineering (PEER) Center with the participation of the University of California, Berkeley. OpenSees is primarily written in C++ and allows users to create finite element computer applications for simulating the response of structural and geotechnical systems subjected to earthquakes

The inconvenient of OpenSees is the lack of any graphical interface. The input data (geometry, mechanical parameters, external actions and analysis options) are assigned by means of a file written in the TCL language and the output consists of simple text files that report the results of the structural analysis without any post-processor that makes them suitable for the design or verification of the structure. This characteristic of the software could cause some problems in the realization of a model that requires an elevated numbers of nodes, elements and sections as the building that is used in the study case of this thesis. For this reason the model was realized using the software OpenSees Navigator that is a graphical user interface (GUI) pre- and post-processor for the OpenSees software framework.

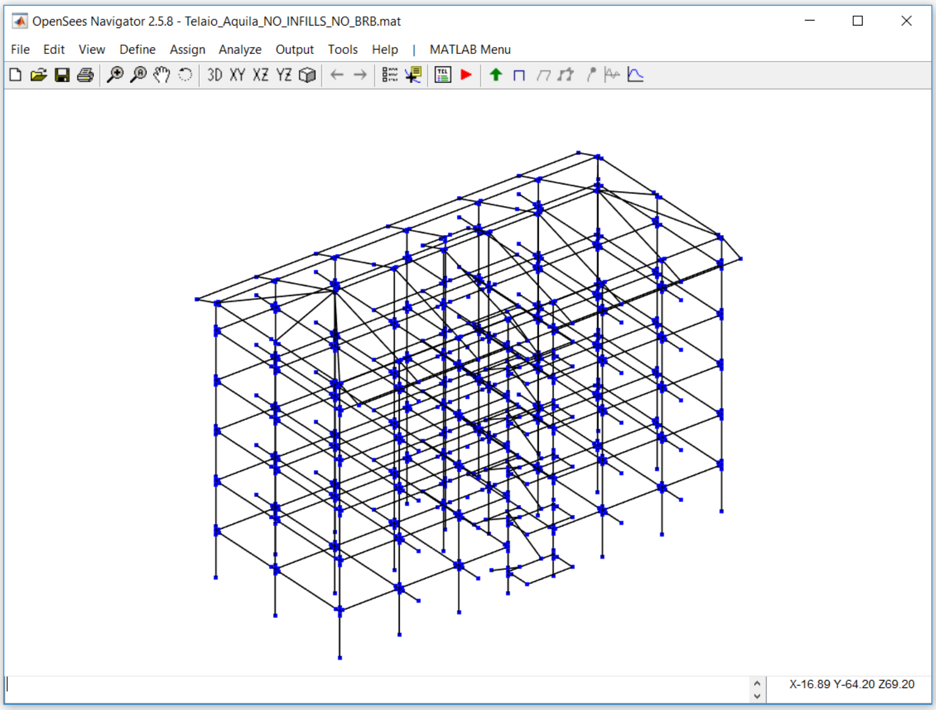

Figure 6-16. Opensees Navigator interface.

6.2.1 Definition of the geometry

The geometry of the model is defined creating the nodes and the line elements through the commands *edit>node* and *edit>element*. It is also possible to import the position of the nodes and of the elements from models realized with other finite elements software through a .s2k file.

In this particular case the geometry of the building was realized using Sap2000 that permits to define faster and with simpler commands the position of all the elements and then it was imported into OpenSees navigator using the .s2k file.

In order to take into account the increased stiffness in the beam-to-column joints it was necessary to define two rigid zone at the end of each column and beam. These rigid zones were defined as *ElasticBeamColumn* elements with increased values of elastic modulus E, cross sectional area A and moments of inertia around the two local axis in order to obtain higher values of stiffness compared to that of the columns and the beams.

Some views of the model realized in OpenSees Navigator are shown in the following images.

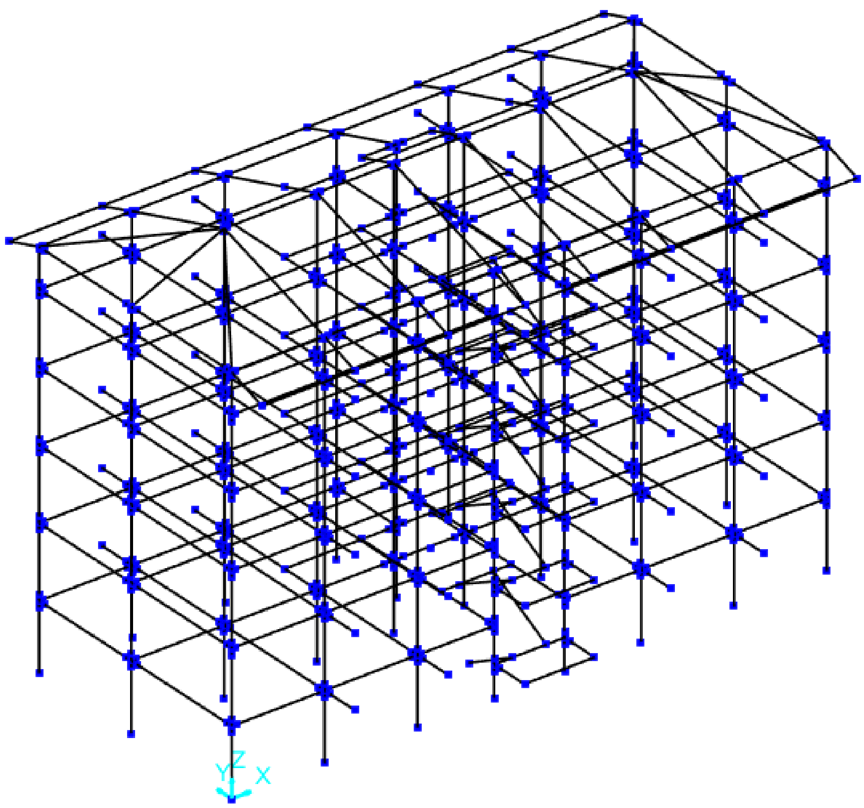

Figure 6-17. 3D view of the model.

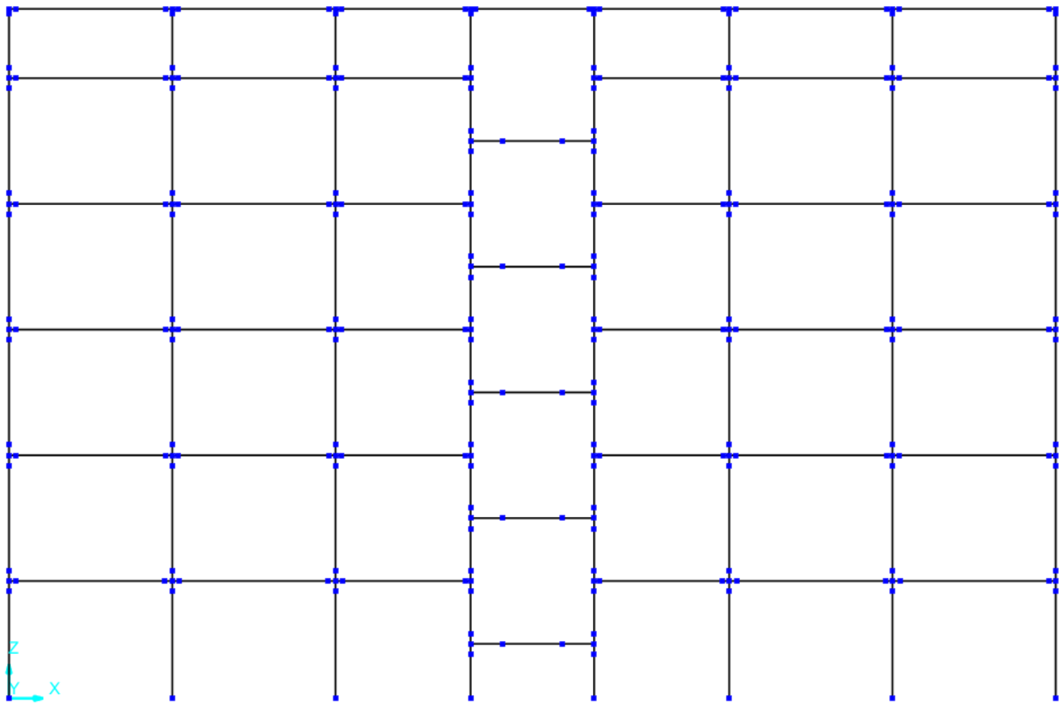

Figure 6-18. XZ plan view of the frame Y=0 m.

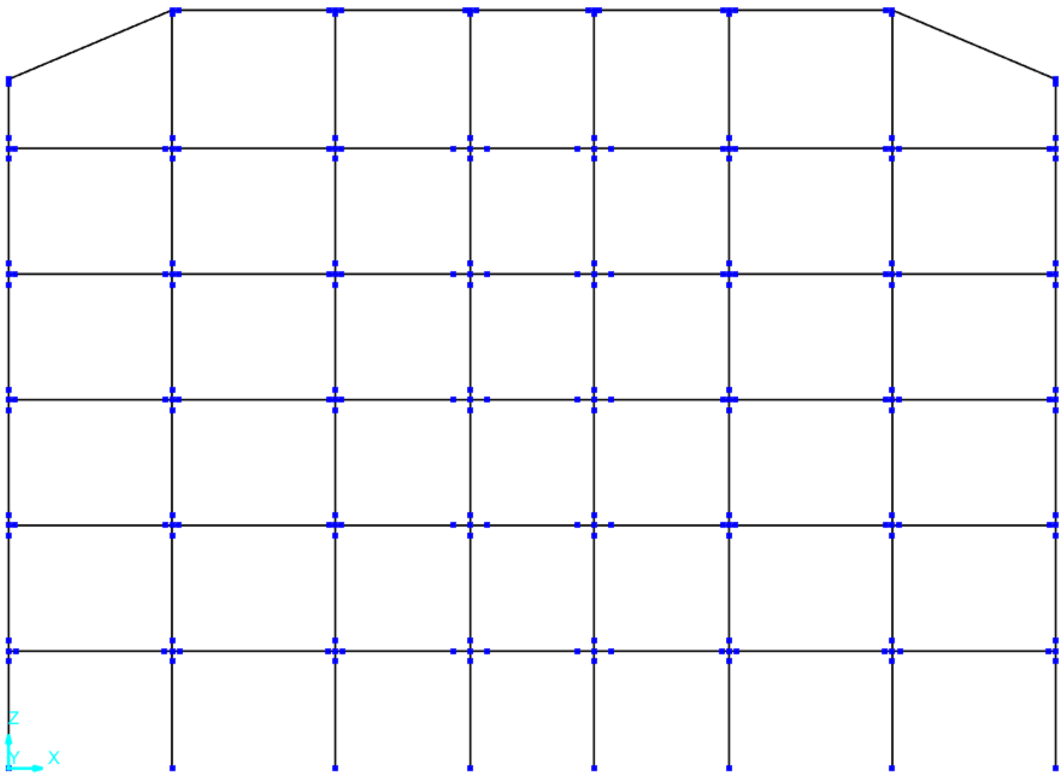

Figure 6-19. XZ plan view of the frame Y=5.5 m.

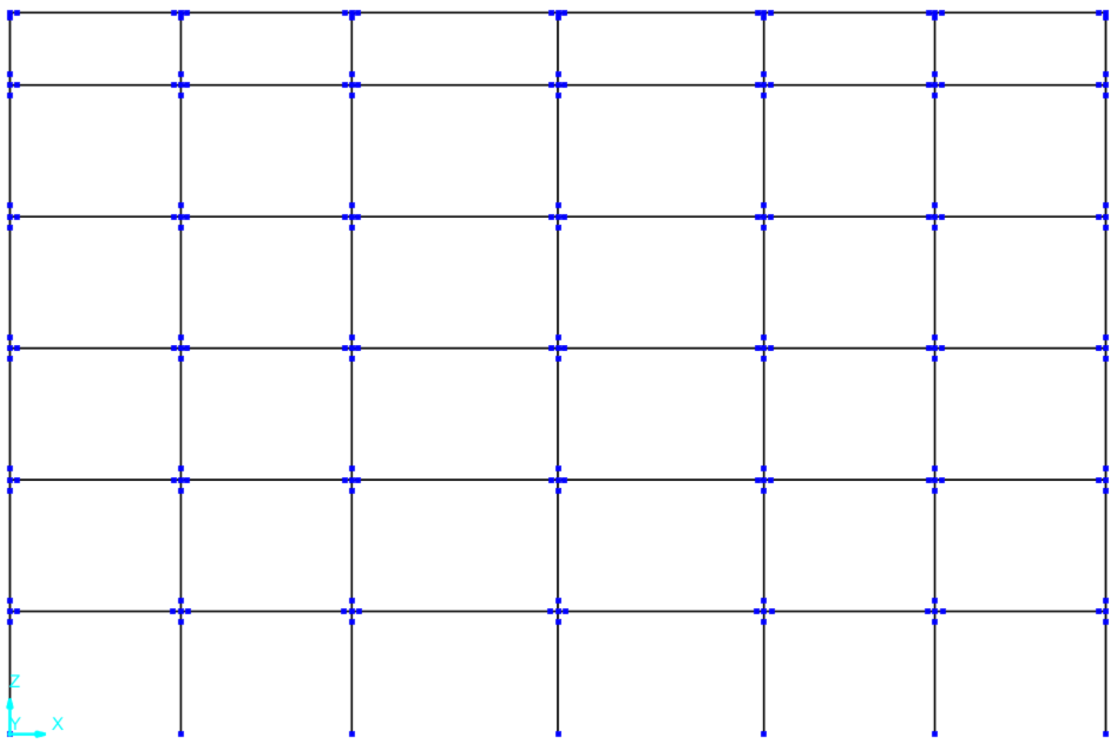

Figure 6-20. XZ plan view of the frame Y=10.55 m.

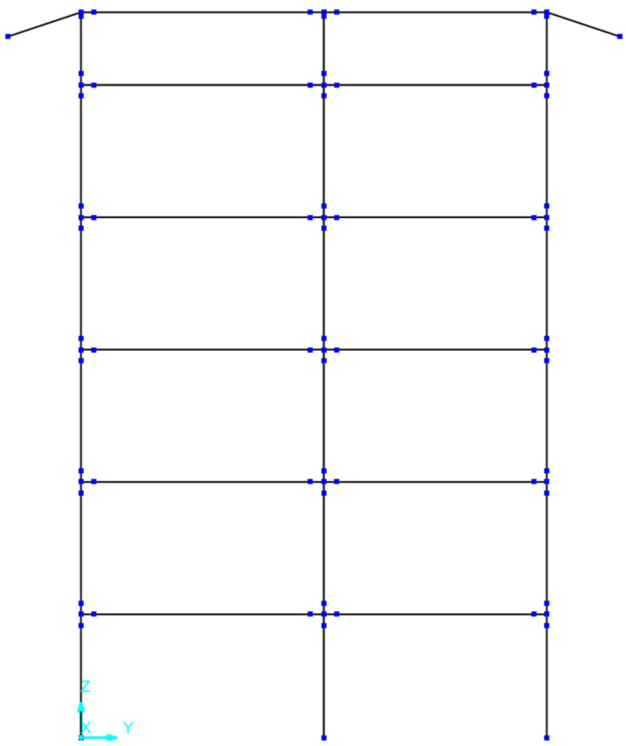

Figure 6-21. YZ plan view of the frame X=0 m.

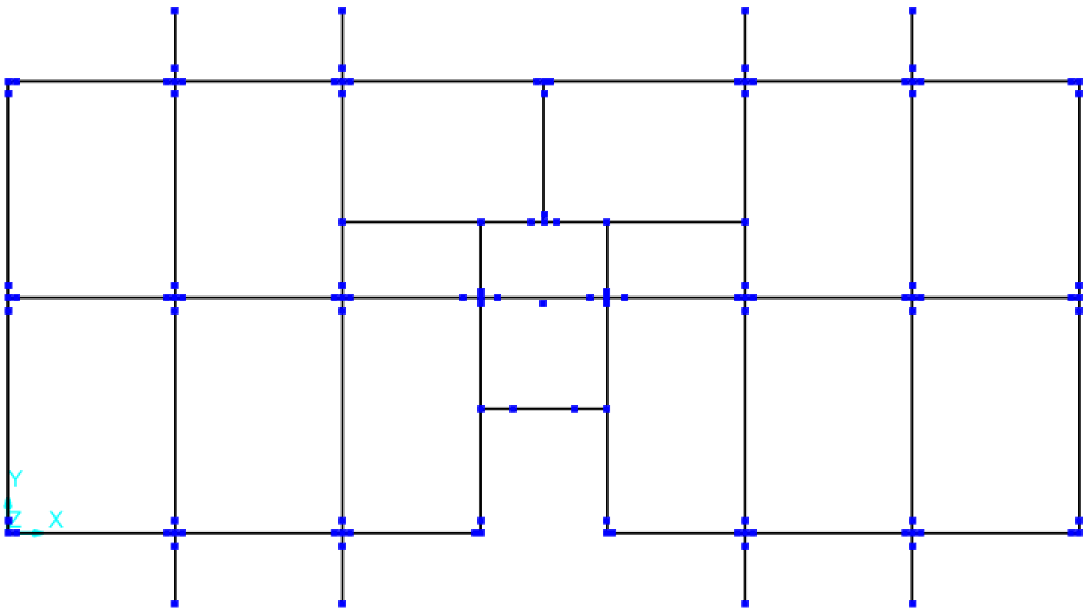

Figure 6-22. XY plan view of the typical floor (Z=2.8, 5.8, 8.8, 11.8, 14.8).

6.2.2 Definition of the materials

CONCRETE

In order to define the concrete parameters were used the average values defined in Table 7. The constitutive law used for the unconfined and confined concrete is given by the OpenSees *uniaxialMaterial Concrete02* command. This command is used to construct a uniaxial concrete material object with tensile strength and linear tension softening. The command string for generating this material is

uniaxialMaterial Concrete02 $matTag $fpc $epsc0 $fpcu $epscu $lambda $ft $Ets

where

- $fpc: is the compressive strength (input as a negative value);
- $epsc0: is the strain at compressive strength (input as a negative value);
- $fpcu: is the crushing strength (input as a negative value);
- $epscu: is the strain at crushing strength (input as a negative value);
- $lambda: is the ratio between unloading slope at $epscu and initial slope;
- $ft: is the tensile strength;
- $Ets: is the slope of the linear tension softening branch.

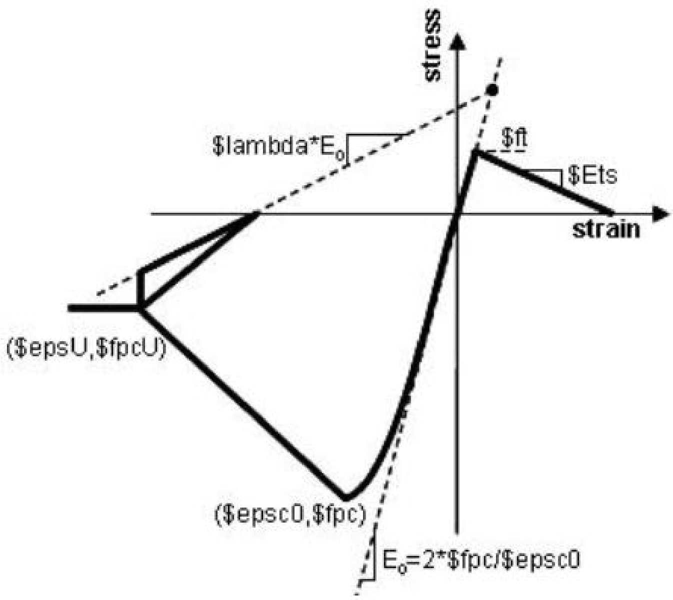

Figure 6-23. UniaxialMaterial Concrete02 stress-strain relationship.

The stress-strain relationship for this type of material is shown in Figure 6-23. The tensile strength was set to 0.1fcp. The problem of this type of uniaxial material is that the stress-strain relationship after the reaching of the crushing strength continues with a plateau without decreasing under monotonic load. This can cause an unrealistic response of the structure, especially in the evaluation of the pushover curve. To avoid this problem was necessary to construct a MinMax material object by means of the command *uniaxialMaterial MinMax*. This command constructs a material that has the same stress-strain behavior of a uniaxial material defined previously but if the strain falls above or below certain threshold values the material is assumed to fail and the values of stress and tangent are set to 0. The string command for this type of material is

```
uniaxialMaterial MinMax $matTag $otherTag <-min $minStrain> <-max $maxStrain>
```

where

- \$otherTag: is the tag of the other material that define the stress-strain relationship;
- \$minStrain: is the minimum value of strain;
- \$maxStrain: is the maximum value of strain.

In the realization of the model was taken into account the confinement of the core concrete of the beams and of the columns. The confined concrete constitutive law was obtained using Mander's model (*Mander et al.* 1988). Mander et al. developed this model because was noticed that the confinement of concrete by transverse reinforcement results in a significant increase in both the strength and the ductility of the compressed material. This effect can be seen in Figure 6-24.

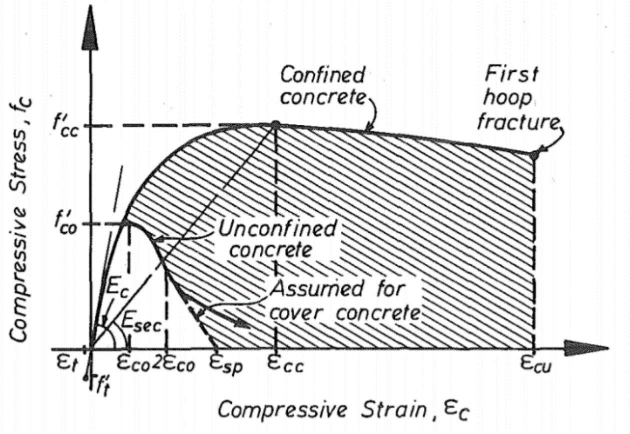

Figure 6-24. Stress-strain model for confined and unconfined concrete (Mander et al. 1988).

The compressive strength of the confined concrete is increased thanks to the compressive effect provided by the stirrups and the longitudinal reinforcement. For this reason the confinement of the material depends on the geometry of the section and of the reinforcements.

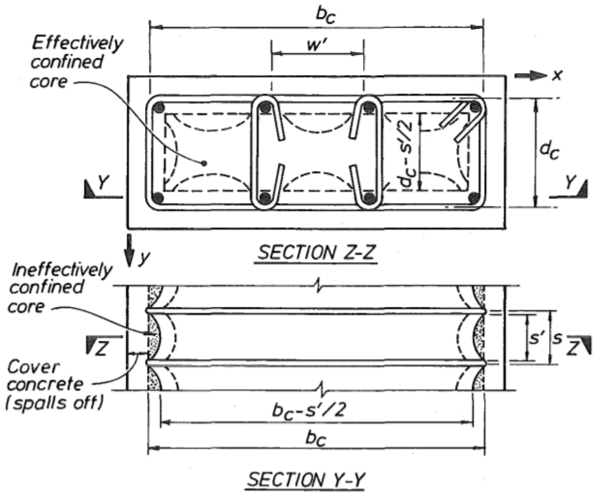

Figure 6-25. Effectively confined core.

The compressive strength of the confined concrete is given by eq.

$$f'_{cc} = f'_{co}\left(-1.254 + 2.254\sqrt{1+\frac{7.94 f'_l}{f'_{co}}} - 2\frac{f'_l}{f'_{co}}\right) \tag{6.2.1}$$

where f'_{co} is the compressive strength of the unconfined concrete and f'_l depends on the geometry of the section and of the reinforcements.

The ultimate compressive strain ε_{cu} corresponds to the rupture of the firs hoop and it can be found using a method (*Mander* 1984) that is based on an energy balance approach. This approach considers the additional ductility given by the confinement to be due to the energy stored in the transverse reinforcement.

The values of the parameters assigned to the concrete02 materials, calculated taking into account Mander's model in case of confined concrete are shown in Table 17.

As anticipated before an equal number of MinMax materials, to which the Concrete02 materials were assigned, was created setting as maximum value of compressive strain equal to -0.012 for the confined materials and -0.0035 for the unconfined cls.

Table 17

CONCRETE02 MATERIALS							
Name	**fpc [kN/m^2]**	**epsc0**	**fpcu [kN/m^2]**	**epsU**	**lambda**	**ft [kN/m^2]**	**Ets [kN/m^2]**
0_Pil25x30_liv6_ConfinedCls	-24476	-0.0033	-16490	-0.0161	0.5	2448	2000000
0_Pil25x60_liv123_ConfinedCls	-24348	-0.00327	-17440	-0.01334	0.5	2435	2000000
0_Pil25x60_liv456_ConfinedCls	-22610	-0.00247	-11600	-0.01406	0.5	2261	2000000
0_Pil30x60_liv23_ConfinedCls	-24089	-0.00315	-17370	-0.01219	0.5	2409	2000000
0_Pil30x60_liv456_ConfinedCls	-22824	-0.00257	-13140	-0.01265	0.5	2282	2000000
0_Pil30x80_liv123_ConfinedCls	-23333	-0.0028	-15410	-0.01175	0.5	2333	2000000
0_Pil35x60_liv1_ConfinedCls	-23867	-0.00305	-17230	-0.0114	0.5	2387	2000000
0_Tr20x20_Elev12345_ConfinedCls	-25031	-0.00359	-17350	-0.01752	0.5	2503	2000000
0_Tr25x50_Elev12345(11-12 14-12)_ConfinedCls	-23683	-0.00296	-13730	-0.0176	0.5	2368	2000000
0_Tr25x50_Elev12345Cop_ConfinedCls	-22876	-0.00259	-13460	-0.01242	0.5	2288	2000000
0_Tr30x20_Elev12345_ConfinedCls	-24131	-0.00317	-15870	-0.01544	0.5	2413	2000000
0_Tr30x50_Cop_ConfinedCls	-23530	-0.0029	-16400	-0.01117	0.5	2353	2000000
0_Tr30x50_Elev12345_ConfinedCls	-22931	-0.00262	-14310	-0.01135	0.5	2293	2000000
0_Tr35x50_Elev1_ConfinedCls	-22958	-0.00263	-14910	-0.01062	0.5	2296	2000000
0_Tr40x20_Scale_ConfinedCls	-23335	-0.0028	-13880	-0.0146	0.5	2334	2000000
0_Tr45x20_Cop_ConfinedCls	-22981	-0.00264	-12810	-0.01436	0.5	2298	2000000
0_Tr60x20_Elev12345_ConfinedCls	-22024	-0.00219	-8210	-0.01649	0.5	2202	2000000
0_Tr65x20_Cop_ConfinedCls	-21608	-0.002	-6390	-0.01649	0.5	2161	2000000
0_Tr70x20_Cop_ConfinedCls	-21600	-0.00185	-5710	0.01399	0.5	2160	2000000
0_UnconfinedCls	-21600	-0.00181	-11570	-0.0035	0.5	2160	2000000

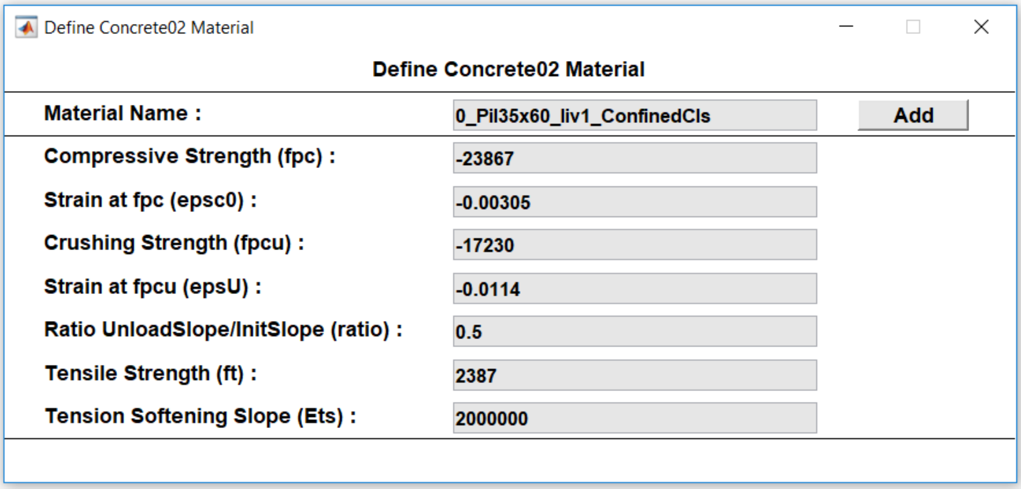

Figure 6-26. Definition of Concrete02 material in OpenSees Navigator.

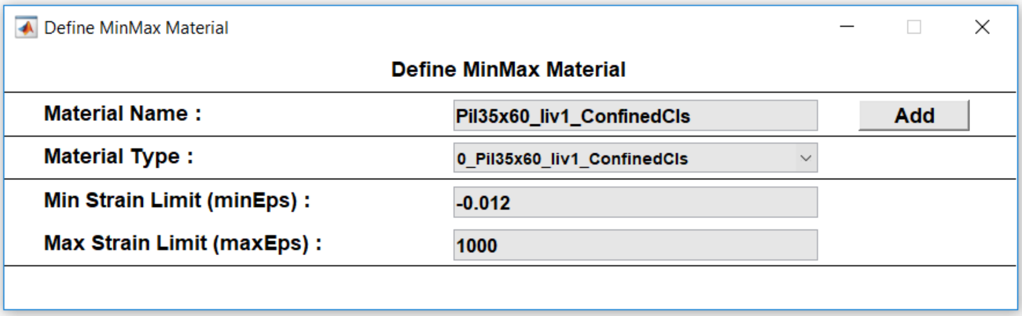

Figure 6-27. Definition of MinMax material in OpenSees Navigator.

STEEL

In order to define the steel parameters were used the average values defined in Table 7. The constitutive law used for the reinforcement steel is given by the OpenSees *uniaxialMaterial Steel01* command. This command is used to construct a uniaxial bilinear steel material object with kinematic hardening and optional isotropic hardening. The command string for generating this material is

uniaxialMaterial Steel01 $matTag $Fy $E0 $b <$a1 $a2 $a3 $a4>

where

- $Fy: is the yield strength;
- $E0: is the initial elastic tangent;
- $b: is the strain hardening ratio (ratio between post-yield tangent and initial elastic tangent);
- $a1,$a2,$a3,$a4: are isotropic hardening parameters.

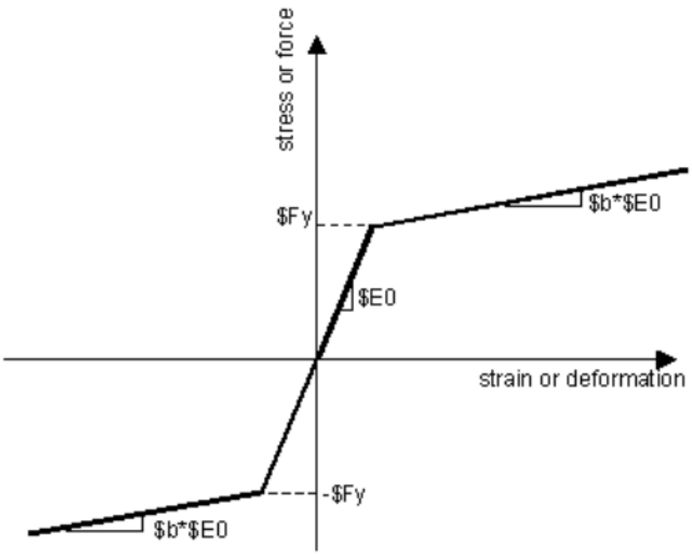

Figure 6-28. UniaxialMaterial Steel01 stress-strain relationship.

As well as the concrete, a MinMax material was introduced to simulate the rupture of the reinforcement bars at a strain of 0.075 both in tension and compression. This threshold was chosen for safety reason even if the ultimate elongation of the Fe B44k is greater than 12% as reported in Table 8.

The values of the parameters assigned to the steel01 material are shown in

Table 18

STEEL01 MATERIAL							
Name	**E [kN/m²]**	**Fy [kN/m²]**	**b**	**a1**	**a2**	**a3**	**a4**
Steel	206000000	430700	0	0	1	0	1

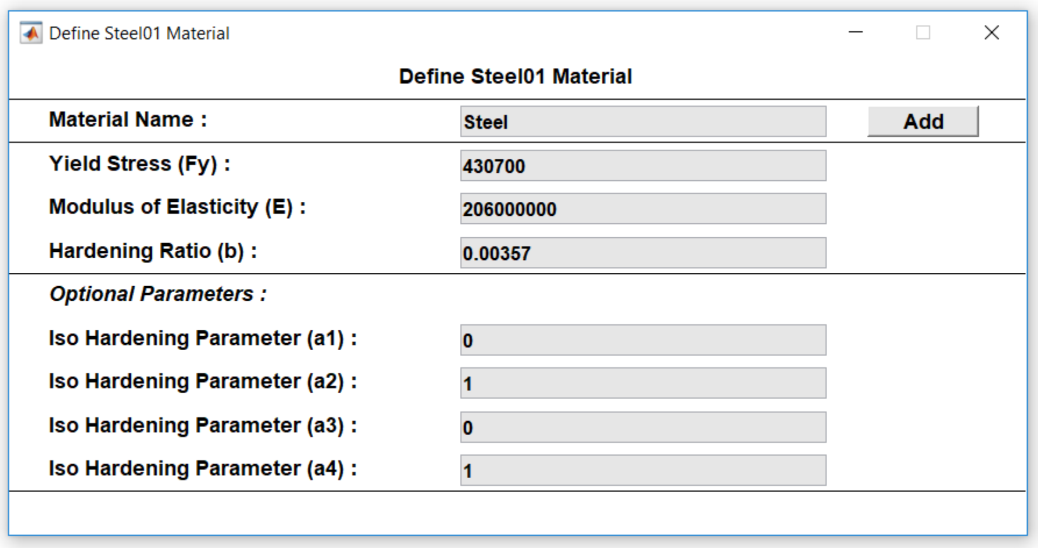

Figure 6-29. Definition of Steel01 material in OpenSees Navigator.

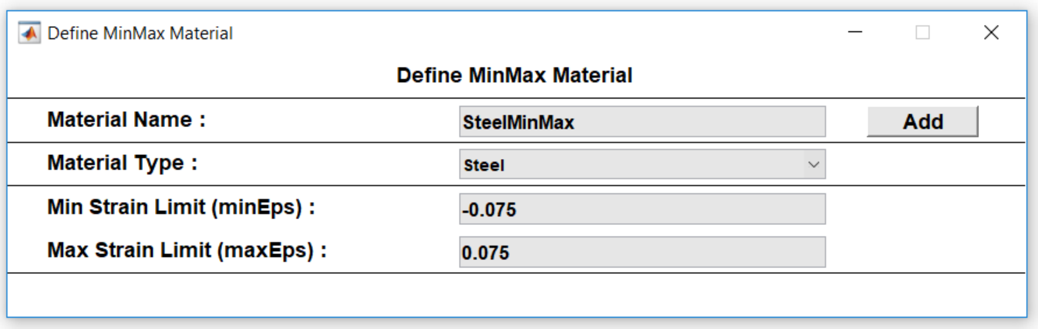

Figure 6-30. Definition of MinMax material in OpenSees Navigator.

6.2.3 Fiber elements

There are two types of nonlinearity

- Geometrical nonlinearity: given by the deformation of the structure that goes out of the hypothesis of small displacements with the consequent displacement of the points of application of loads with respect to the undeformed configuration. This type of nonlinearity is taken into account considering the P-delta effects.
- Mechanical nonlinearity: given by the plasticity and therefore by the constitutive law of the materials that compose a certain section of an element.

In order to take into account the mechanical nonlinearity there are two ways, concentrated plasticity and distributed plasticity.

In case of concentrated plasticity the plasticity is considered only in a single section, in which is placed a plastic hinge modelled as a nonlinear spring that has the same moment-curvature law of the section. The remaining part of the element is considered elastic. It is a simple technique that it is capable of capturing the deterioration under cyclic action but the most important problem are that can capture neither the interaction between bending moment and axial force, that modified the moment curvature relationship, nor the spread of plasticity over the length of the element.

To overcome these problems it is possible to consider the distributed plasticity that can be of three types: plastic hinges with finite length, which identify an area where plasticization will take place, fiber elements and 3D finite elements.

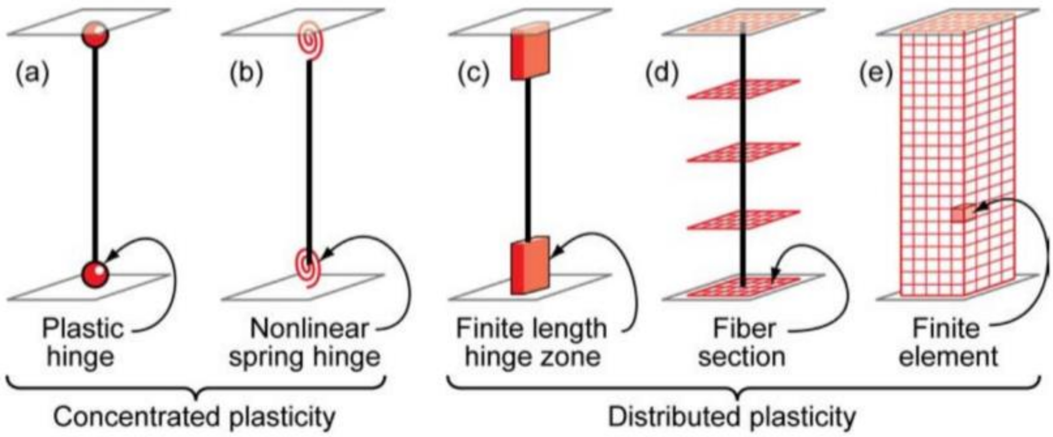

Figure 6-31. Different plasticity modeling.

The idea on which the fiber approach is based consists in the discretization of the element along its length, into a number of section corresponding to the integration points, and of the transverse sections into a number of rectangular fibers with monoaxial behavior, as is shown in Figure 6-32.

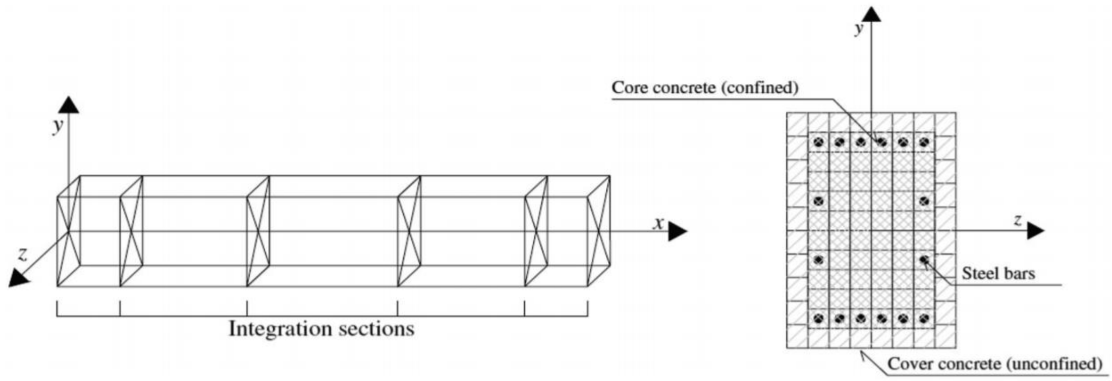

Figure 6-32. Fiber element with distributed plasticity.

To each fiber is assigned the constitutive law of the material that composes it and so in this way it is possible to assign different behaviors to the concrete, confined or not, and to the steel reinforcements. This type of element allows to overcome all the problems related to the concentrated plasticity, but obviously requires greater computational cost. By means of fiber elements it is only possible to describe the flexural and the axial deformations and not other behaviors such as shear deformations and the slippage of the reinforcements.

Fiber elements are divided into two types:

- DBE: displacement based elements;
- FBE: force based elements.

The firs category, DBE, is based on the so-called stiffness method in which the displacement field is discretized and interpolated according to the eq.

$$\mathbf{u}(x)=\mathbf{N}(x)\mathbf{q} \tag{6.2.2}$$

where $\mathbf{q}$ is the vector of the nodal displacement and $\mathbf{N}(x)$ is a matrix containing the interpolation functions, linear for the axial displacement and cubic for the transverse displacement. The deformation field $\mathbf{d}(x)$ is obtained deriving the displacement field

$$\mathbf{d}(x) = \mathbf{B}(x)\mathbf{q} \tag{6.2.3}$$

where $\mathbf{B}(x)$ is a matrix containing the derivatives of the shape functions. Starting from these equations, by means of integrations, is possible to obtain the stiffness matrix $\mathbf{K}$. Once that the deformation field is known is possible to obtain the forces, and so the equilibrium, using the principle of virtual displacements (PVD). For the DBE the axial deformation is constant and the curvature is linear. In order to obtain more precise results it is necessary to refine the mesh.

The second category, FBE, is based on the so-called flexibility method in which the force field is discretized and interpolated according to the eq.

$$\mathbf{D}(x) = \mathbf{b}(x)\mathbf{Q} \tag{6.2.4}$$

Where $\mathbf{b}(x)$ contains the force interpolation functions, that are the equilibrium equations

$$\mathbf{b}(x) = \begin{bmatrix} 1 & 0 & 0 \\ 0 & \dfrac{x}{L} - 1 & \dfrac{x}{L} \end{bmatrix} \tag{6.2.5}$$

and $\mathbf{Q}$ are the generalized nodal forces. In such a way it is possible to obtain the exact solution of the balance between internal stresses and reactions at the nodes, which was not verified in the DBEs. Once that the internal stress field is known is possible to obtain the compatibility between displacements and deformations using the principle of virtual forces (PVF)

$$\mathbf{v} = \int_0^L \mathbf{b}^T \mathbf{e}\, dx \tag{6.2.6}$$

where $\mathbf{e}$ is the vector of the section deformations and $\mathbf{v}$ is the vector of the element deformations. This compatibility relationship is evaluated by numerically

$$\mathbf{v} = \sum_{i=1}^{N_P} \left(\mathbf{b}^T \mathbf{e}\,|_{x=\xi_i} \right) \omega_i \tag{6.2.7}$$

using Gauss-Lobatto quadrature because it places integration points at the end of the element where the bending moment is larger.

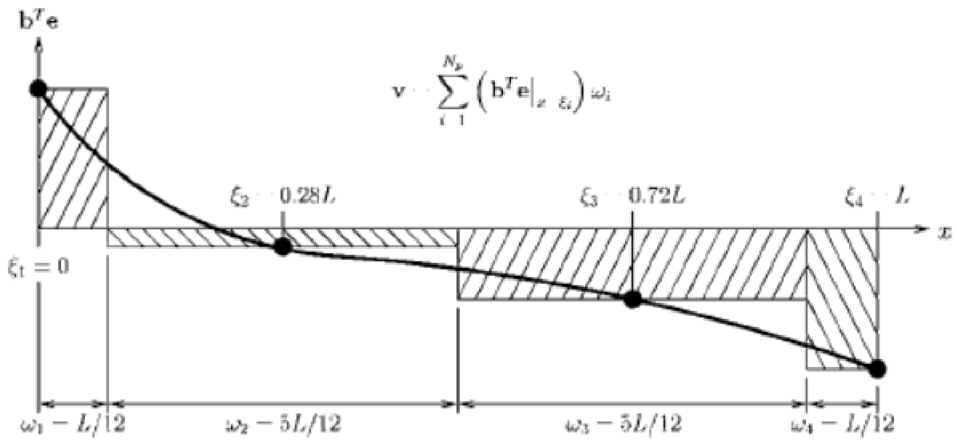

Figure 6-33. Four points Gaus-Lobatto quadrature rule to evaluate FBE compatibility.

FBE elements gives better results than DBEs, generally pillars and beams can be modeled with a single FBE element (with five integration points), while to obtain the same precision with respect to the theoretical solution with DBE are necessary at least four elements (with 3 points of integration each).

In OpenSees a particular type of finite element, called *BeamWithHinges* Element is implemented. This element is based on the flexibility formulation, and so it is a FBE, but the plasticity is concentrated over specified hinge lengths L_{pi} and L_{pj} at the two ends of the element. This type of elements is divides into three parts:

- Two plastic hinges at the ends with fiber sections and nonlinear constitutive behavior;
- One linear elastic region in the middle of the element.

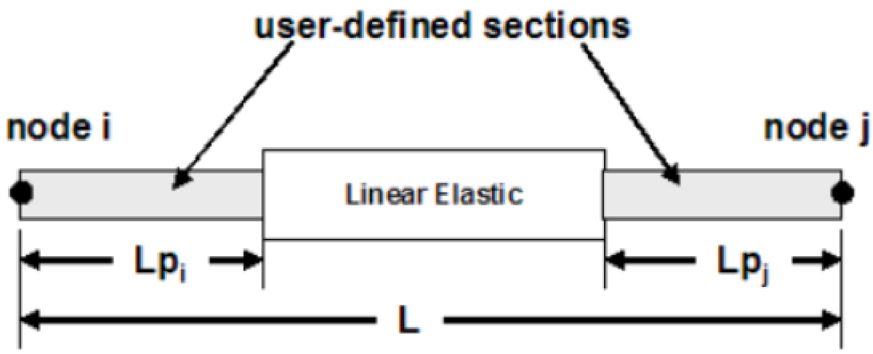

Figure 6-34. Beam with hinges element in OpenSees.

While the integration of distributed-plasticity force-based elements distributes the gauss points along the entire element length, the *BeamWithHinges* element localizes the integration points in the hinge regions. Two integration points per hinge are used to be able represent the curvature distribution accurately by means of Gauss-Radau integration.

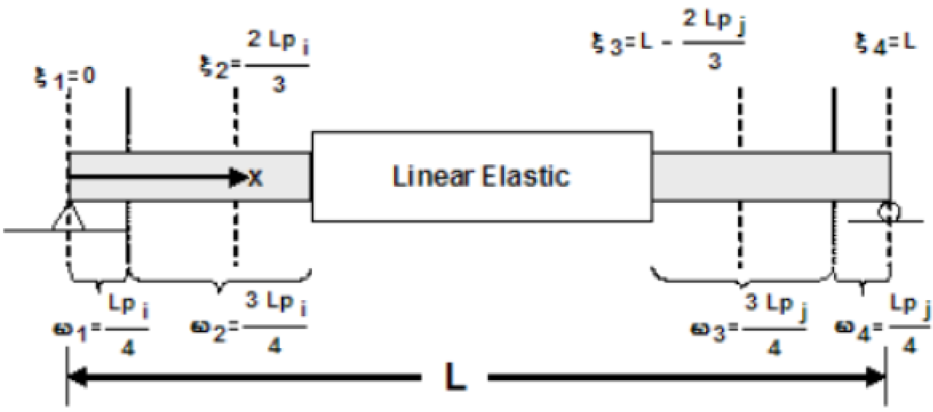

Figure 6-35. Two points Gauss-Radau plastic hinge integration method.

The problem with this formulation of the element is that two integration points per hinge require too much computational cost. For this reason a modified Gauss-Radau integration method developed by *Scott et al.* (2006) has been implemented. This modified integration method applied the Gauss-Radau integration rule over a length of $4l_{pi}$ and $4l_{pj}$ starting from the element ends. In such a way elastic properties are applied to the interior integration points.

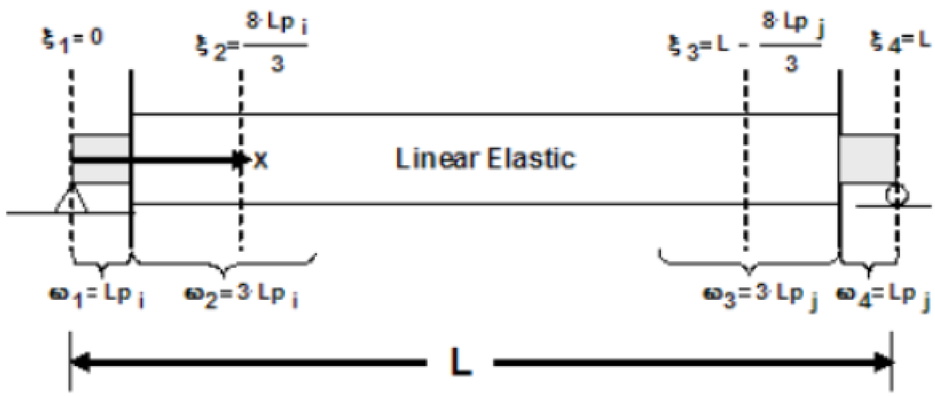

Figure 6-36. Modified Gauss-Radau plastic hinge integration method.

This typology of element was used in the model for both the columns and the beams. In order to define each element is necessary to create the fiber sections of each columns and beams and to define the plastic hinges lengths.

The fiber sections were created referring to the geometry and the reinforcement defined in Table 3, Table 4 and Table 5 and using the editor of OpenSees Navigator. The sections were realized distinguishing the core, to which is applied the confined concrete material, from the four covers, one for each side, to which is applied the unconfined concrete. The definition of each quadrilateral patch requires to specify the position of the four corners into a reference system YZ that coincides with the local system of the element and in this way is defined the orientation of the section.

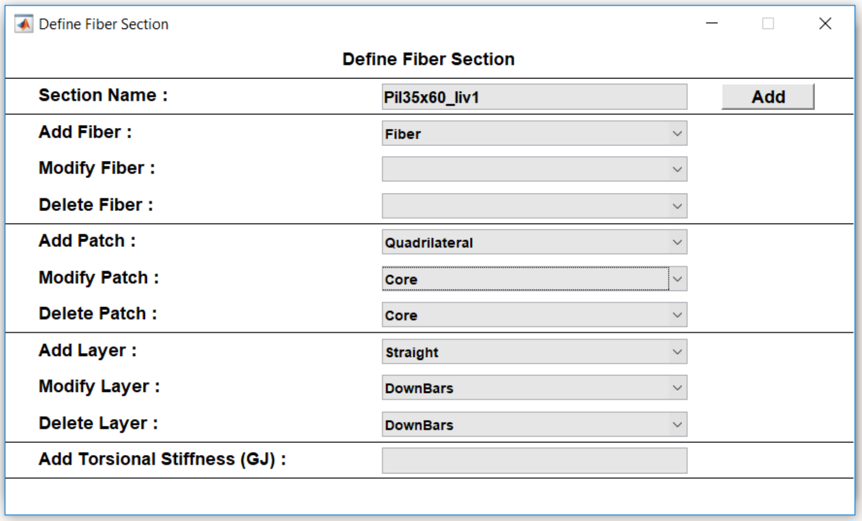

Figure 6-37. Definition of a fiber section in OpenSees Navigator.

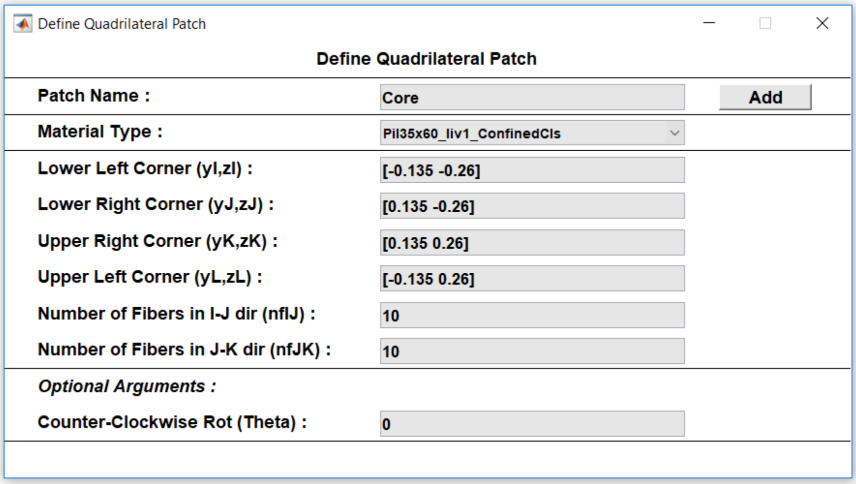

Figure 6-38. Definition of a quadrilateral patch for the core of the section.

All the sections have the same number of fiber

- 10x10 for the core
- 10x2 for the cover, with 10 fibers in the long direction

The steel bars are added to the section with the *layer straight* command that permits to create a line of fibers defining the position of the starting point, of the end point, the numbers of fibers and the area of each fiber.

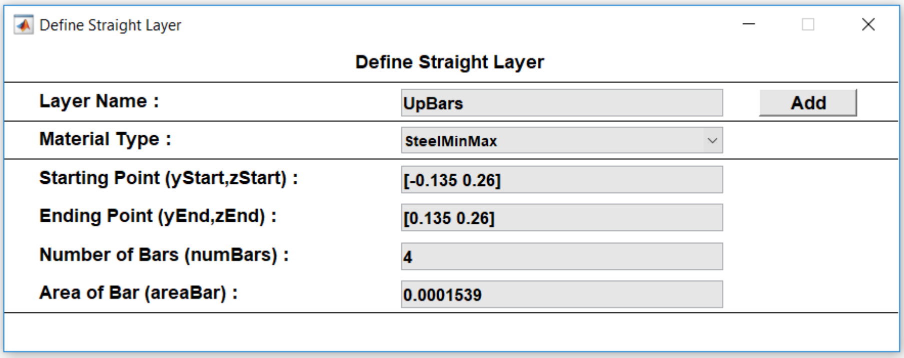

Figure 6-39. Definition of a straight layer of fibers for the reinforcements.

There are various expressions that permits to calculate plastic hinges lengths. The most popular are shown in Table 19.

Table 19

Author	Year	L_p
Priestley and Park	1987	$L_p = 0.08L_V + 6d_b$
Paulay and Priestley	1992	$L_p = 0.08L_V + 0.022f_y d_b$
Panagiotakos and Fardis	2001	$L_p = 0.12L_V + 0.014\alpha_{sl} f_y d_b$
Berry et al.	2008	$L_p = 0.05L_V + 0.1\frac{f_y d_b}{\sqrt{f_c^{'}}}$

In the realization of this model was used the formulation of *Panagiotakos and Fardis* (2001) that depends on the shear span L_V of the element, that for simplicity is considered equal to half of the length, and on the product $f_y d_b$. Considering L_p as a linear function of these two variables gives an expression that provide the best fit to the results of numerous experimental tests.

$$L_p = 0.12 L_V + 0.014 \alpha_{sl} f_y d_b \tag{6.2.8}$$

α_{sl} is a variable that can assume the value 1 if the slippage of the reinforcement bars from the anchorage zone beyond the end section is possible or 0 if is not. For the building that is the object of this study case there were no information about the anchorage of the steel bars so it was necessary to make some assumption considering the slippage possible for the columns and not for the beams.

The last parameters to be set for the BeamWithHinges elements are used to create an elastic section at the two Gauss integration points of the element interior. These values are the cross sectional area, the moment of inertia around Y, Z and X, the elastic modulus E (in this case was set equal to the elastic modulus of the cracked concrete) and the shear modulus G.

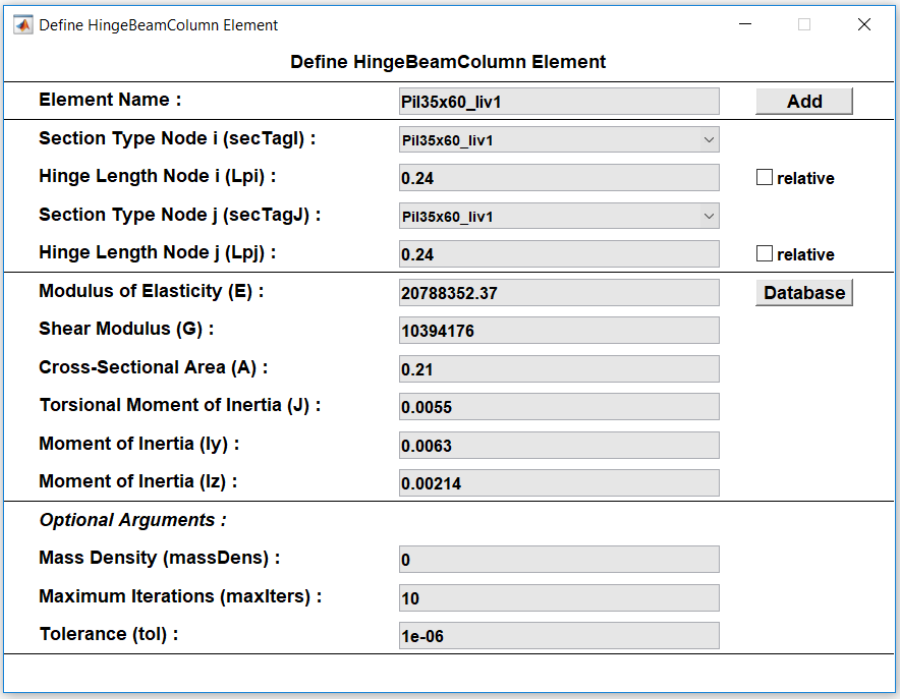

Figure 6-40. Definition of the BeamWithHinges element in OpenSees Navigator.

6.2.4 Geometric transformation of the elements

The geometric-transformation command (*geomTransf*) is used to construct a coordinate transformation object, which transforms beam element stiffness and resisting force from the basic system to the global-coordinate system. It was possible to choose between two type of geometrical transformation:

- *Linear*: it is used to performs a linear geometric transformation of beam stiffness and resisting force from the basic system to the global-coordinate system.
- *P-delta*: performs a linear geometric transformation of beam stiffness and resisting force from the basic system to the global coordinate system, considering second-order P-Delta effects.

The transformation chosen for the model was the P-delta in order to take into account the second order effects that are necessary for not over estimate the member strength and under estimate the deflections, particularly in lateral directions.

The command string to generate a P-delta geometric transformation for an element is

geomTransf PDelta $transfTag $vecxzX $vecxzY $vecxzZ

where $vecxzX, $vecxzY and $vecxzZ are the three components, in the global coordinate system, of a vector vecxz that is used to construct the local coordinate system. The element coordinate system is specified as follows: the x-axis is the axis connecting the two element nodes; the y- and z-axes are then defined using the vector vecxz that lies on a plane parallel to the local x-z plane. Local y-axis is given by the cross product of local x-axis with vecxz and local z-axis is given by the cross product of local x and y.

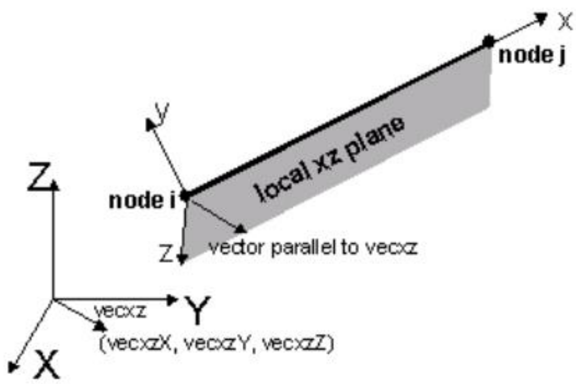

Figure 6-41. Definition of the local axis of an element according to the command geomTransf PDelta.

6.3 Design of the hysteretic devices

In order to proceed with the design of the dissipative bracing system it is necessary to know the modal characteristics of the structure. For this reason it is necessary to perform firstly a modal analysis in order to find the periods of vibration and the eigenvectors of the structure associated to the first vibration modes. Once that the characteristics of the first vibration mode are known it is possible to define the lateral load pattern for the pushover analysis and to begin with the design of the BRB system as explained in chapter 5.

The bracing system is designed only along X direction because this is the weak direction of the structure, without an appropriate resisting system as well as the Y direction.

6.3.1 Modal analysis of the structure

Performing a modal analysis requires the application of the seismic masses to the nodes and the definition of rigid diaphragms at each floor. In order to simplify the modeling the masses of each floor were concentrated in the center of gravity (corresponding to the nodes from 300 to 304). The value of the mass at each floor was found applying on the structure the load combination deriving from eq.(6.1.1) considering a combination coefficient of 0.3 for the variable load of the floors and of 0.6 for the variable loads of the stairs and the balconies. The mass associated to the roof was concentrated at the fifth floor.

The values of the masses associated to each floor are shown in Table 20

Table 20

DISTRIBUTION OF THE MASSES			
Floor	**Joint**	**Z**	**Mass**
-	-	[m]	[$kN/m/s^2$]
Floor 5	4	14.8	526.98
Floor 4	3	11.8	334.45
Floor 3	2	8.8	334.45
Floor 2	1	5.8	334.45
Floor 1	0	2.8	345.32

The results of the first five vibration modes of the modal analysis are shown in Table 21.

Table 21

VIBRATION MODES OF THE BARE FRAME				
Mode	**Type**	**ω [rad/s]**	**T [s]**	**f [s^{-1}]**
1	Translational X	7.388	0.850	1.176
2	Rotational	9.371	0.670	1.491
3	Translational Y	9.496	0.662	1.511
4	Translational X	23.432	0.268	3.729
5	Rotational	30.300	0.207	4.822

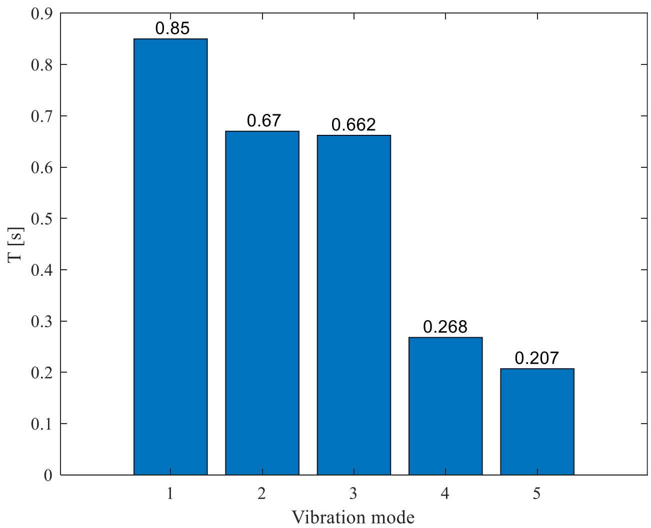

Figure 6-42. Periods of vibration of the first five modes.

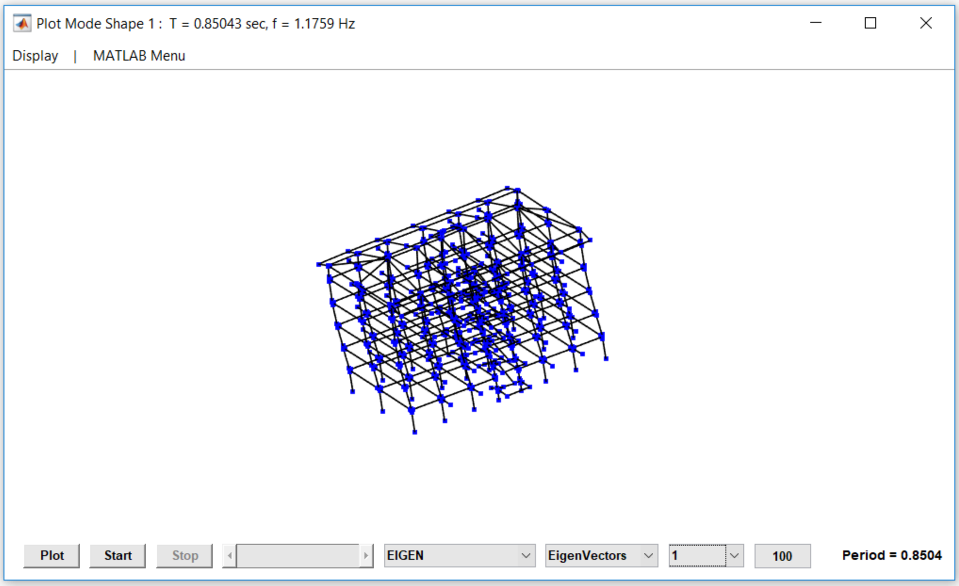

Figure 6-43. Plot of the first vibration mode in OpenSees Navigator.

6.3.2 Nonlinear static analysis of the bare frame

The design procedure of the BRB system requires the evaluation of the system capacity curve by means of a nonlinear static (pushover) analysis as explained in subparagraph 5.2.1.

According to eq.(5.2.8) the lateral load pattern for the pushover analysis is determined in order to have a distribution of the loads that is proportional to a certain deformed shape. In this case the deformed shape coincide with the first vibration mode of the structure in order to obtain a distribution of the loads equal to the effective earthquake forces. The deformed shape is obtained normalizing the first modal shape respect to the top displacement, so

$$\Phi_x^i = \frac{x^i}{x^5} \tag{6.3.1}$$

where x^i is the displacement of the i-th floor in x direction for the first vibration mode and x^5 is the displacement of the last floor in the same direction. The product of Φ_x^i for the mass of the i-th floor gives the load that has to be applied to the gravity center at that floor. The values of the loads applied at each floor for the pushover analysis of the bare frame are summarized in Table 22.

Table 22

PUSHOVER LOAD PATTERN						
Floor	Joint	H	x^i	$\varphi_x{}^i$	Mass	Fx
-	**-**	**[m]**	**-**	**-**	**[$kN/m/s^2$]**	**[kN]**
Floor 1	300	2.8	0.0045725	0.1439	345.323	49.69
Floor 2	301	5.8	0.0128288	0.4037	334.446	135.02
Floor 3	302	8.8	0.0209037	0.6578	334.446	220.01
Floor 4	303	11.8	0.0275006	0.8654	334.446	289.44
Floor 5	304	14.8	0.0317769	1.0000	526.980	526.98

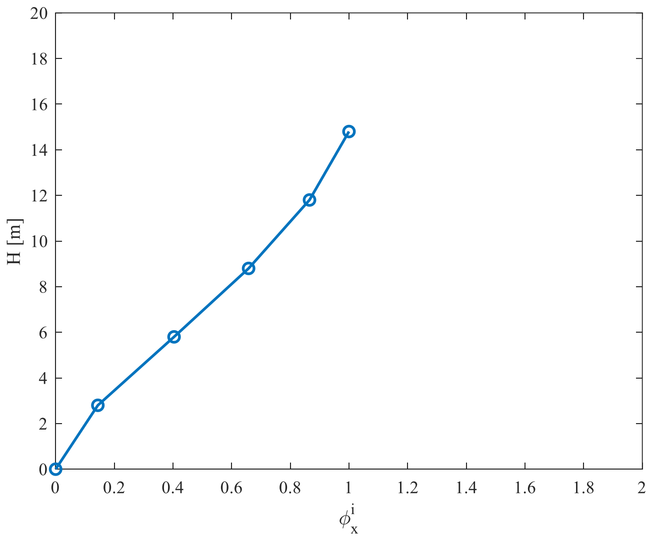

Figure 6-44. Normalized deformed shape of the first vibration mode of the bare frame.

Once that the lateral load pattern is defined is possible to perform the pushover analysis applying the loads to the center of gravity of each floor and controlling the increment of the loads in time with a multiplication factor λ that corresponds to the *p* factor of eq.(5.2.8) . Pushover analysis is performed starting from the condition of the structure subjected to the gravity loads. Instead of increasing directly the multiplication factor of the lateral loads λ is necessary to control the analysis through the displacement of a control node along a fixed dof, setting a constant increment of displacement at each step. In this case the control node is the center of gravity of the last floor (node 304) and the direction in which the displacement is increased is the global X. The increment of displacement at each step is set equal to 0.001 m.

At each step is recorded the displacement of the node 304 and the sum of the base shear of each columns of the ground floor. Plotting all the couples of values at each step of the analysis gives the pushover curve of the structure. The base shear is indicated with V and the displacement of the control node with d_{304}.

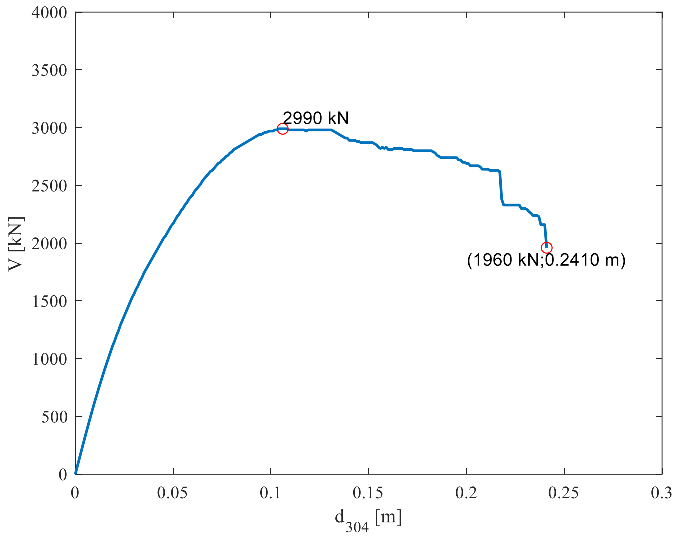

Figure 6-45. Pushover curve of the unretrofitted structure.

The ultimate displacement of the node 304 is equal to 0.2410 m and the maximum base shear is equal to 2990 kN. The capacity curve shows a drop of resistance at its ultimate displacement of the 34.4%.

As anticipated in subparagraph 5.2.1 it is necessary to transform the capacity curve of the MDOF system into the capacity curve of an inelastic SDOF equivalent system. In order to do that it is necessary to obtain the value of the equivalent mass m^* of the SDOF system and of the modal participation factor Γ using the eq.(5.2.15) and eq.(5.2.17). The values of these parameters are calculated in Table 23.

Table 23

Node	H	m^i	x^i	Φ^i	$m_i\Phi_i$	$m_i\Phi_i^2$	m*	Γ
-	[*m*]	[$kN/m/s^2$]	-	-	[$kN/m/s^2$]	[$kN/m/s^2$]	[$kN/m/s^2$]	-
304	14.8	526.98	0.0318	1.00	526.97	526.97		
303	11.8	334.45	0.0275	0.87	289.43	250.48		
302	8.8	334.45	0.0209	0.66	220.00	144.72	**1221.137**	**1.2411**
301	5.8	334.45	0.0128	0.40	135.02	54.50		
300	2.8	345.32	0.0046	0.14	49.68	7.15		

Dividing the base shear V and the displacement of the node 304 d_{304} by the modal participation factor gives the capacity curve of the equivalent SDOF system shown in Figure 6-46.

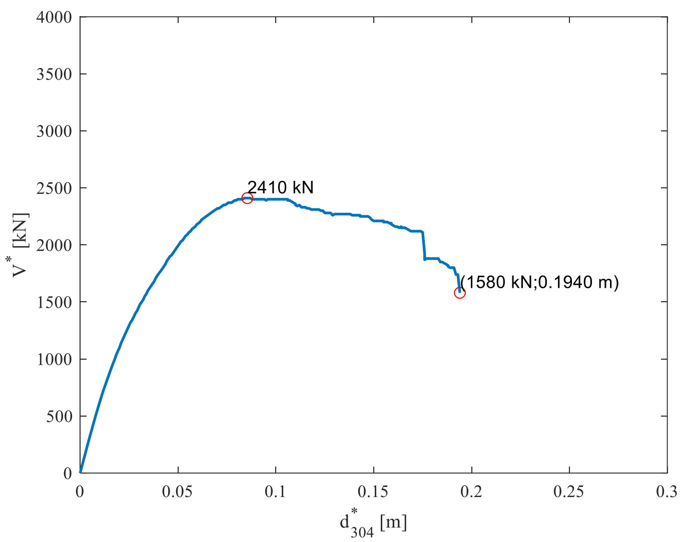

Figure 6-46. Capacity curve of the equivalent SDOF system.

This capacity curve is than bilinearized according to the procedure proposed in NTC 2008 code (CS.LL.PP. 2008; 2009) that is explained in subparagraph 5.2.1.

The perfectly plastic branch of the bilinearized curve is stopped when it is reached a drop of resistance equal to the 15% and so the ultimate displacement is lower than 0.1940 m.

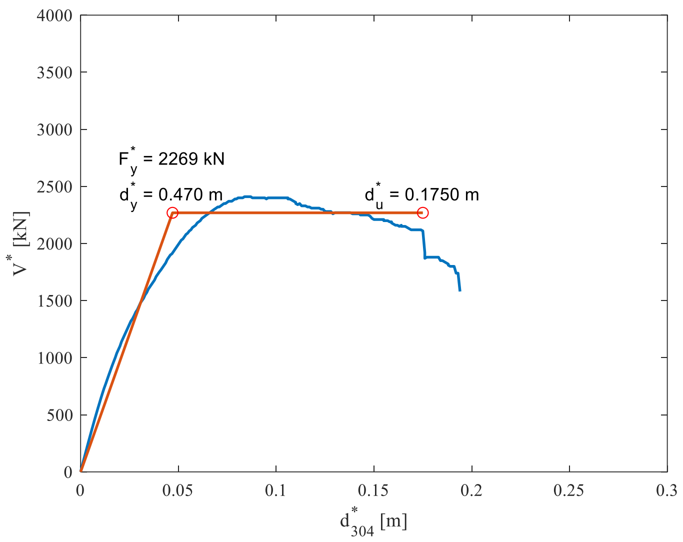

Figure 6-47. Bilinearization of the capacity curve of the unretrofitted structure

The characteristics of the bilinear system are shown in Table 24. It can be easily observe that the ductility μ offered by the system is quite high.

Table 24

k*	**m***	**T***	**μ**
kN/m	**kNm/s²**	**s**	
48522.65	1221.137	0.996	3.7385

6.3.3 Comparison between the capacity and the seismic demand

The bilinear capacity curve of the structure has to be compared with the seismic demand represented by the inelastic response spectrum, obtained from the elastic one by means of the eq.(5.2.25) and eq.(5.2.26), in the acceleration-displacement plane. In order to do that it is necessary to transform the bilinear curve from the force-displacement plan to the acceleration-displacement dividing the force by the equivalent mass m^* .

The elastic spectrum considered in the design procedure is the SLV spectrum shown in Figure 6-12 and Figure 6-13.

The comparison between the demand and the capacity is shown in Figure 6-48.

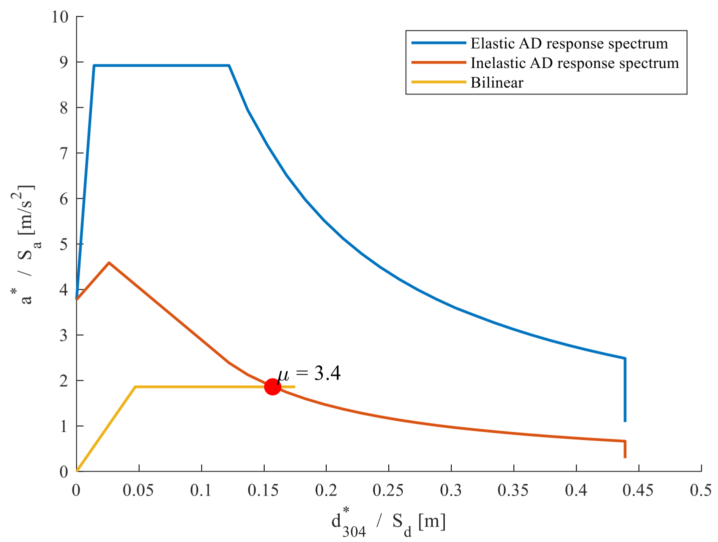

Figure 6-48. Comparison between capacity of the structure and seismic demand.

The ductility demand is μ=3.4 and it is very close to the maximum ductility of 3.7 that the structure can offer. This means that the structure needs to show high plastic deformations in order to withstand the seismic demand. For this reason the damages on the structure will be much extended after the earthquake and most likely it will be necessary the demolition.

In order to avoid this problem it is necessary to reduce the demand of ductility required to the structure imposing a limit to the maximum μ that can be offered.

Diminishing the value of μ has an influence also on the seismic demand represented by the inelastic spectrum and for this reason it is expected that the performance point will not be reached and so it will be necessary an upgrading of the structure by means of a hysteretic devices (BRB) system.

The imposition of a lower value of ductility is connected to the choice of an adequate parameter that can describe the structural damage. In this case the design parameter chosen for this aim was the maximum interstorey drift. In fact limiting the interstorey drift it is possible to reduce the amount of damages on the structure. Some provisions about the maximum interstorey drift angle regarding immediate occupancy (IO) performance level are contained in the American code FEMA 365 (2000) that prescribes a value of 1%. Choosing this value would have led to a too onerous dimensioning of the dissipative bracing system so has been decide to set the maximum value of the interstorey drift to 1.5% that is also an acceptable value for limiting the structural and nonstructural damage.

In order to find the step of the pushover analysis at which the maximum drift value of 1.5% is reached it is necessary to plot the trend of the drifts at each floor for every loading step.

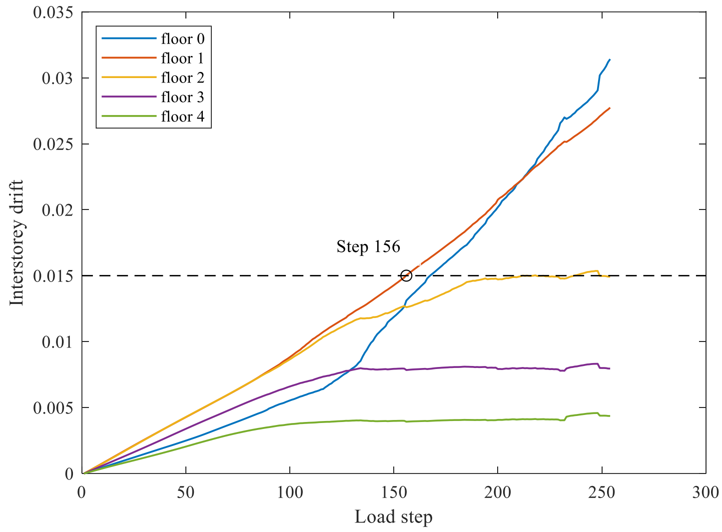

Figure 6-49. Interstorey drifts at each load step.

An interstorey drift of 1.5% is reached at the load step 156 in floor 1 so it is necessary to stop the pushover analysis at this step in order to set a limit to the ductility offered by the structure.

The pushover curve stopped at the reaching of an interstorey drift of 1.5% is shown in Figure 6-50 while in is shown the capacity curve of the equivalent SDOF system and its bilinearization.

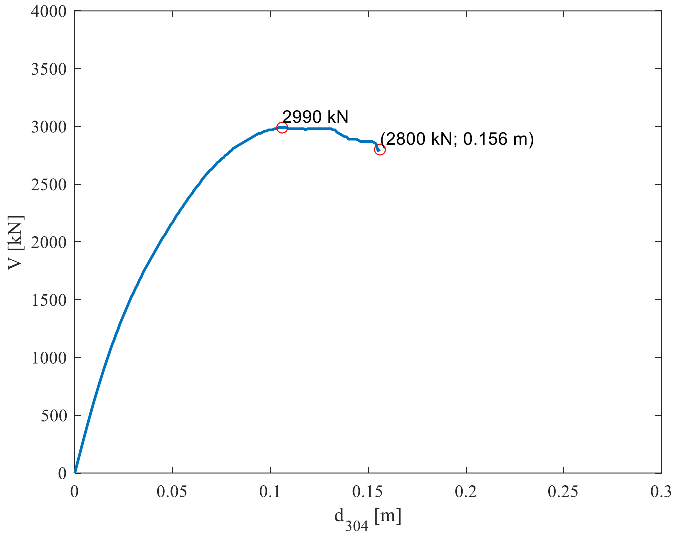

Figure 6-50. Pushover curve at 1.5% of interstorey drift.

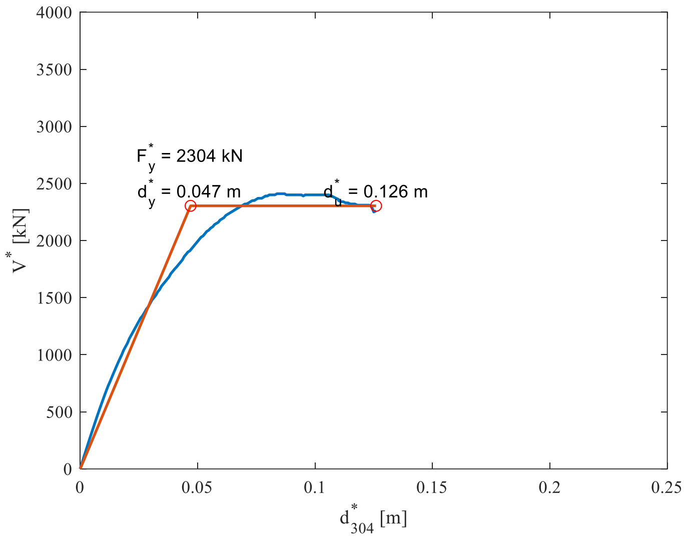

Figure 6-51. Equivalent SDOF system capacity curve and its bilinearization.

The perfectly plastic branch of the bilinearized curve is stopped when it is reached the ultimate displacement d_u^* because the drop of resistance is smaller than the 15%.

The characteristics of the bilinear system are shown in Table 25. Obviously the ductility μ is lower than the previous case.

Table 25

k*	m*	T*	μ
[kN/m]	[kNm/s^2]	[s]	-
48522.65	1221.137	0.9962	2.646

The comparison between the new demand curve, for a lower value of μ and the capacity is shown in Figure 6-52.

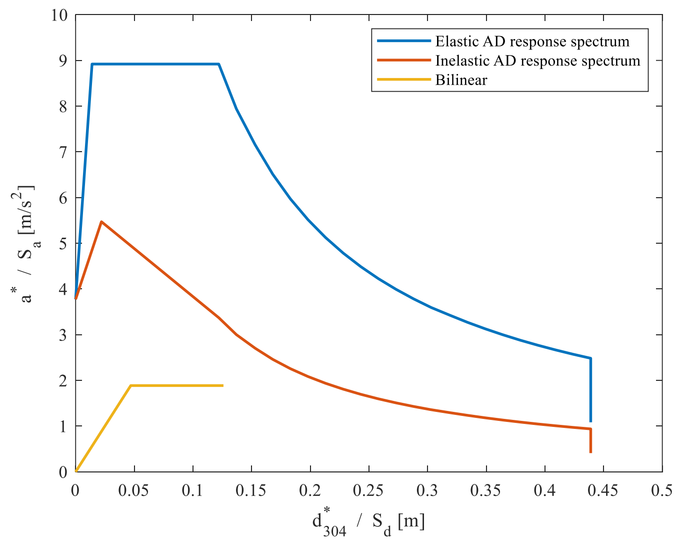

Figure 6-52. Comparison between the reduced capacity and the seismic demand.

6.3.4 Design of the BRB system

To design the BRB system according to the procedure explained in chapter 5 it is necessary to define the characteristics of the coupled system (frame + BRB system) that permits to withstand the seismic action. The design parameters are:

- μ_d : ductility of the dissipative bracing system;
- V_d^1 : base shear of the dissipative bracing system;
- μ_0 : ductility of the dissipative devices (BRBs).

As explained in paragraph 5.1 the ratio between the ductility of the entire bracing system and the ductility of a single dissipative device should be lower than 0.7-0.8. The ductility of the BRB can vary in a high range as reported in chapter 4. In this case a value of μ_0 equal to 15 was chosen so μ_d should be lower than 11-12.

The base shear V_d^1 is chosen in such a way to obtain a capacity curve of the coupled system that intersect the inelastic spectrum.

Summing the capacity curve of the bare frame with that of the BRB system gives a trilinear curve that is than bilinearized using the areas equivalence criterion obtaining the bilinear curve for the coupled system. The base shear and the ductility are given by eq.(5.2.30) and (5.2.31).

The design parameters chosen and the characteristics of the coupled system are summarized in Table 26.

Table 26

V_d^1	μ_d	μ_0	μ_d/μ_0	$V^1 = V_d^1 + V_f^1$	μ
[kN]	-	-	-	[kN]	-
900	10	15	0.66	3204	3.335

The capacity curve of the bare frame, the BRB system and the coupled system are shown in Figure 6-53 while the comparison between the capacity curve of the coupled system and the seismic demand in the acceleration-displacement plane is represented in

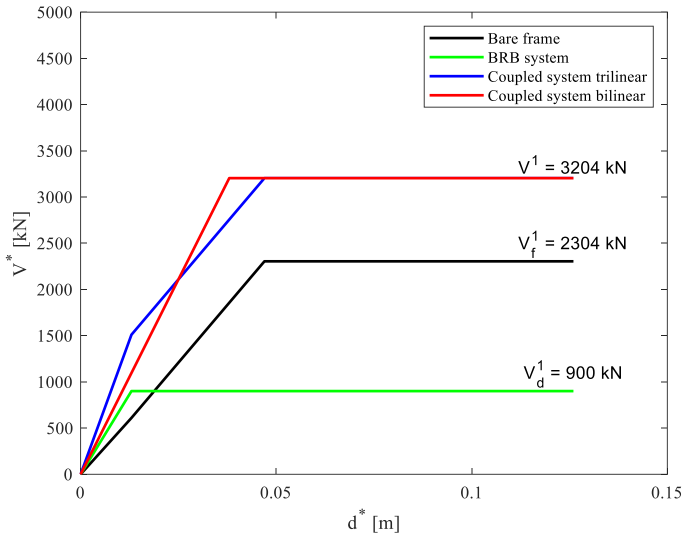

Figure 6-53. Bilinearized capacity curve of the SDOF coupled system.

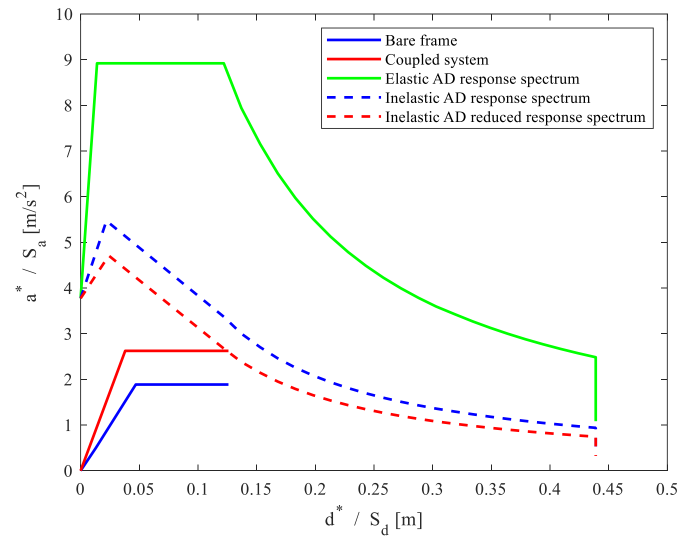

Figure 6-54. Capacity vs demand in AD plane

The design of the characteristics of the BRB system at each floor follows the procedure explained in paragraph 5.2. Since the building is regular in height it is possible to choose as the objective deformed shape the modal shape of the first vibration mode of the bare frame. Choosing an objective deformed shape is possible to obtain the corresponding distribution of the shears and stiffness at each floor applying the equations from (5.2.1) to (5.2.7). The results of this procedure are in Table 27.

Table 27

Floor	**H**	**m^i**	**U^i**	**Δ^i**	**u^i**	**δ^i**	**V^i/ω^2**	**v^i**	**K^i/ω^2**	**k^i**
-	**[m]**	**[kN/m/s^2]**	**[m]**	**[m]**	**[m]**	**[m]**	**-**	**-**	**-**	**-**
4	14.8	526.98	0.0318	0.0043	1.000	0.135	527.0	0.432	123233	0.461
3	11.8	334.45	0.0275	0.0066	0.865	0.208	816.4	0.669	123758	0.463
2	8.8	334.45	0.0209	0.0081	0.658	0.254	1036.4	0.849	128352	0.481
1	5.8	334.45	0.0128	0.0083	0.404	0.260	1171.4	0.959	141885	0.531
0	2.8	345.32	0.0046	0.0046	0.144	0.144	1221.1	1.000	267062	1.000

Once that is known the distribution in height of the forces and of the stiffness deriving from the objective deformed shape is possible to design the bracing system in order to have the same behavior also for the retrofitted structure. In order to obtain reasonable values of yielding forces and axial stiffness it was necessary to place four brace for each floor, two for each external frame, placed symmetrically in the external span of the frame. The characteristics of each brace were obtained by means of the equations from (5.2.35) to (5.2.41). The results are shown in Table 28.

Table 28

DISSIPATIVE BRACES YIELD FORCES AND STIFFESS										
Floor	H	v^i	δ^i	V_d^i	K_d^i	α	$F_{c,tot}^i$	$K_{c,tot}^i$	F_c^i	K_c^i
-	**[m]**	**-**	**[m]**	**[kN]**	**[kN/m]**	**-**	**[kN]**	**[kN/m]**	**[kN]**	**[kN/m]**
4	14.8	0.432	0.135	482.1	229698	0.6557	608.2	365615	**152.0**	**91404**
3	11.8	0.669	0.208	746.8	230677	0.6557	942.2	367173	**235.6**	**91793**
2	8.8	0.849	0.254	948.1	239240	0.6557	1196.1	380802	**299.0**	**95200**
1	5.8	0.959	0.260	1071.6	264465	0.6557	1352.0	420954	**338.0**	**105238**
0	2.8	1.000	0.144	1117.1	497787	0.6227	1375.1	754371	**343.8**	**188593**

After this step of the design procedure the yielding force F_c^i and the axial stiffness K_c^i of the overall diagonal are known and it is possible to proceed with the design of the characteristics of the two components of the brace, the dissipative BRB and the elastic connection arm. The geometrical characteristics of the two members are obtained applying the equations (5.1.1), (5.1.4), (5.1.5) and from (5.2.42) to (5.2.46) while the critical buckling load of the steel connecting arm is calculated using the equations from (5.2.47) to (5.2.53).

The design parameter of the materials are shown in Table 29.

Table 29

μ_0	**E**	**f_{y0}**	**f_{yb}**
-	**[N/mm^2]**	**[N/mm^2]**	**[N/mm^2]**
15	210000	250	355

The dimensioning of the BRBs is shown in Table 30

Table 30

BRB CHARACTERISTICS				
Floor	**K_0^i**	**F_0^i**	**A_0^i**	**L_0^i**
-	**[kN/mm]**	**[kN]**	**[mm$^{2]}$**	**[mm]**
4	142.18	152.05	608.19	898.3
3	142.79	235.56	942.23	1385.7
2	148.09	299.04	1196.14	1696.2
1	163.70	337.99	1351.97	1734.3
0	293.37	343.78	1375.14	984.4

The dimensioning of the connecting arms is shown in Table 31

Table 31

CONNECTING ARMS CHARACTERISTICS						
Floor	**K_b^i**	**L_b^i**	**A_b^i**	**F_b^i**	**t**	**r**
-	**[kN/mm]**	**[mm]**	**[mm2]**	**[kN]**	**[mm]**	**[mm]**
4	255.93	4022	4901	1740	10	78
3	257.02	3534	4326	1535	10	69
2	266.56	3224	4092	1452	10	66
1	294.67	3186	4470	1587	10	72
0	528.06	3816	9597	3407	10	153

The geometric characteristics and the material elastic modulus and shear modulus are in Table 32.

Table 32

Floor	**A_b^i**	**L_b^i**	**$I_{y,z}$**	**E**	**ν**	**G**	**J (tors)**	**$A_{Vx,Vz}$**
-	**[m^2]**	**[m]**	**[m^4]**	**[KN/m^2]**	**-**	**[kN/m^2]**	**[m^4]**	**[m^2]**
4	0.004902	4.0	1.4978E-05	210000000	0.30	91304347.83	2.9956E-05	0.002451
3	0.004326	3.5	1.0308E-05	210000000	0.30	91304347.83	2.0616E-05	0.002163
2	0.004093	3.2	8.7326E-06	210000000	0.30	91304347.83	1.7465E-05	0.002046
1	0.004471	3.2	1.1372E-05	210000000	0.30	91304347.83	2.2745E-05	0.002235
0	0.009597	3.8	1.1208E-04	210000000	0.30	91304347.83	2.2416E-04	0.004799

Both the resistance and buckling checks are verified and the bucking critical loads are calculated in Table 33.

Table 33

BUCKLING CHECKS									
Floor	**λ_1**	**$I_{x,y}$**	**ρ**	**λ**	**λ^***	**Φ**	**χ***	**χ**	**$F_{b,inst}^i$**
-	**-**	**[mm^4]**	**[mm]**	**-**	**-**	**-**	**-**	**-**	**[kN]**
4	76.41	14977984	55.2	89	1.165	1.28	0.5525	0.5525	874
3	76.41	10308007	48.8	101	1.319	1.49	0.4597	0.4597	641
2	76.41	8732649	46.1	107	1.394	1.60	0.4208	0.4208	555
1	76.41	11372326	50.4	98	1.277	1.43	0.4835	0.4835	697
0	76.41	112079016	108	44	0.581	0.71	0.8968	0.8968	2777

The yielding and ultimate displacement for each brace are calculated as follow:

$$d_y^i = \frac{K_c^i}{F_c^i} \tag{6.3.2}$$

$$d_u^i = \mu_d d_y^i \tag{6.3.3}$$

and the values for the braces of each floor are reported in Table 34.

Table 34

Floor	**d_y^i**	**d_u^i**
-	**[mm]**	**[mm]**
4	1.66	16.63
3	2.57	25.66
2	3.14	31.41
1	3.21	32.12
0	1.82	18.23

6.3.5 Modelling of the BRBs

The dissipative bracing system was modelled in OpenSees in two different ways.

A first simplified model of the braces was realized using a single truss element for the entire length of the diagonal. The *element truss* command permits to construct a truss element object defining the cross sectional area of the element and associating a previously-defined uniaxial material. The truss element considers the constitutive law provided by the uniaxial material as a stress-strain relationship and so the axial force is given by the value of the stress multiplied by the cross sectional area

$$F = \sigma A \tag{6.3.4}$$

while the axial stiffness is given by

$$K = \frac{EA}{L} \tag{6.3.5}$$

where E is the elastic modulus of the material and L is the length of the element. Since that the truss element was used to model the entire brace was necessary to assign to the material the characteristics of the overall brace F_c and K_c. To define the material was used the *UniaxialMaterial Steel02* command that construct a Giuffre-Menegotto-Pinto steel material object with isotropic strain hardening. The command string is

```
uniaxialMaterial Steel02 $matTag $Fy $E $b $R0 $cR1 $cR2 <$a1 $a2 $a3 $a4 $sigInit>
```

where:

- $Fy: is the yield strength;
- $E: is the initial elastic tangent (elastic modulus);
- $b: is the strain hardening ratio;
- $R0, $cR1, $cR2: are parameters that controls the transition from elastic to plastic branches.

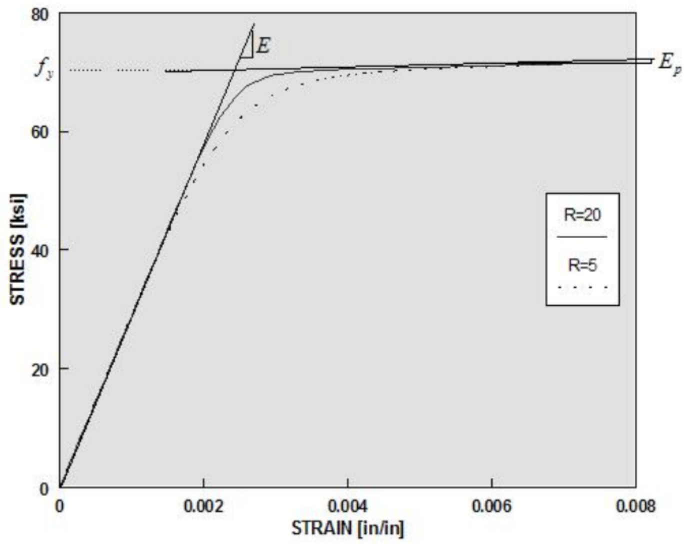

Figure 6-55. Steel 02 constitutive law.

The value of F_c is a force so ti was necessary to assign to the truss element a unit area in order to use this value as $Fy for the uniaxial material. In the same way K_c is a stiffness so in order to obtain a value of elastic modulus to be assigned to $E it was necessary to multiply it for the length of the element since the area of the truss is unit. In this way the truss elements are able to represent the behavior of the entire brace.

Table 35

Name	E [kN/m]	F_y [kN]	b	a1	a2	a3	a4	R0	cR1	cR2
BRB_0	905245	343	0.01	0	1	0	1	18.5	0.925	0.15
BRB_1	517773	337	0.01	0	1	0	1	18.5	0.925	0.15
BRB_2	468386	299	0.01	0	1	0	1	18.5	0.925	0.15
BRB_3	451622	235	0.01	0	1	0	1	18.5	0.925	0.15
BRB_4	449705	152	0.01	0	1	0	1	18.5	0.925	0.15

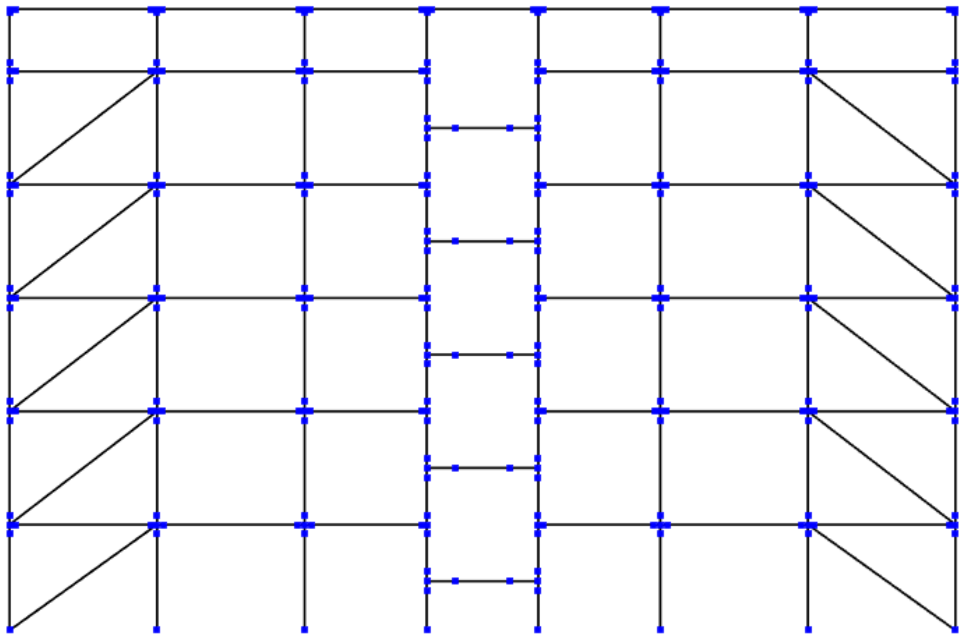

Figure 6-56. Modeling of the BRB with a single truss element.

The other modelling approach consists in dividing the brace into the two parts that compose it, the proper BRB and the elastic connecting arm. In this way is possible to obtain a more realistic response of the dissipative bracing because the hysteretic behavior is localized only in the element that represent the BRB. Using this approach the connecting arm was modelled as a forceBeamColumn element assigning an elastic section with the geometrical properties present in Table 32. The BRB, instead, was modelled as a truss element assigning the real cross sectional area A_0^i to each element. The material assigned to each BRB is always the same and it is constructed with the *uniaxialMaterial SteelBRB* command. This command constructs a steel material according to the elastoplastic model of *Zona and Dall'Asta* (2011). This model, as explained in paragraph 4.4, was developed in order to take into account the particular behavior of the BRBs, characterized by a significant role of isotropic hardening and a tension-compression asymmetry. This model is particularly suitable for describing the hysteretic energy dissipation provided by the BRB in dynamic nonlinear (time history) analysis.

The command string for the construction of this type of material is:

uniaxialMaterial SteelBRB $mTag $E $sigmaY0 $sigmaY_T $alpha_T $beta_T $delta_T $sigmaY_C $alpha_C $beta_C $delta_C $tol

where

- $E: is the elastic modulus of the steel core material
- $sigmaY0: is the yielding strength of the steel core material
- $sigmaY_T $alpha_T $beta_T $delta_T $sigmaY_C $alpha_C $beta_C $delta_C: are the parameters that characterize the material response and their meaning is explained in the paragraph 4.4.

According to the values of Table 29 the elastic modulus is 210000 N/mm^2 and the yielding strength is 250 N/mm^2. The others parameters were set according to the results of experimental tests performed on BRB subjected to a deformation history with a non-zero mean strain portion of the cyclic path (*Tremblay et al. 2004*).

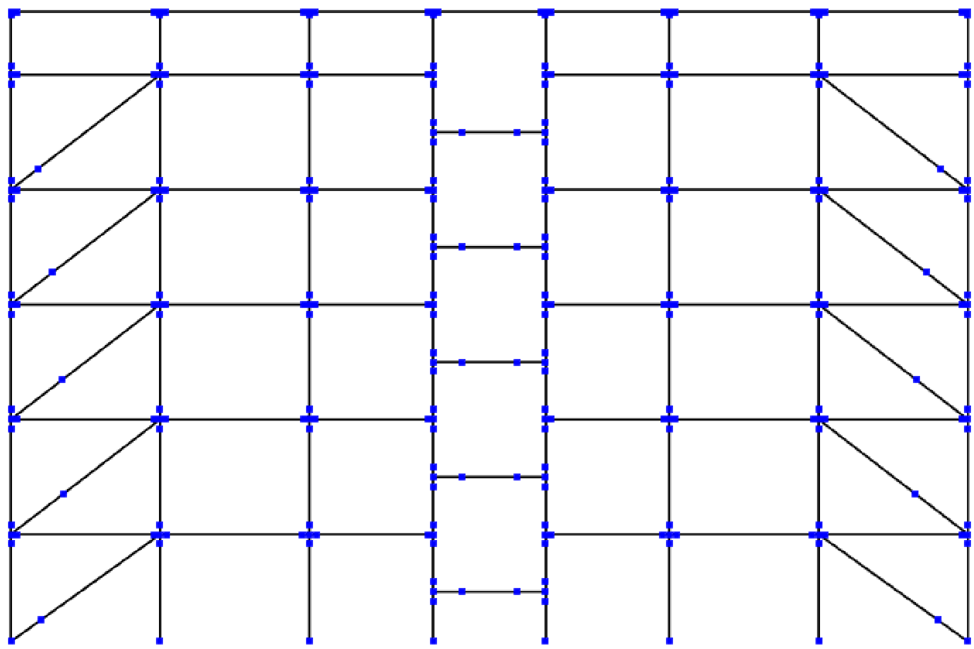

Figure 6-57. Modeling of the BRB with two elements (truss + elastic forcebeamcolumn).

6.4 Modelling of the infills

The model of the building was further improved taking into account the presence of the infills. The infills were modelled using the *Decanini et al*. (1993) model that considers the contribution of the masonry infill panel to the frame by means of a system of two diagonal. The masonry struts are ineffective in tension but the combination of two diagonals provides a resisting mechanism both for positive and negative direction of loading. The force-displacement relationship considers four branches. A first linear elastic branch corresponds to the uncracked stage; the second branch refers to the post-cracking phase up to the reaching of the maximum strength (H_{mfc}). The peak corresponds to the complete cracking stage of the infill panel. The descending third branch of the curve describes the post-peak strength deterioration until the reaching of the residual strength and displacement; after that the curve continues horizontally.

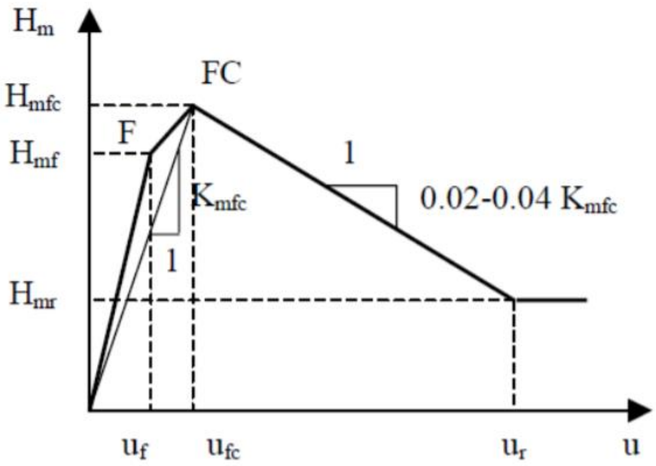

Figure 6-58. Bertoldi, Decanini et al. model force-displacement law.

The model requires the definition of three parameters in order to obtain the shape of the curve.

The width of the equivalent strut ω

$$\omega = d\left(\frac{K_1}{\lambda_h} + K_2\right) \tag{6.4.1}$$

Where K_1 and K_2 are two empirical coefficient, λ_h is a non-dimensional parameter introduced by *Stafford Smith* (1963) that takes into account the relative stiffness of the frame and infill and d is the diagonal length of the panel.

The stiffness of the equivalent strut at complete cracking

$$K_{mfc} = \frac{E_m e\omega}{d}\cos^2\vartheta \tag{6.4.2}$$

Where E_m is the Young modulus of the infill, e is the thickness and ϑ is the inclination of the strut.

The maximum strength of the equivalent strut

$$H_{mfc} = \sigma_{br(\min)} e\omega \cos\vartheta \tag{6.4.3}$$

Where $\sigma_{br(min)}$ is the minimum of four values that correspond to four mode of infill failure.

The ratio between the cracking force and the maximum force is about 0.8, while between the residual force and the maximum force is 0.35. The the initial elastic stiffness is obtained taking into account the stiffness of the frame and K_{mfc}.

Two cross diagonals per frame were modelled in OpenSees by means of twoNodeLink elements. This type of element requires the definition of a force-displacement law to apply along one of the six degrees of freedom of the element (3 translational and 3 rotational). In this way, once that is known the force-displacement law derived from Decanini model it is possible to apply it along the axial direction of the element.

The various force-displacement laws for the infills were introduced in the model using the *uniaxialMaterial Hysteretic* command that construct a uniaxial bilinear hysteretic material object with pinching of force and deformation, damage due to ductility and energy, and degraded unloading stiffness based on ductility. The definition of this material requires the specification of three points in the stress-strain or force-displacement plane and for this reason is suitable for describing the force-displacement law of the infills.

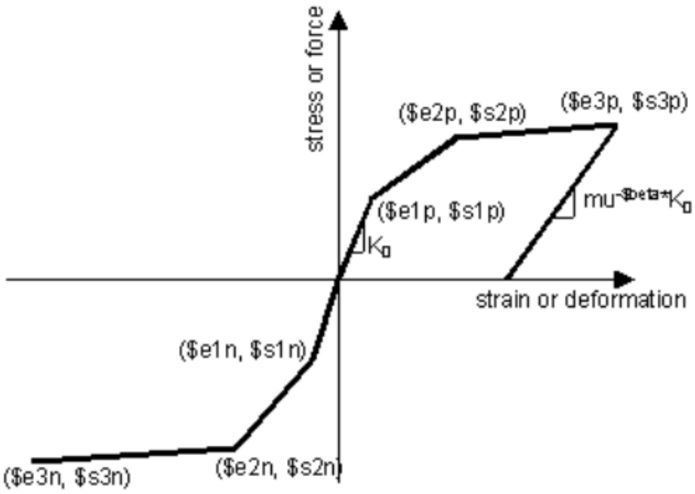

Figure 6-59. Hysteretic material constitutive law.

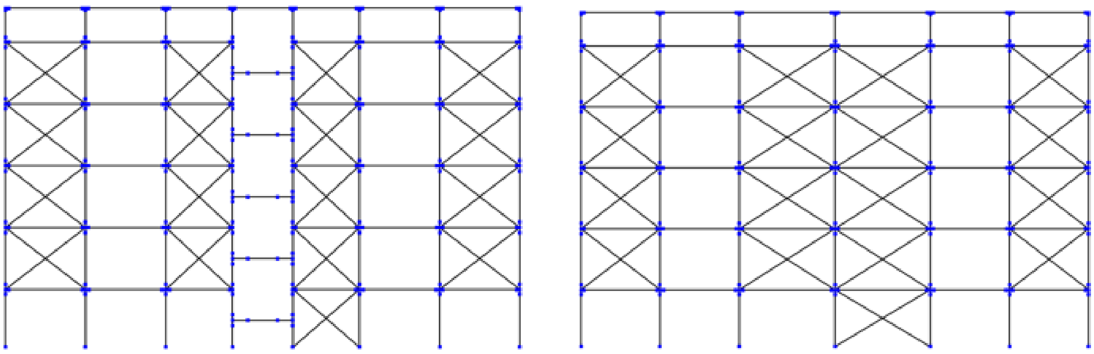

Figure 6-60. Infills along the frame Y=0m and Y=10.55m.

Chapter 7

7 Comparison of the results

7.1 Modelling of the brace with a single element

The results of the modal analysis of the retrofitted structure are presented in Table 36.

Table 36

VIBRATION MODES OF THE RETROFITTED STRUCTURE				
Mode	**Type**	**ω [rad/s]**	**T [s]**	**f [s^{-1}]**
1	Translational Y	9.497	0.662	1.512
2	Translational X	9.859	0.637	1.569
3	Rotational	10.158	0.619	1.617
4	Translational X	30.393	0.207	4.837
5	Translational Y	30.574	0.206	4.866

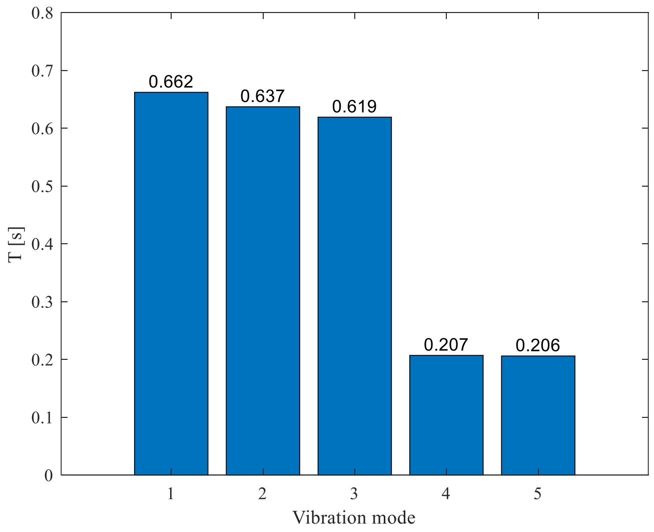

Figure 7-1. Periods of vibration of the first five modes of the retrofitted structure.

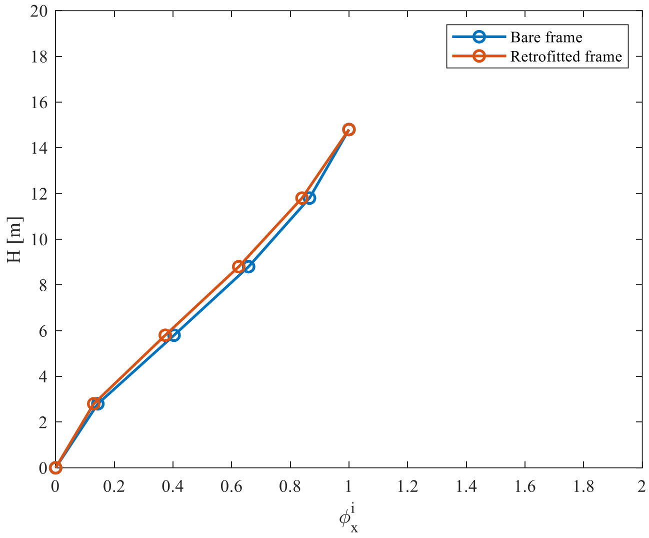

Figure 7-2. First translational modal shape in X direction of the bare frame and the retrofitted (single element brace).

Modeling the dissipative bracing system with a single truss element and the material Steel02 gives the pushover curve of Figure 7-3.

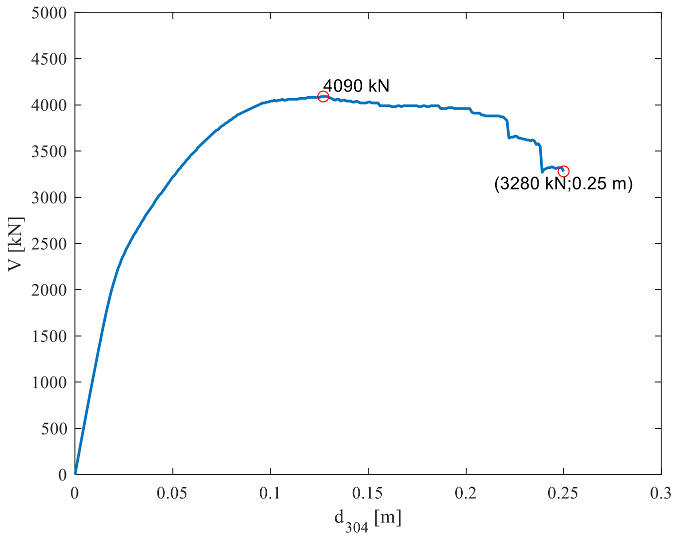

Figure 7-3. Pushover curve of the retrofitted structure (single element brace).

The ultimate displacement of the curve was stopped at 0.25 m corresponding to a drop of resistance of the 20% respect to the peak of 4090 kN. For higher displacements the decreasing of the resistance becomes bigger and the response of the structure is no more reliable.

Since that the aim of the retrofitting is to obtain a structure that is able to withstand the design seismic demand whit a maximum interstorey drift of 1.5% the pushover curve was stopped at the reaching of this condition at the step number 163.

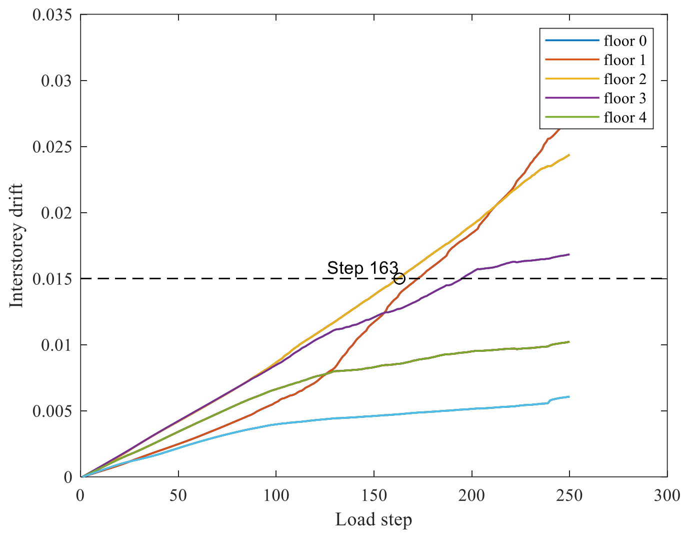

Figure 7-4. Interstorey drift at each load step (single element brace).

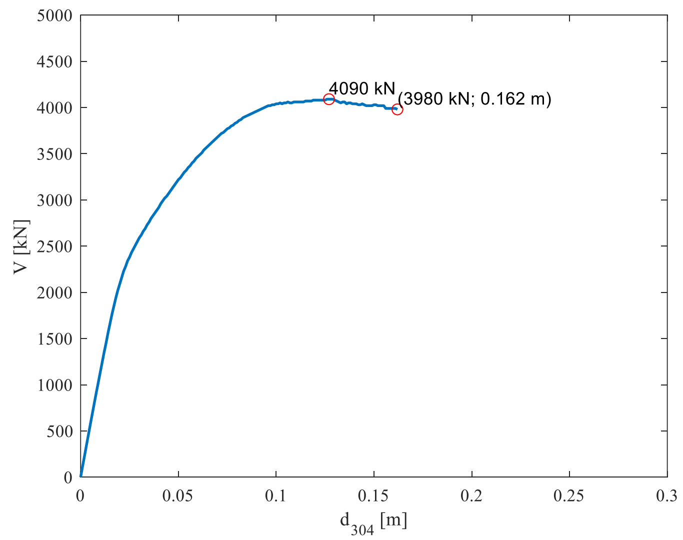

Figure 7-5.Pushover curve of the retrofitted structure stopped at 1.5% drift (single element brace).

The bilinearization of this curve and the comparison between the capacity of the retrofitted structure and the seismic demand are shown in Figure 7-6 and Figure 7-7.

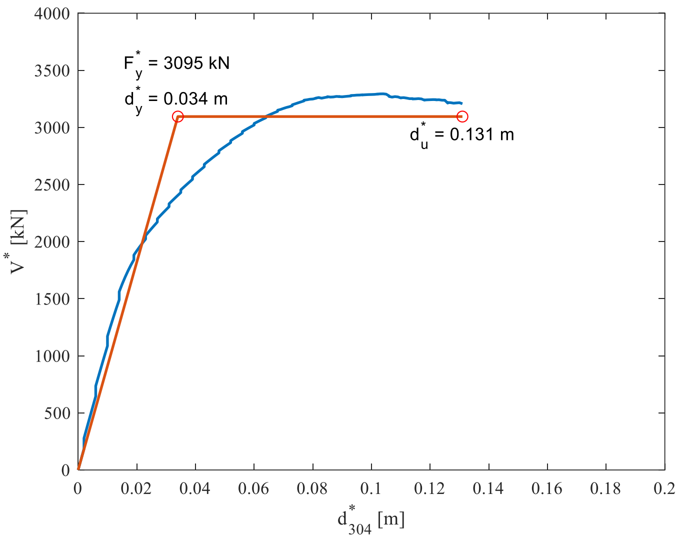

Figure 7-6. Equivalent SDOF system capacity curve and its bilinearization (single element brace).

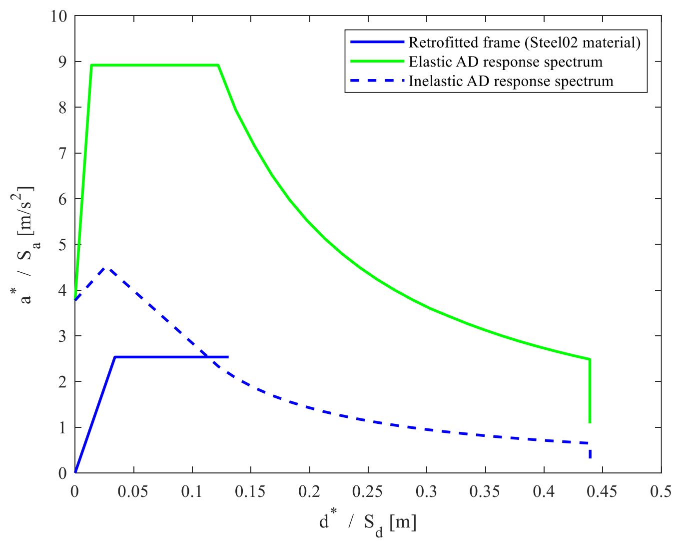

Figure 7-7. Comparison between capacity of the retrofitted structure and seismic demand (single element brace).

The characteristics of the bilinear capacity curve are in Table 37.

Table 37

k*	m*	T*	μ
[kN/m]	[kN/m/s^2]	[s]	-
90896.105	1221.137	0.727895688	3.833

Since the resisting shears of the dissipative bracing system are proportional to the normalized shears of the bare frame v^i that depends on the modal shape of the first vibration mode it is expected to obtain an almost contemporary yielding of all the BRB as shown in Figure 7-8.

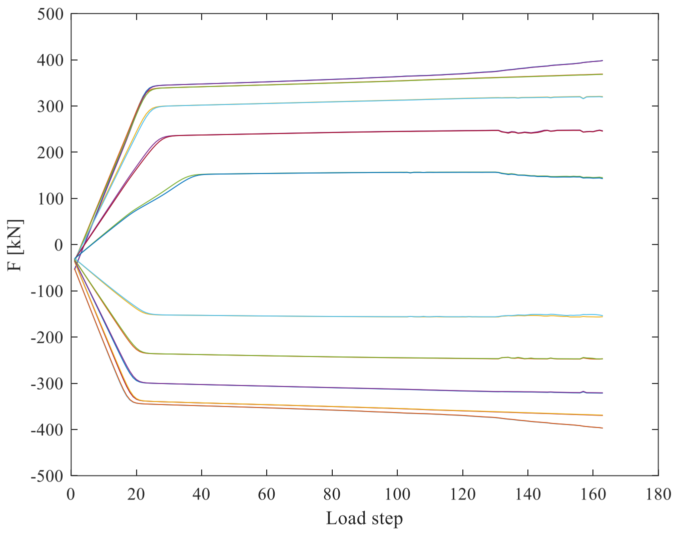

Figure 7-8. Contemporary yielding of all the BRB (single element brace).

7.2 Modelling of the brace with two elements

The results of the modal analysis of the retrofitted structure are presented in Table 38.

Table 38

VIBRATION MODES OF THE RETROFITTED STRUCTURE				
Mode	**Type**	**ω [rad/s]**	**T [s]**	**f [s^{-1}]**
1	Translational Y	9.504	0.661	1.513
2	Translational X	9.860	0.637	1.569
3	Rotational	10.167	0.618	1.618
4	Translational X	30.394	0.207	4.837
5	Translational Y	30.593	0.205	4.869

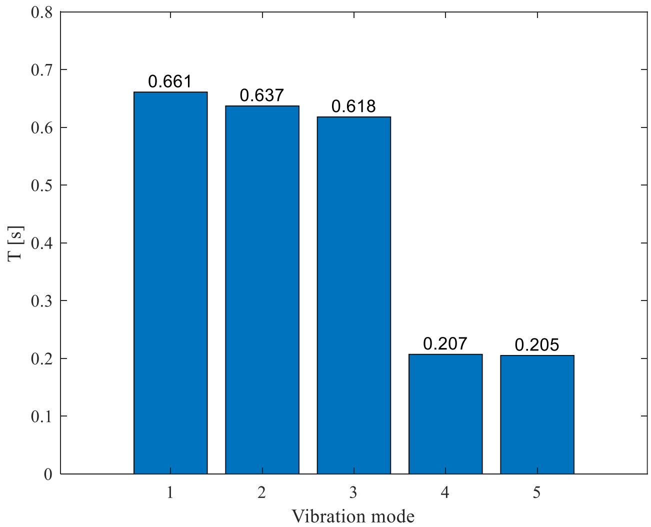

Figure 7-9. Periods of vibration of the first five modes of the retrofitted structure.

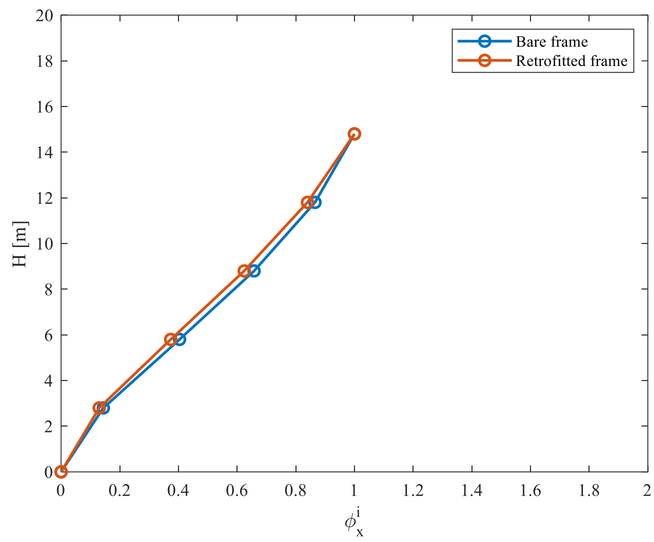

Figure 7-10. First translational modal shape in X direction of the bare frame and the retrofitted (two elements brace).

Modeling the dissipative bracing system with two elements, a ForceBeamColumn with an elastic section for the connecting arm and a truss element with the steelBRB material for the dissipative device, gives the pushover curve of Figure 7-11.

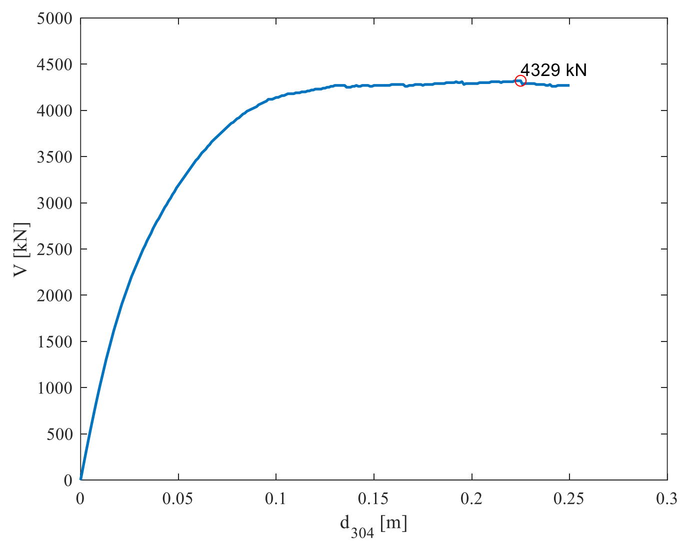

Figure 7-11. Pushover curve of the retrofitted structure (Two elements brace).

In this case the pushover curve was stopped at a ultimate displacement of 0.25m as was done in the previous case. The capacity curve does not show a drop of resistance and this is due to the higher hardening ratio assigned to the *SteelBRB* material according to the results of experimental tests.

Even in this case the pushover curve was stopped at the reaching of an interstorey drift of 1.5%.

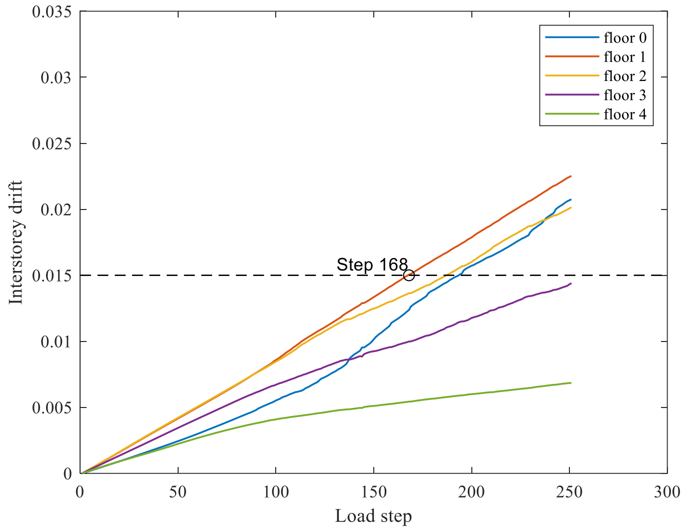

Figure 7-12. Interstorey drift at each load step (Two elements brace).

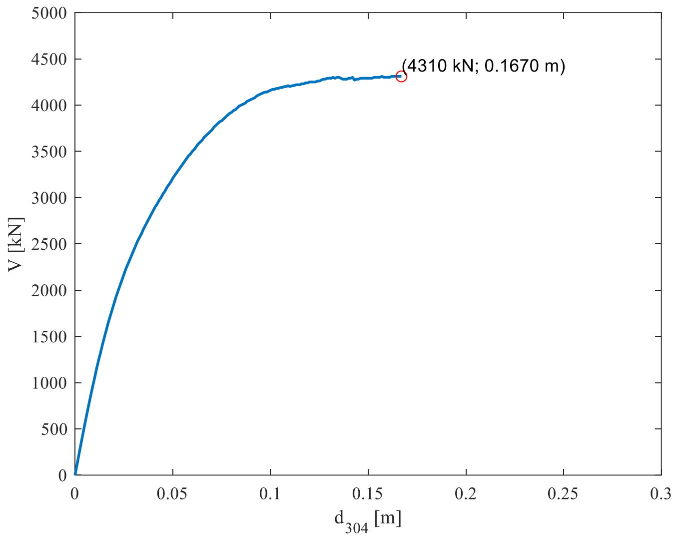

Figure 7-13. Pushover curve of the retrofitted structure stopped at 1.5% drift (two elements brace).

The bilinearization of this curve and the comparison between the capacity of the retrofitted structure and the seismic demand are shown in Figure 7-14 and Figure 7-15.

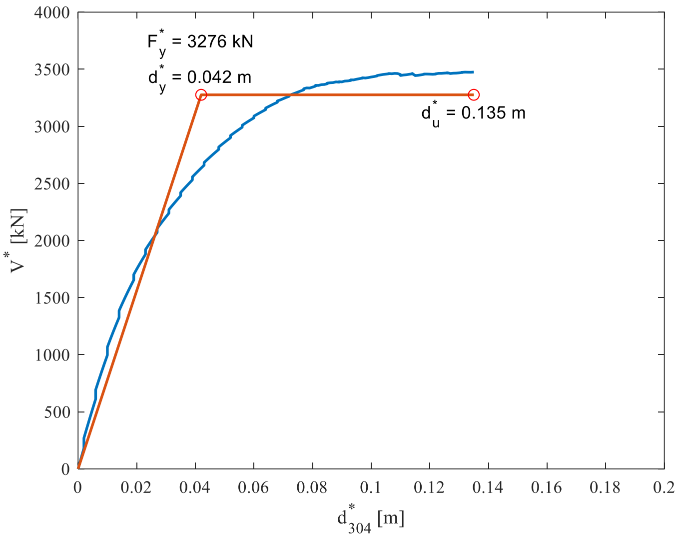

Figure 7-14. Equivalent SDOF system capacity curve and its bilinearization (two elements brace).

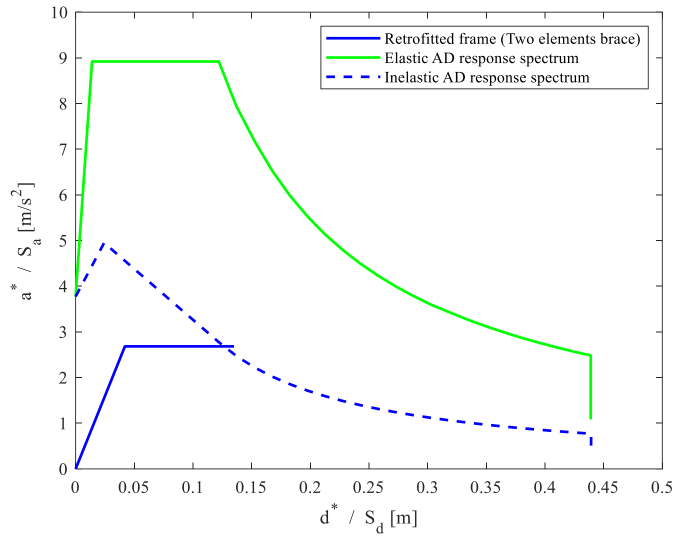

Figure 7-15. Comparison between capacity of the retrofitted structure and seismic demand (two elements brace).

The characteristics of the bilinear capacity curve are in Table 39.

Table 39

k*	m*	T*	μ
[kN/m]	[kN/m/s^2]	[s]	-
78457	1221.1	0.783	3.222

Since the resisting shears of the dissipative bracing system are proportional to the normalized shears of the bare frame v^i that depends on the modal shape of the first vibration mode it is expected to obtain an almost contemporary yielding of all the BRB as shown in Figure 7-16.

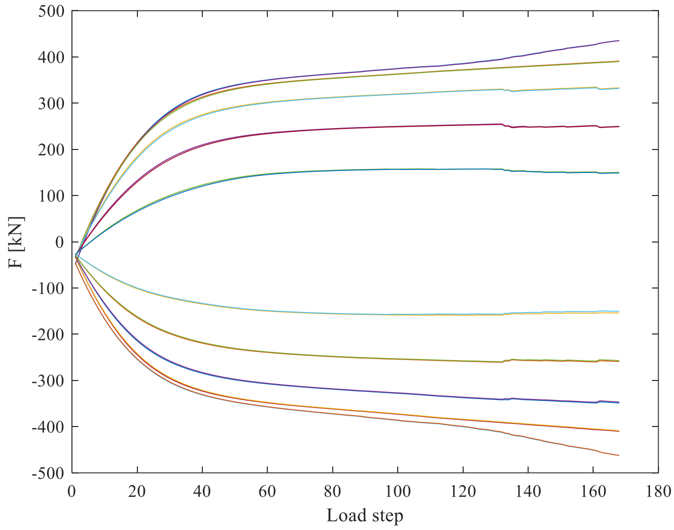

Figure 7-16. Contemporary yielding of all the BRB (two elements brace).

The design of the dissipative bracing system was realized starting from the bare structure, without considering the presence of the infills. For this reason the BRB system modelled using two elements for each brace was added also to the model of the structure with the infills in order to investigate the influence of the stiffening provided by the nonstructural elements on the response of the retrofitted structure.

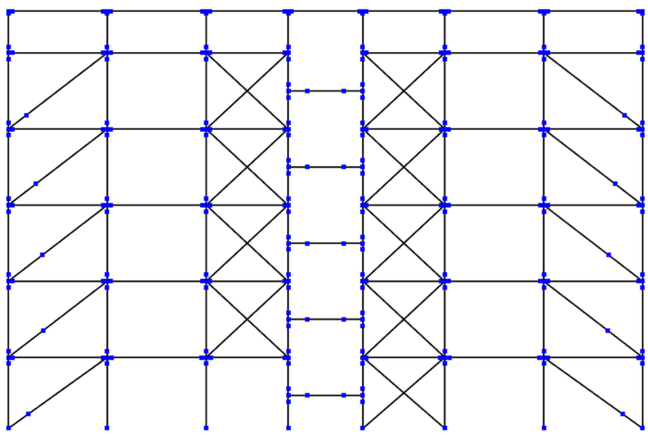

Figure 7-17. Retrofitted model with the infills.

The results of the modal analysis of the model with both the infills and the BRB system is presented in Table 40.

Table 40

VIBRATION MODES OF THE RETROFITTED STRUCTURE				
Mode	**Type**	**ω [rad/s]**	**T [s]**	**f [s^{-1}]**
1	Translational Y	9.740	0.645	1.550
2	Translational X	9.933	0.633	1.581
3	Rotational	10.545	0.596	1.678
4	Translational X	30.542	0.206	4.861
5	Translational Y	31.173	0.202	4.961

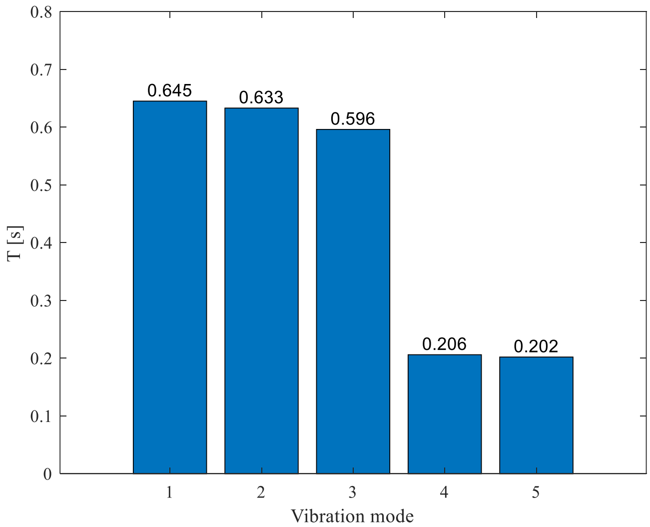

Figure 7-18. Periods of vibration of the first five modes of the retrofitted structure considering the infills.

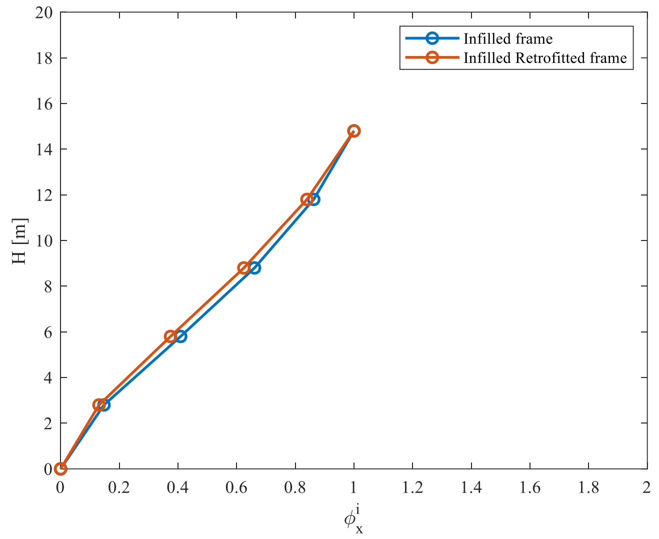

Figure 7-19. First translational modal shape in X direction of the infilled frame and the retrofitted (two elements brace).

The procedure used to obtain the bilinear capacity curve of the infilled retrofitted structure is the same of the two previous case. The pushover curve was stopped at the reaching of a 1.5% interstorey drift obtaining the capacity curve represented in Figure 7-20

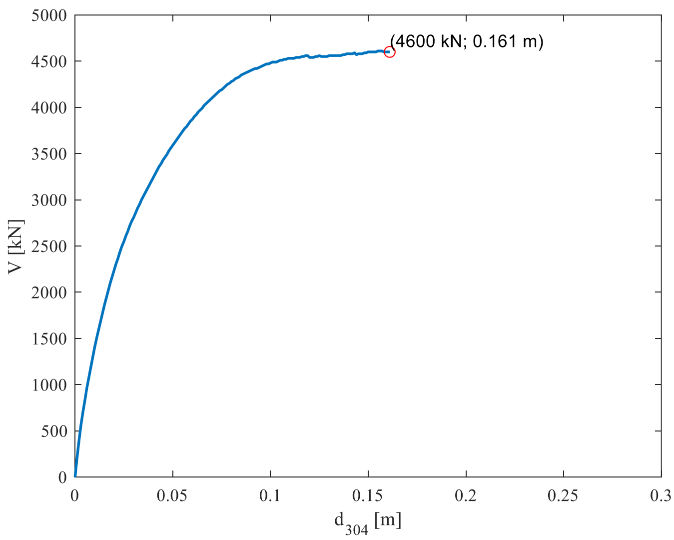

Figure 7-20. Pushover curve of the infilled retrofitted structure stopped at 1.5% drift (two elements brace).

The comparison between the capacity of the retrofitted structure and the seismic demand are shown in Figure 7-21.

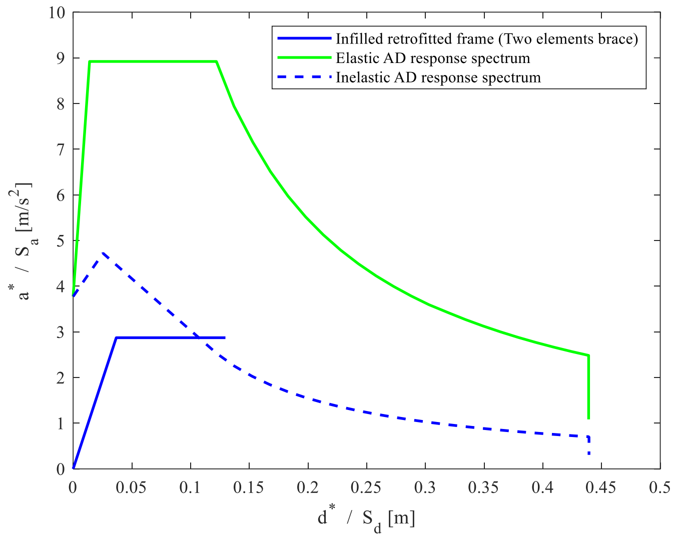

Figure 7-21. Comparison between the capacity of the infilled retrofitted structure and seismic demand (two elements brace).

The characteristics of the bilinear capacity curve are in

k*	**m***	**T***	**μ**
[kN/m]	**[kN/m/s²]**	**[s]**	**-**
95487.368	1221.1	0.710180631	3.531

7.3 Comparison of the pushover curves.

It is interesting to make a comparison of the pushover curves obtained from the unretrofitted structure and from the retrofitted ones in order to look at the differences in the structural behavior obtained with different modelling approaches.

The three pushover curves of the bare frame and of the retrofitted frame, modelling the BRB with a single element diagonal or with two elements, are shown in

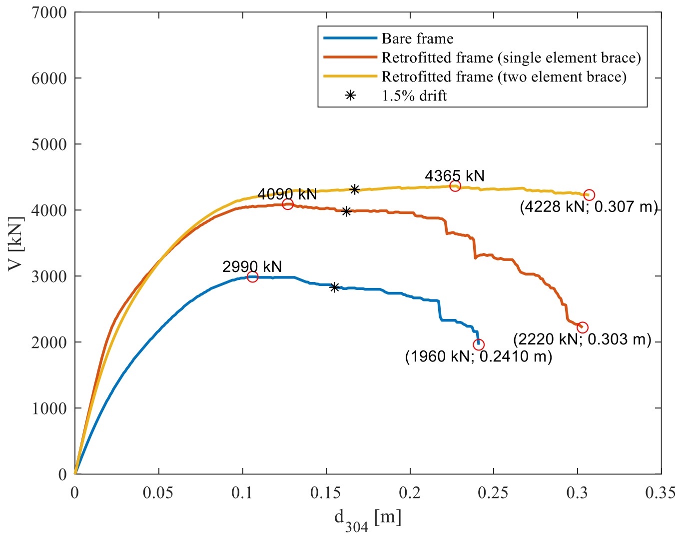

Figure 7-22. Comparison between pushover curves of the bare frame and the retrofitted structure.

The pushover curves plotted in Figure 7-22 arrive until the ultimate displacement of the system that corresponds to the failure and at this stage the interstorey drift is much higher than the 1.5% considered in the design phase. An interstorey drift of the 1.5% is reached at the asterisk markers and the corresponding displacement of the control node 304 is almost the same in the three cases.

The adding of the BRB system to the model increases the maximum strength of the capacity curve with respect to the unretrofitted structure as can be seen in Table 41. Modelling the bracing system dividing each brace in two components gives an higher peak resistance because the hardening ratio assigned to the material used for the BRB, chosen according to the results of experimental tests, is higher than the hardening ratio assigned to the steel02 material, used in the modeling of the brace with a single truss element. This is also the reason why the pushover curve does not show the same softening behavior after the reaching of the peak.

Table 41

Model	Peak resistance	variation
-	[kN]	%
Bare frame	2990	-
Retrofitted (single element brace)	4090	37
Retrofitted (two elements brace)	4365	46

Considering the presence of the infills gives the pushover curves of Figure 7-23.

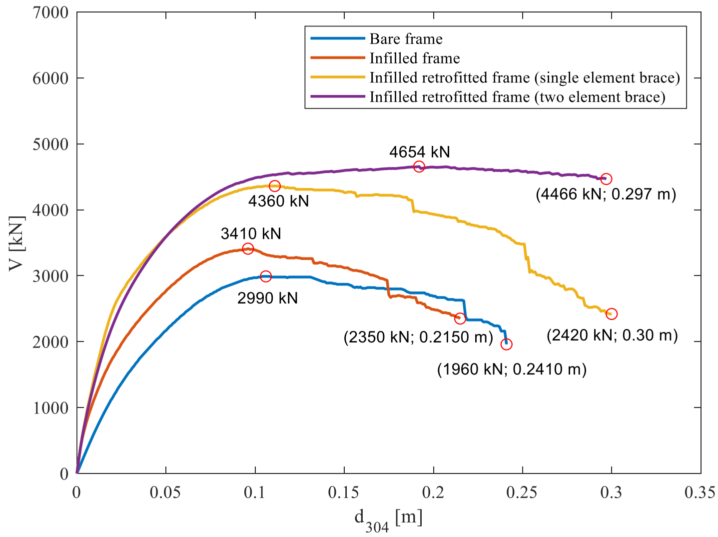

Figure 7-23. Comparison between pushover curves of the infilled frame and the infilled retrofitted structure.

Even in this case the pushover curves arrive at the ultimate displacement of the system, corresponding to the failure.

Taking into account the presence of the infills increase the strength of the system and the variations respect to the bare frame are presented in Table 42. It can be seen that the increasing of maximum resistance, given by the infills only, respect to the bare frame is the 14%. The increasing of resistance of the infilled retrofitted structure respect to the infilled frame is lower than the case without taking into account the infills because the positioning of the BRBs in the external spans of the frame requires the elimination of the infills placed in those position and therefore the loss of their contribution.

Table 42

Model	Peak resistance	Variation respect to the bare frame	Variation respect to the infilled frame
-	[kN]	%	%
Bare frame	2990	-	-
Infilled frame	3410	14	-
Infilled retrofitted (single element brace)	4360	-	28
Infilled retrofitted (two elements brace)	4654	-	37

Chapter 8

8 Conclusive remarks and further developments.

The recent seismic events that affected the Italian territory, starting from that of L'Aquila of the 2009, highlighted the numerous design deficiencies of the buildings situated in areas with high seismic hazard that were realized before the introduction of the seismic codes. For this reason, the seismic retrofitting or upgrading of the existing buildings has become of paramount importance in recent years because it is necessary both for limit the number of victims, and for limit the costs necessary for the repair or the construction of new buildings.

The aim of this thesis is the retrofitting of an existing RC building situated in L'Aquila that suffered extensive damage after the earthquake of 2009. The biggest problem of the structure is the absence of a resisting system in both directions that therefore causes an inadequate response of the building along the weaker direction.

The seismic retrofitting was carried out by means of a system of dissipative buckling restrained braces, which are suitable for application in RC structures and are able to provide a high energy dissipation thanks to the development of large and stable hysteretic loops.

The dissipative bracing system was designed by means of a method based on the result of the pushover analysis. Choosing two design parameters, the ductility of the bracing system and its base shear, it was possible to design a bilinear capacity curve of the SDOF coupled system (frame + BRB) that was able to reach the performance point intersecting the seismic demand represented by the inelastic spectrum. The bracing system was designed in order to obtain a retrofitted structure that was able to withstand the seismic demand associated to the SLV design spectrum showing a maximum interstorey drift of 1.5% in order to limit damage on structural and non-structural elements.

The results of the design procedure were validated adding the designed bracing system to the finite element model of the structure, realized previously to perform the nonlinear static analysis. The modeling of the braces was performed in two ways, one simpler and one more refined, and in both cases the pushover analyses performed on the retrofitted structure gave a positive result because the design earthquake could be withstand by the structure exhibiting a maximum interstorey drift lower than 1.5% validating in this way the design procedure.

It was seen that even considering the presence of the infills, not taken into account in the design phase, the retrofitted structure reached the required performance point. For these reasons, the design procedure used in this thesis turns out to be suitable for the purpose and allows obtaining a regular response of the structure under the seismic action.

Further nonlinear dynamic analysis can be performed on the model applying a set of spectrum-compatible ground motion to investigate the dynamic response of the structure evaluating the mean values of the maximum interstorey drifts. It is also possible to perform incremental dynamic analysis (IDA) scaling a set of ground motion at different values of intensity measure and realizing fragility curves for different engineering demand parameters (EDP).

The finite element model realized for the execution of the nonlinear analysis can also be used for future research concerning the accumulation of damage on BRBs given by multiple earthquakes (main shock and aftershock). The material used for modeling the BRBs allows obtaining as output also the accumulation of plastic strain on the dissipative device due to the hysteretic cycles. In this way, it is possible to obtain the cumulative plastic ductility (CPD) through which is possible to evaluate the damage status of the dissipative device and compare it with appropriate models.

A further improvement of the finite element model can also be done by modeling the infills with more precise techniques that are able to simulate the influence of the infills at the local level of the individual elements.

BIBLIOGRAPHY

Black C., Makris N., Aiken I., (2002). Component Testing, Stability Analysis and Characterization of Buckling-Restrained Unbonded Braces. Report No. PEER 2002/08, Univ. of California, Berkeley, CA.

Bozorgnia Y., Bertero V. V. (2004). *Earthquake Engineering: From Engineering Seismology to Performance-Based Engineering.* ICC-CRC Press, Boca Raton, Florida, USA.

Chopra A. (1995). *Dynamics of structures: Theory and Applications to Earthquake Engineering*. USA: Prentice Hall

Constantinou, M. C., Soong, T. T., and Dargush, G. F. (1998). *Passive energy dissipation systems for structural design and retrofit*, MCEER Monograph Series, No. 1, Multidisciplinary Center for Earthquake Engineering Research, Buffalo, N.Y.

Dall'Asta A., Ragni L., Tubaldi E., Freddi F., (2009). Design methods for existing r.c. frames equipped with elasto-plastic or viscoelastic dissipative braces. Conference: XIII National Conference ANIDIS: L'Ingegneria sismica in Italia.

De Luca F., Vamvatsikos D., Iervolino I., (2013). Improving Static Pushover Analysis by Optimal Bilinear Fitting of Capacity Curves. Computational Methods in Earthquake Engineering. Springer, 2013. p. 273-295 (Computational Methods in Applied Sciences; Vol. 30).

Di Sarno L., Manfredi G., (2009). Seismic retrofitting of existing RC frames with buckling restrained braces. ATC & SEI 2009 Conference on Improving the Seismic Performance of Existing Buildings and Other Structures.

Fajfar P., (2000). A nonlinear analysis method for performance-based seismic design. Earthquake Spectra 2000,16(3):573-592.

Iwata M., Kato T., Wada A., (2000). Buckling-restrained braces as hysteretic dampers. Proc. STESSA 2000 Conf., 33-38, Montreal, Canada, August 2000.

Kim J., Choi H., Chung L., (2004). Energy-based seismic design of structures with buckling-restrained braces. Steel and Composite Structures, Vol. 4, No. 6 (2004) 437-452.

Liberatore L., Decanini L.D. (2011). Effect of infills on the seismic response of high-rise RC buildings designed as bare according to Eurocode 8. Ingegneria Sismica 28(3):7-23.

Mander J. B., Priestley M. J., Park R. (1988). Theoretical Stress-Strain Model for Confined Concrete. Journal of Structural Engineering, Vol. 114, Issue 8 (September 1988).

Panagiotakos T. B., Fardis M. N., (2001). Deformations of Reinforced Concrete Members at Yielding and Ultimate. ACI Structural Journal, Vol 98, Issue 2, Pages 135-148.

Scott M. H., Fenves G. L., (2006). Plastic Hinge Integration Methods for Force-Based Beam–Column Elements. Journal of Structural Engineering, Vol 132, Issue 2, Pages 244-252.

Symans M. D., Charney F. A., Whittaker A. S., Constantinou M. C., Kircher C. A., Johnson M. W., McNamara R. J, (2008). Energy Dissipation Systems for Seismic Applications: Current Practice and Recent Developments. Journal of Structural Engineering 134, January 2008.

Tubaldi E., Freddi F., Zona A., Dall'Asta A., (2017). Seismic performance of structural systems equipped with buckling-restrained braces. Conference: ANIDIS 2017, Pistoia, Italy.

Zona A., Dall'Asta A., (2011). Elastoplastic model for steel buckling-restrained braces. Journal of Constructional Steel Research, Volume 68, Issue 1, January 2012, Pages 118-125.

<u>CODES</u>

ASCE, (2000). Prestandard and Commentary for the Seismic Rehabilitation of Buildings. Report No. FEMA-356, Building Seismic Safety Council, Federal Emergency Management Agency, Washington, D.C.

Eurocode 8 (2004). Design of structures for earthquake resistance-Part 1: General rules, seismic actions and rules for buildings.

NTC 2018 (2018). Aggiornamento delle “Norme tecniche per le costruzioni”.